NOVEL APPROACHES TO LARGE SCALE PROTEIN PURIFICATION AND ANALYSIS.

A Thesis Submitted by
Mark Andrew Snoswell, B.Sc.(Hons)

to the University of Adelaide,
South Australia for the degree
of Doctor of Philosophy.

Department of Biochemistry,

University of Adelaide,

Australia December, 1990

SUMMARY

New inventions are described in the areas of electrophoresis and spectroscopy.

A new class of separation and apparatus was invented and developed. The new technique is named Counter-current Electrophoretic Filtering (CEF). CEF opposes electrophoresis and hydrodynamic forces to effect an efficient, high resolution, continuous separation technique, applicable to any ion or mixture of ions. The apparatus developed is very efficient and easy to scale up.

Spectral enhancement techniques have been developed which permit enhancement to gas phase resolution from liquid phase spectra. For Gaussian bands it is shown that an ideal filter function exists for both band broadening (smoothing), and band narrowing (enhancement). Ideal band broading is practically achievable, while ideal band narrowing is not practically achievable. Approaches to the ideal band narrowing filter are developed and evaluated and a 'best solution' is given.

STATEMENT

This thesis contains no material which has been accepted for the award of any other degree or diploma in any university. To the best of my knowledge, it contains no material that has been previously published or written by another person except where due reference is made in the text.

Mark. A. Snoswell.

ERRATA
======

page 2-3, paras 4 & 5	- isoachophoresis should be isotachophoresis (5 occurences)
page 2-11, para 3	- Wiers should be Weirs
page 7-3, para 4	- gaol should be goal

ACKNOWLEDGEMENTS

I wish to acknowledge the guidance of my supervisors Dr John Wallace and Dr Julian Wells.

I am grateful for the assistance of Tam Vu and Nicholass Abbot who participated in the spectral and electrophoretic work respectively.

I also wish to thank all of my 'PGH (Porcine Growth Hormone) team' who contributed in various ways, particularly with respect to the production of PGH.

I am particularly indebted to Dr Tom Kurucsev for his assistance with the preparation of this thesis and in particular the mathematics involved in the spectral enhancement section.

Finally I want to thank my wife Helen for her support and help in the preparation of this thesis.

DEDICATION

For my fa ther
Dr Alan Snoswell. B.Sc. (Hons), Ph.D., D.Sc.
(1930-1990)

Abbreviations and Nomenclature.

S/N		Signal to noise ratio.
RMS	s	Root mean square.
sigma	σ	Band width parameter in time domain.
theta	θ	Band limit parameter in time domain.
delta	δ	Half height band width in time domain.
beta	β	Convolution width parameter = 2m + 1.
PGH	PST	Porcine Growth Hormone or Porcine Somatotrophin.
gamma	γ	Band width parameter in Fourier domain.
alfa	α	Interval in Fourier domain.
delta	δ	Reduced band Width %.
PGH		Porcine Growth Hormone.
BGH		Bovine Growth Hormone.
HGH		Human Growth Hormone.
GH		Growth Hormone.
PEG		Poly Ethelene Glycol.
CEF		Counter-current Electrophoretic Filtering
SND		S/N degradation, (source S/N)/(output S/N).

Table of Contents

Continuous electrophoretic filtering

Spectral Enhancement

Discussion

Counter-current electrophoretic filtering

Introduction

Purification of proteins is of major concern to those industries wishing to utilize biotechnology to produce their products. In particular the economical purification of a desired product at high throughput and high resolution is often the determining factor when assessing the worth of manufacturing many medium to low value protein products. [1] [2] Often a crude product can be manufactured in large quantities with relative ease, however final purification to remove closely related contaminants (even incorrectly folded forms of the desired product) can be extremely difficult.

Unfortunately many techniques suitable for purifying proteins in the laboratory (such as gel filtration and gel electrophoresis) cannot be scaled up economically. This is due to the inherently wasteful use of relatively expensive media that highly reproducible manufacturing processes demand. For instance, the techniques of gel filtration and gel electrophoresis have loading capacities of less than 5% of the matrix volume. From a process capacity point of view, these techniques are wasting over 95% of the media at any given time.

Of the commonly applied laboratory techniques, liquid chromatography is the most widely used at moderate process levels. However it is unlikely that liquid chromatographic techniques would be suitable to purify recombinant proteins above the 100Kg per day levels. Companies such as Monsanto are pioneering the use of truly massive ion-exchange columns in their processes to manufacture BST (Bovine Somatotrophin).[3] Even with the several thousand litre volume columns used in these processes, capacities are still only around 20Kg per day. To meet the demand for PGH in Asia and China alone would require production column capacities in excess of 500Kg per day.

Clearly there is a need to develop new high resolution, low cost purification techniques that scale well (from mg to tonne levels). This chapter discloses details of a newly invented purification technique which may well be capable of serving the needs of research scientists and production engineers alike. Before describing the invention it is appropriate to consider the merits and drawbacks of the techniques currently available.

---

1 M. Snoswell,D.Petridies, C. Cooney, B. Evans, R. Field. Bioprocess Simulation: An Integrated approach to Process Development. Computers in Chemical Engineering 1988

2 A. Middelberg, M. Snoswell, A. Zwahlen, S. Bastiras, C. Senn. An Economic and Technical Analysis of a Manufacturing Process for PST. Internal publication April 1990

3 T. Keuer, J. Ryland. Industrial-scale ion Exchange Chromatography for Purification of Proteins. Engineering Foundation Conference on Recovery of Biological Products V. May 1990

Current technology

Traditional protein purification processes are of a partitioning nature and can be divided into two broad groups as follows.

> Processes dependent on protein-protein and/or protein-solution interactions. This group of separations can be further divided into two subclasses: (a) liquid-liquid partitioning such as selective extraction into liquid phases of differing PEG concentrations; and (b) protein precipitation in which agents such as ammonium sulphate or ethanol are used to selectively precipitate proteins.
>
> Processes involving partitioning onto and/or through some solid support. This group of separations can also be divided into two major subclasses: (a) filtration; and (b) adsorption (also known as liquid chromatography).

Group 1 processes are cheap and easy to implement and scale up. Unfortunately they usually offer little selectivity.

Of the group 2 processes filtration is cheap and easily scaled up. Unfortunately it also suffers from a lack of selectivity, although the selectivity is often much higher than for group 1 processes. If electrical forces are utilized for filtration (ie. gel electrophoresis), then extremely high selectivities are achievable. Unfortunately gel electrophoresis is **very** hard to scale up mainly because of problems associated with ohmic heating and heat removal. Liquid chromatography offers medium selectivity and, although not easily scaled up, is currently the most widely utilized preparative protein purification process.

Following is a brief discussion of the merits and disadvantages of the most commonly used protein purification processes. The goal is to assess the various processes and design a new purification process with few disadvantages but with all the benefits of current processes.

Liquid chromatography

Liquid chromatography in packed gel beds is the traditional and most widely used method for preparative separation of proteins. At present nearly all purified protein products on the market have undergone liquid chromatographic purification. While liquid chromatography has been successfully used for moderate scale production of proteins, it is limited by two factors.

First, components to be purified must be bound to, or entrapped wholly within, the porous gel bed. Therefore, the volume of gel required is in direct proportion to the quantity of material to be purified. In commercial applications the chromatographic gel is a consumable item. Replacement gel can often be the most significant cost item in the purification process.

Second, no matter what sort of chromatography is applied, process volume will increase, although product volume may decrease in extraction/concentration modes. It is not possible to perform any chromatographic separation without the aid of some eluting buffer. This adds process volume and considerable capital, consumable and labour costs to the purification process[1] [2].

While most recombinant proteins require processing at low concentrations, the final formulations are often very concentrated (ie. controlled release formulations). Process quality water, product dewatering, and waste treatment all add considerable cost and risk to any production process. Ion exchange (IEX) and hydrophobic interaction chromatography (HIC) are the most commonly applied forms of liquid chromatography[3]. Both of these modes permit trace enrichment by extracting low concentration products from process streams. Although this concentrates the product stream, overall process volume increases due to the requirement for eluting and equilibrating buffers.

One area in which liquid chromatography is commonly applied is desalting as a final step. For proteins with molecular weights greater than 3,500 g mol^{-1}, and for process throughputs less than several hundred litres per day, desalting competes favourably with ultra-filtration as a buffer exchange method. However the closely related technique of gel filtration is only ever applied to the highest value, and lowest volume products. The reason for this is the disparate relative efficiencies of gel utilisation (and therefore running costs) of the two methods. Loading capacity for both methods is volume limited: desalting allows batch process volumes up to 33% of the gel bed volume; gel filtration requires batch volumes of less than 5% of the bed volume for adequate resolution.

1 M. Snoswell, D.Petridies, C. Cooney, B. Evans, R. Field. Bioprocess Simulation: An Integrated approach to Process Development. Computers in Chemical Engineering 1988

2 A. Middelberg, M. Snoswell, A. Zwahlen, S. Bastiras, C. Senn. An Economic and Technical Analysis of a Manufacturing Process for PST. Internal publication April 1990

3 O'Hare

Ultrafiltration

Ultrafiltration is often used in commercial scale protein purifications. The advantages of filtration over chromatography are several: process volumes do not necessarily increase; throughput is proportional to filter area and not volume; operation is simple and cheap; and filter costs are less than chromatographic gel. Unfortunately filtration has relatively low resolution and will usually only give complete separation of proteins whose hydrodynamic radii differ by at least an order of magnitude.

The ability to operate in a continuous mode is a considerable advantage over techniques such as chromatography which can only be operated in a batch mode. The higher degree of control and consistency with reduced monitoring requirements, automation costs and risk combine to make continuous processes preferred. In particular, on-line process optimisation is a goal which is practically impossible to achieve with batch processes.

Electrophoresis

Gel electrophoresis is the highest resolution separation technique for proteins. Two dimensional techniques are capable of resolving hundreds of proteins in a single gel. Unfortunately gel electrophoresis is limited by the same constraints as liquid chromatography, with the additional problem of ohmic heating severely limiting gel volumes. With the process stream entrapped wholly within a gel it becomes extremely difficult to scale up, control, and monitor the process. Added to problems of power costs and heat removal, the gels are expensive and delicate. To date it has not been possible to scale up this method. In fact, gel electrophoresis is a method that benefits from scaling down!

Free Flow Electrophoresis

There have been many published and patented reports of free flow electrophoresis systems designed to retain resolution while allowing them to be scaled up. It is argued that, in a free flow system, heat may

be dissipated and separated samples can be easily removed in a continuous fashion. Also sample recovery is simplified and there is no expensive and delicate gel matrix to maintain. To the best of the author's knowledge, none of these apparatus and methods retains the resolving power of gel electrophoresis while yielding a practical and scaled up separation method. Even utilizing complex stabilization techniques[1] [2] resolution is poor and the scale up potential severely limited by the complexity of the devices.

Of the available methods of applying forces to protein molecules to effect separations, electro-mechanical means are attractive. There are only three field types that can be readily generated:

Mechanical, such as gravitational/accelerational or pressure. In such a field, migration of proteins is a function of the various hydrodynamic forces acting in relation to the protein's mass and density.

Electro-mechanical, wherein a charged ion experiences a force proportional to its charge and the imposed electric field strength.

Electromagnetic, wherein an ion experiences a force proportional to its vector velocity and the imposed magnetic field.

Of the last two, electro-mechanical forces are of the greatest magnitude and electromagnetic forces the weakest (being almost too weak for practical use).

The forces which are practically unavailable include the Strong and Weak nuclear forces due to their extremely short ranges.

Clearly a combination of the two strongest forces, mechanical and electro-mechanical, would offer great scope for designing practical new separation techniques.

Mechanical forces can be applied in two ways: gravitational/accelerational; and pressure. (I shall refer to the first type solely in terms of accelerational fields as it is not possible at present to readily manipulate gravitational fields.) In considering the design of the CEF technique, it is important to note that while acceleration and electric fields are penetrating, pressure fields are non-penetrating. The CEF

1 P.T.Noble, Evaluation of Rotational Flow Stabilized Continuous Electrophoreses for Protein Fractionation, Biotechnology Progress (Vol.1,No.4) 1985, 237-249.

2 T.Vermeulen et al, Design Theory and Separations in Preparative-Scale Continuous-Flow Annular-Bed Electrophoresis, Ind.Eng.Chem.Process Des.Develop (Vol.10,No.1) 1971, 91-102

technique utilises pressure (generated by fluid flow) and electrical fields. While an ion is influenced by both fields in a free solution, the ion's interaction with the pressure field is modified within the confines of a matrix material. Within a gel matrix there are many 'pockets' accessible to the ion where the pressure field (fluid flow) is effectively zero, while the electric field is undiminished. By modulating the ion's interaction with the two fields within two adjoining regions of free flow and gel matrix there is great scope to design many new types of separation process. CEF embodies one such particular configuration as constrained by the following design goals.

Design goals

Taking the best characteristics of each of the techniques described, a new separation technique would:

not add to the process volume;

concentrate the desired product;

operate in a continuous mode;

be as cheap and easy to scale up as ultrafiltration;

be tuneable over a very wide range of selectivity;

have the resolution of gel electrophoresis;

draw on existing materials and technology;

be easy to monitor and control; and

work from pico gram to tonne scales.

With these design criteria in mind, the technique of Counter-current Electrophoretic Filtering (CEF) was invented.

The current invention was designed with the clear conviction that a dynamic combination of hydrodynamic and electric forces would offer the best solution to the separations problems at hand. [1]

1 The technique and apparatus described fully in the following chapter were the result of a thought experiment. The intent was to explore the possibility of developing an entirely new process complete with apparatus design, working principals, control mechanisms and operating principals limitations without once setting pen to paper. This approach proved very powerful and permitted the rapid evolution through a number of processes to the final CEF design.

CEF : THE INVENTION

Method and apparatus for Counter-current Electrophoretic Filtering (CEF)[1]

Abstract

Novel new methods and apparatus for the purification and/or concentration of ions in a mixture of differing molecular species are provided. The process described opposes electromotive and hydrodynamic forces across a membrane. Dynamic equilibria (within, and adjacent to, the membrane) produce a tuneable filter element which filters ions on the basis of electromobility. Selectivity is achieved by varying one or more of the following parameters:

bulk fluid flow rate;

electric field strength;

bulk fluid pH; and

membrane material and construction.

One or more apparatus in series can be utilized to concentrate and purify a single component from a mixture.

Background: Description of prior art

The principles of electrophoresis are well known. Separation of a mixture of ions can be effected in an electric field since ionic species will migrate towards an opposite charged electrode at a rate determined by their charge to mass ratio. Hydrated polymeric gels such as acrylamide and aggarose are commonly used as the matrix within which the migration takes place. Such gels impede the passage of ions but also prevent mixing, allowing high resolution separation of ions. In addition to 'pure electrophoresis', interactions of the ions and the gel matrix also provide for separations influenced by properties other than the ions' charge mass ratio.

1 This section is written in the form of a patent, as is appropriate for describing an invention.

Electrophoresis is most commonly used as an analytical tool for the separation of biomolecules. Analytical electrophoresis methods do not usually include the recovery of samples. The separation, detection and quantitation of a mixture are carried out entirely within a gel. The simplest preparative electrophoresis systems operate on the same principles as analytical methods, wherein a mixture of ions are applied as a zone at the origin and the ions are driven through the gel matrix by electrical forces. These batch processes include methods for recovering the separated ions as they emerge from the gel. Apparatus for performing such separations are available from several sources[1] [2]. U.S. Pat. No. 3,847,785 is illustrative of such techniques.

These techniques are very limited in scale, due mainly to problems of ohmic heating. Moreover the samples must be in concentrated form, while these batch processes significantly dilute the ions being separated.

Methods for the continuous separation of ionic species by the action of an electric field perpendicular to the fluid flow were reported as early as 1967[3]. Continuous operation permits higher throughput and more sophisticated control. Due to mixing. these processes still have low capacity and low resolution . Ohmic heating also severely limits the scale at which these processes will work.

Ornstein in U.S. Pat. No. 3,384,564 describes the principles of a process known as isoachophoresis, or displacement electrophoresis. In isoachophoresis, ions of intermediate electrophoretic mobility are 'sandwiched' between ions of higher and lower mobility. The equilibrium forces counteract diffusion and can also concentrate the sample. However the individual bands are difficult to collect without contamination from neighbouring bands. Capacity is severely limited by the requirement for electrophoresis over a long distance to obtain adequate separation.

Many of the problems of isoachophoresis are reduced in a method described by Preetz and Pfeifer[4] in which the bulk fluid flow counteracts isoachophoresis. This counterflow permits the process of isoachophoresis to be performed in a small chamber, or column, for a long time. As disclosed in U.S. Pat. No. 3,705,845 this dramatically reduces the power

1 Gradipore Ltd. Sydney. NSW. Australia. Gradiprep[tm] apparatus.

2 Applied Biosystems Ltd. Foster City. CA. USA.

3 Ravoo, Gelings & Vermculen, Anal. Chim. Acta 38(1967) 219-232

4 U.S. Pat. No. 3,705,845

requirement and problems associated with ohmic heating. Furthermore this system permits continuous modes of operation.

The use of dynamic equilibria between hydrodynamic and electromotive forces to achieve separations of ions has more recently been described by O'Farell[1] [2]. In U.S. Pat's. No. 4,290,855 & 4,323,439 O'Farell describes a process he calls CounterActing Chromatographic Electrophoresis (CACE). The process opposes electrophoresis and gel filtration chromatography and involves the desired ions being trapped at a discontinuity in the gel chromatography bed. While electromotive forces oppose the bulk fluid flow, ions can penetrate the first portion of the gel. The second portion of the gel bed is selected to further oppose the hydrodynamic forces (ie a more porous gel filtration media), where the opposing electromotive forces predominate on the desired ion species. As disclosed, the method describes separations of proteins wholly within a porous chromatographic gel bed. This method suffers from all the drawbacks of both gel chromatography and electrophoresis without offering any significant advantages.

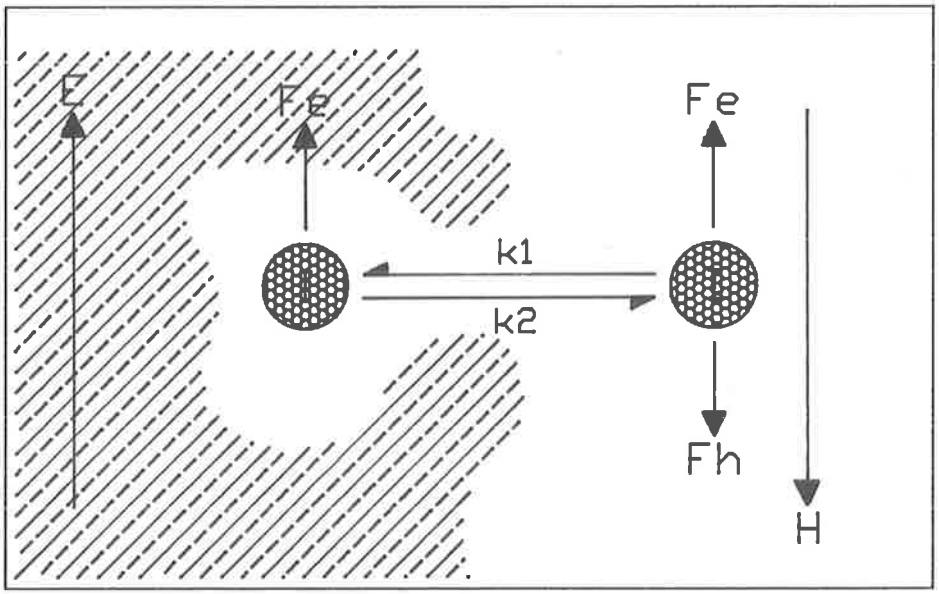

Figure 2.1 *FORCES ACTING on an ion in the membrane of a CEF device. An ion (I), will exhibit a net migration in a direction determined by electromotive (Fe), and hydrodynamic (Fh) forces generated in superimposed electric (E) and pressure (H, hydrodynamic) fields. In addition the hydrodynamic force will be reduced by the interaction of the ion with the membrane material. This will occur when the protein molecule enters some pore or convolution where the fluid flow is reduced or zero, but where the electromotive force is unimpeded. The effective hydrodynamic force (eFh = Fh x Af) is the result of the hydrodynamic force (Fh) multiplied by the availability fraction (Af = k2 / k1).*

1 P.H.O'Farell, J.Biol.Chem, 250(1975) 4007

2 P.H.O'Farell, Science, 227(1985) 1586-1589

Summary of the invention

The invention comprises a novel method and apparatus for isolating, purifying and/or concentrating any species capable of carrying a non-zero charge, ie. any atom, molecule, compound or particle capable of possessing an ionic character. The process can be succinctly described as a Counter-current Electrophoretic Filter (CEF), and utilizes the phenomenon of a dynamic equilibria between hydrodynamic and electromotive forces. The equilibria, when established in a thick membrane, produces a very high resolution filter whose selectivity is based on an ion's electrophoretic mobility. The hydrodynamic forces acting on the sample are generated by the bulk flow of fluid through the membrane. The electrophoretic forces are generated by an electric field antiparallel to the net fluid flow. Under these circumstances the parameters determining permeability of the membrane for a particular ion are:

electrophoretic mobility of the ion;

fluid velocity through the membrane;

electric field strength within the membrane;

interaction of the ion and the membrane; and

pH of the fluid.

The forces acting on an ion within the apparatus are depicted in figures 2.1 and 2.2. The fluid chambers adjacent to the membrane are vigorously mixed to counteract any free flow electrophoresis, and to present all molecules in the solution to the membrane surface. By diffusive processes all molecules presented to the membrane surface will enter it to some degree. Once inside the membrane a selection process will result in the molecule continuing to cross the membrane or being ejected back the way it came.

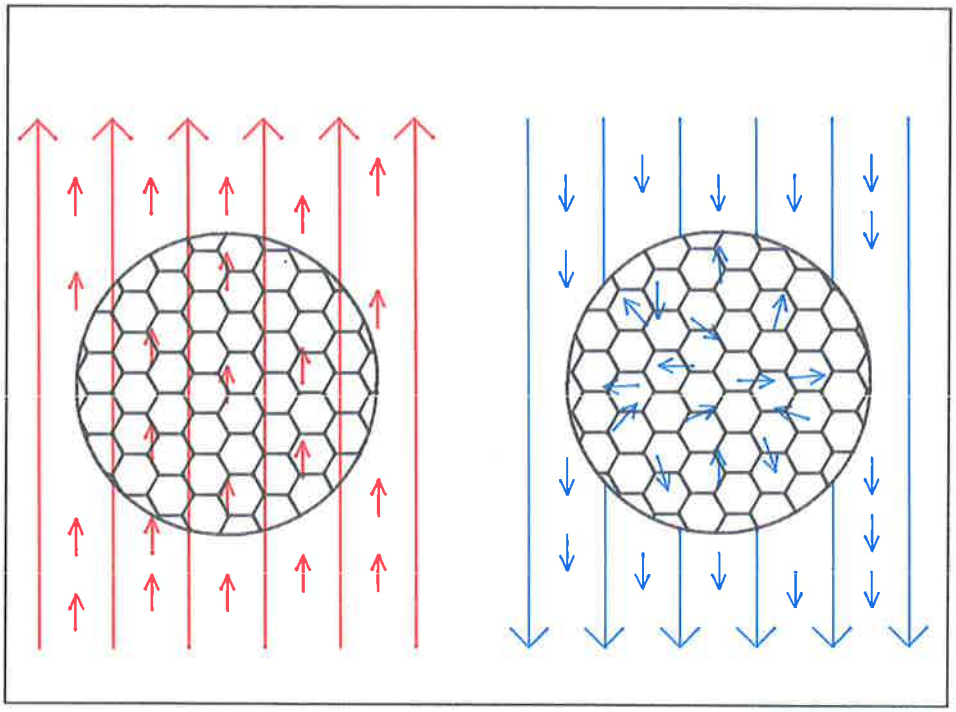

Figure 2.2 ELECTRIC FORCES *penetrate the matrix while hydrodynamic forces do not. The force experienced by an ion in an electric field is undiminished within any non-conducting matrix. The bulk hydrodynamic gradient has no effect within the matrix where (in the absence of any electrodynamic forces) diffusive processes predominate. If the matrix has a distribution of pore sizes within its structure then the rate of diffusion into and out of the matrix will be dependent upon the 'intermatrix volume' available to the ion (ie. gel filtration).*

Selective purification of one ion from a complex mixture can be achieved using two or more CEF units in series, with each tuned to just pass or just retain the desired ion.

Figures 2.3 and 2.4 depict this selective process.

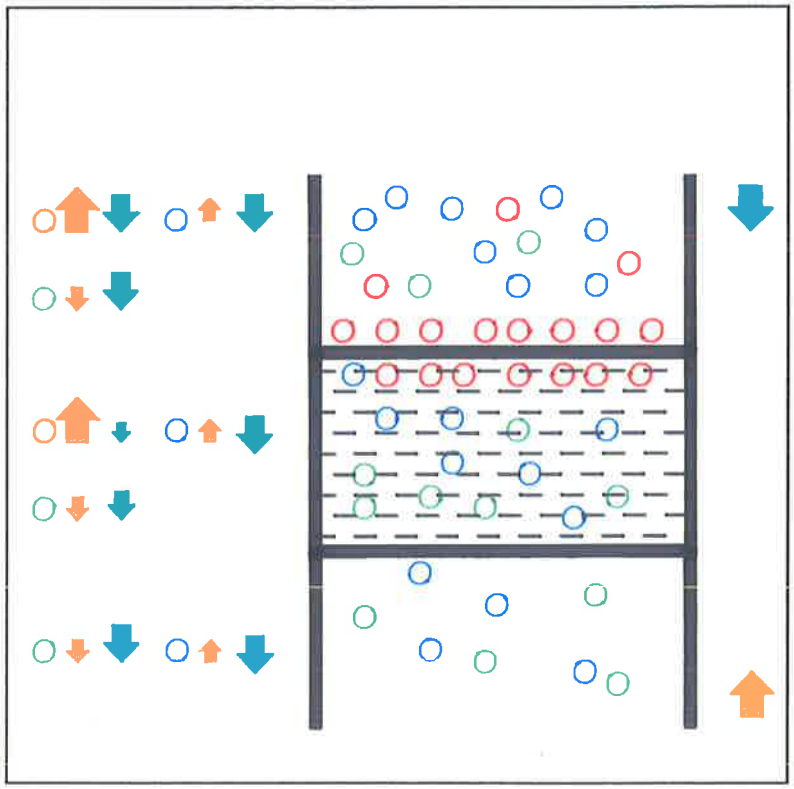

Figure 2.3 *THE SELECTION PROCESS by which the CEF filter works. Electrophoretic forces predominate on ions coloured red, driving them against the bulk fluid flow. Ions coloured blue are predominated by hydrodynamic forces carrying them along with the bulk fluid flow. Ions coloured green experience a superposition of electrophoretic and hydrodynamic forces and are very rapidly swept through the membrane.*

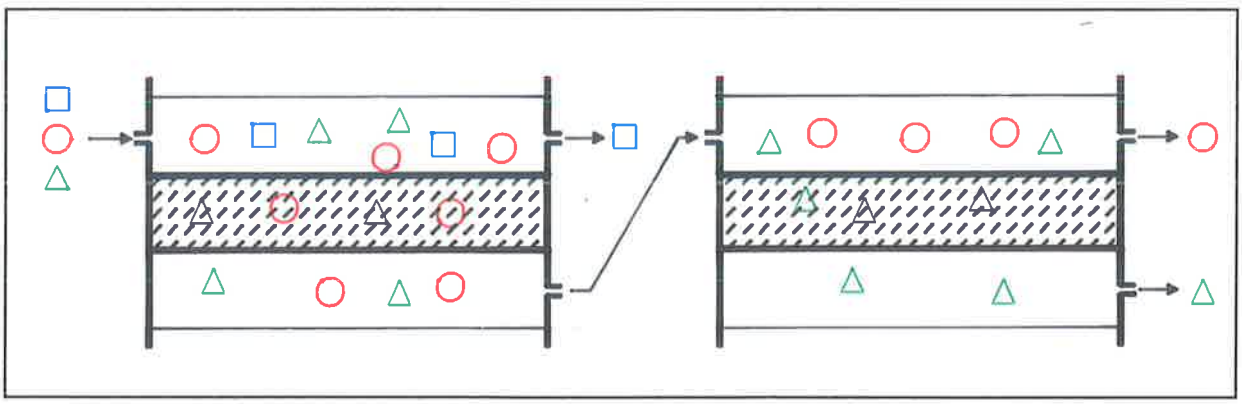

Figure 2.4 *PURIFICATION of a single ion from a complex mixture. The ions represented as circles are the desired product. The contaminating ions (squares and triangles) have higher and lower electrophoretic mobilities respectively. The first CEF unit is set to retain all ions with greater electrophoretic mobility then the desired ions. The filtrate from the first unit contains the desired product and all ions of lower electrophoretic mobility. The second CEF unit is set to trap only the most electrophoretically mobile ions. The final purity is a function of the ratio of filtrate to retentate streams in the second unit.*

Apparatus design

The minimum required components for the apparatus are:

Physical components.

A thick membrane with a tuneable electrophoretic permeability.

Vigorously mixed buffer chambers, above and below (inlet/outlet or retentate/eluent chambers) the thick membrane.

Electrodes, which may be isolated in electrode chambers and separated from the buffer chambers by low molecular weight membranes.

Plumbing and pumping components.

Feed pump to supply the bulk fluid flow through the apparatus.

Concentrate bleed pump to bleed the concentrate from the inlet buffer chamber.

Buffer chamber pumps and/or agitation system.

Electrode buffer recirculation system to maintain the ion balance between the electrodes and therefore permit continuous operation.

Feedback control systems.

Ef (electric field) stat. Electric field control system, whereby the voltage across the thick membrane (in particular the voltage gradient WITHIN the inlet side of the thick membrane) is actively maintained at a pre-determined set point.

pH stat. pH control system, whereby the pH of the inlet buffer chamber is actively maintained at a pre-determined set point.

In all, five major versions of the apparatus were constructed. Each version embodied significant technical improvements over the last, in addition to utilizing improved materials.

Figure 2.5 shows the arrangement of the components that comprise the 'core apparatus', while figure 2.6 shows the entire apparatus.

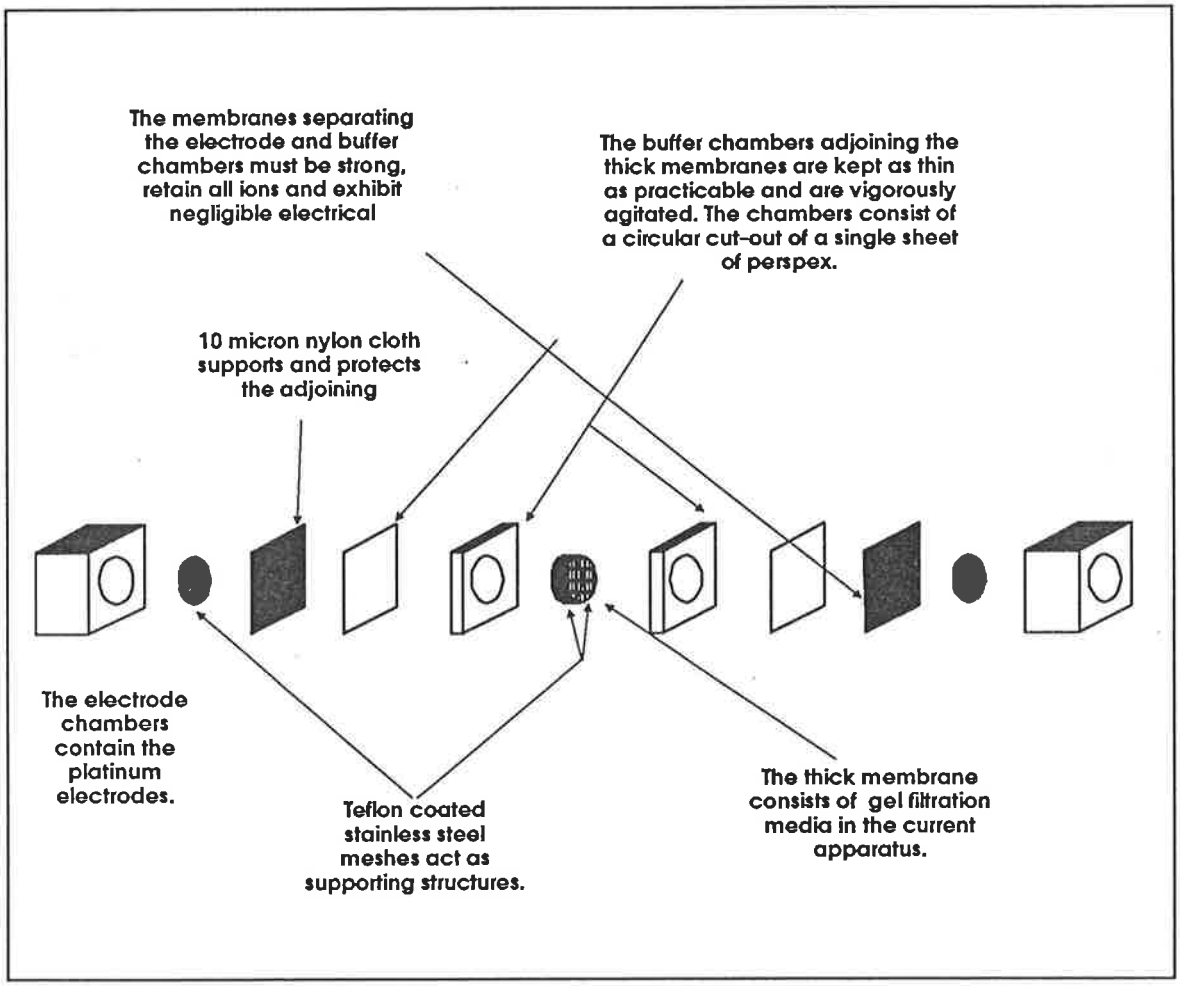

Figure 2.5 *EXPLODED SCHEMATIC of a CEF apparatus. The CEF apparatus consists of five segments: the thick membrane, which was constructed as a thin gel filtration bed in the current design; two buffer chambers, which are above and below (relative to the bulk fluid flow) the membrane and are vigorously agitated; and two electrode chambers, which are isolated from the adjacent buffer chambers by low molecular weight dialysis membranes.*

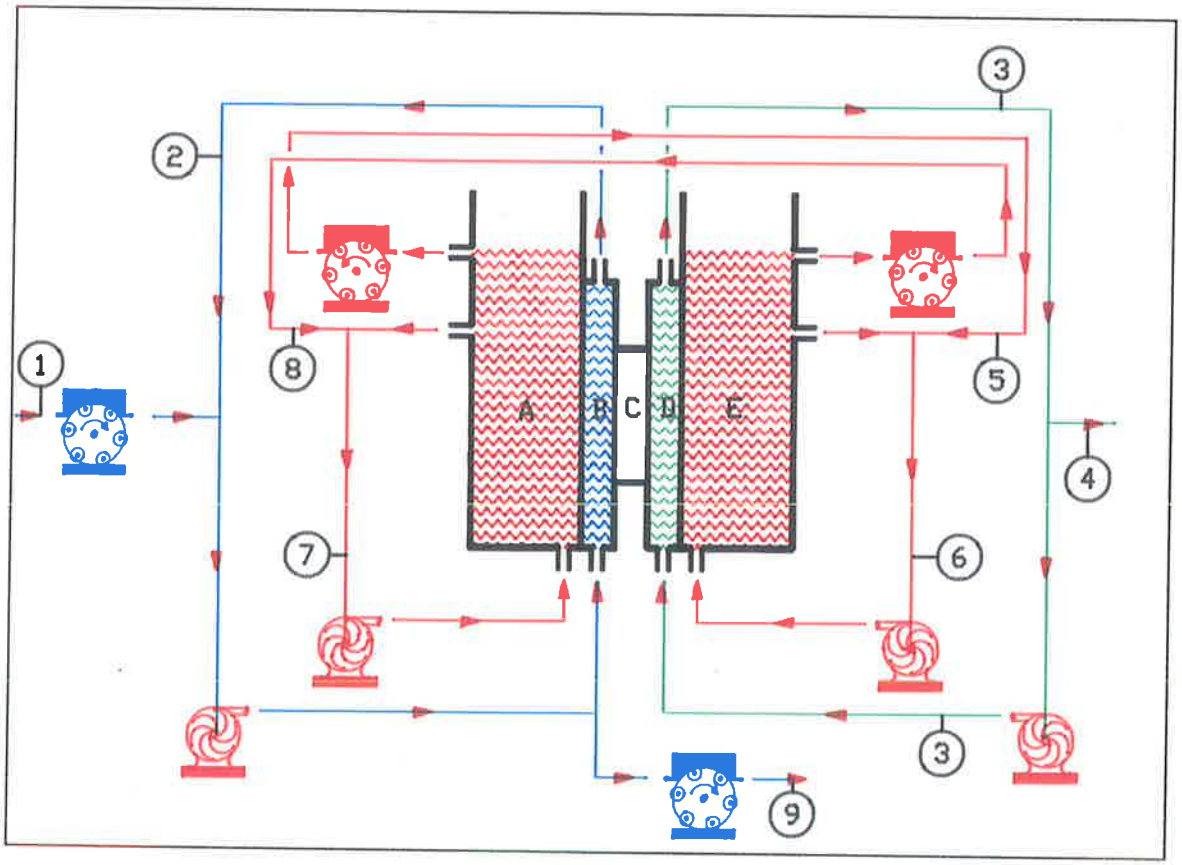

Figure 2.6 *SIMPLIFIED FLOW DIAGRAM of the CEF apparatus. The key to the streams is: 1, Feed stream containing ions to be separated; 2, Retentate recycle; 3, Eluent recycle; 4, Eluent bleed; 5, Anode exchange stream; 6, Cathode recycle; 7, Anode recycle; 8, Cathode exchange; 9 Retentate bleed stream. The apparatus chambers are labelled as follows: A, Anode buffer; B, Retentate; C, Thick membrane; D, Eluent; E, Cathode buffer. The colours correspond to: red, feed and retentate streams; blue, eluent (filtrate); green, buffers. The flow in the eluent stream equals the feed - retentate bleed. Any ion isolated from the retentate stream can only be purified by a factor equal to or less than the ratio of the feed and retentate stream flows. There is no theoretical limit to the possible purification factor of an ion isolated in the eluent stream.*

Design constraints

Membrane materials for isolating electrode chambers.

It proved quite difficult to find low molecular weight cut-off membranes which did not exhibit significant electrical resistance under operational conditions. Of the many membranes tested, the most suitable membrane found was a Spectra/por 3 cellulose dialysis membrane with a rated molecular weight cutoff of 3500.

Support materials for the electrode membranes and gel bed (thick membrane).

A combination of teflon coated 304 stainless steel mesh and 10u warp nylon mesh proved most suitable. The stainless steel mesh provided the required structural strength while the nylon mesh distributed the stresses and protected the membranes from damage against the mesh.

Agitation of the buffer chambers.

This was achieved using external pumps to generate a cross flow over the surface of the thick membrane. The ratio of cross flow to net flow through the apparatus was more than 100 (ie cross flow of 2 l/min to net flow of 20 ml/min). Wiers were utilized to maintain an even cross flow over the entire cross section.

Recirculation of electrode buffers.

This was achieved by a pair of peristaltic pumps which also provided electrical isolation between the electrode chambers. The electrode chambers were open to allow escape of evolved gases. To allow for non-equal pump rates, the peristaltic pumps withdrew fluid near the top of the electrode chambers. Therefore, if one of the pumps ran slightly fast it would lower the liquid level in its electrode chamber until it ran dry, and would not overfill the other electrode chamber.

Minimisation of wasted electrical energy.

Wasted power is generated across potential drops other than in the thick membrane. The electrical potential drop across the electrode membranes, and the major potential drop associated with the boundary layer surrounding the electrodes themselves, must be reduced. A suitable solution was turbulent flow around the electrodes, provided by centripetal recirculation pumps for each

electrode chamber. In addition to these measures, the total path length between the electrodes was kept to an absolute minimum to maximize the proportion of the total applied potential that appeared across the thick membrane.

Control of the electric field within the thick membrane.

One of the major factors determining the selectivity is the electric field WITHIN the THICK MEMBRANE. Accurate measurement and control of the potential gradient is therefore essential. To achieve this, small platinum electrodes were inserted through the walls of the apparatus, a short distance into the thick membrane. The external voltage was varied manually to maintain a constant voltage gradient within the inlet side of the thick membrane. Although not ready in time, two constant ΔV feedback power supplies were made. These power supplies were designed to vary the external voltage by maintaining a constant potential drop (NOT absolute voltages) across a pair of electrodes within the total current path.

CEF : The apparatus.

Materials and Methods

All HPLC traces were generated on a gradient system: Kortec K25 pumps, Kortec gradient controller, Rheodyne 7215 injector with 500µl injection loop, Kortec K95 UV/VIS absorbance detector, Brownlee 4.6mm id x 3cm length C4 Aquapore Guard cartridge, and Servigour chart recorder. Alternately, a Varian LC5000 Gradient HPLC system, with Vista 4000 control/analysis station was used. Gradient elution was performed at room temperature (25deg C), at a flow rate of 1ml/min in a gradient of acetonitrile in 0.1% Trifluroacetic acid. Acetonitrile was HPLC grade from Waters Associates. Trifluroacetic acid AR from Tokyo Kasei. Water was purified from Millipore Milli Q water system with organic removal and 0.22µ filter. All solutions and samples were filtered, on the day of use, through Millipore 0.22µ filters. Bovine serum albumin and haemoglobin were AR grade from Sigma. All pH measurements were made at 25deg C with an Activon pH meter equipped with an Activon ROS401 protein resistant probe. Solution conductivities were measured at 15deg C with a Radio Spares WD332 conductance meter.

Constant current and voltage power supplies used were custom made in the Biochemistry Department. Constant Delta V feedback power supplies were constructed in the Electrical Engineering Department. Materials used in construction of CEF apparatus were: perspex for all major structural elements; teflon coated 304 stainless steel mesh and 10u warp nylon mesh for membrane supports; 304 stainless steel mesh for both anode and cathode; Spectra/por 3 dialysis membrane for electrode membranes; Nikkiso-seven CP-08G centrifugal pumps for cross flow recirculation; Gilson Minipulse 6 channel peristaltic pump for electrode buffer cross-circulation; and Chempulse Electronic Solenoid Pump for retentate feed.

Results

Initial investigations were carried out using Bovine Haemoglobin only. Haemoglobin was chosen because it was available in large quantities and allowed for direct visualization of the action of the CEF apparatus.

The first objective met was to demonstrate that with increasing potential the thick membrane became impermeable to the passage of the Haemoglobin. The CEF apparatus was equilibrated with a solution of 2.5g/l haemoglobin, in 5 mm Tris acetate buffer (pH 9.4), without any applied electric field. When the concentration of haemoglobin emerging from the apparatus was the same as the feed solution the electric field was applied. At pH 9.4 haemoglobin carries a net negative charge. Therefore the electric field was oriented so that haemoglobin was attracted up-stream, (toward the positive anode) against the net fluid flow. When a suitable potential was applied, the haemoglobin was prevented from penetrating further than the top millimetre of the thick membrane. Selective permeability was a product of interactions WITHIN the up-stream portion of the thick membrane.

The voltage drop, associated with the formation of an impermeable equilibrium band of haemoglobin, was measured across short platinum electrodes inserted into the thick membrane at intervals across its thickness. Contrary to expectations, as the concentration of conducting species increased (haemoglobin band and associated counter ions), the voltage across the trapped band rose dramatically. The voltage rise was proportional to the concentration of retained haemoglobin (and haemoglobin band in the top of the thick membrane). Fifteen

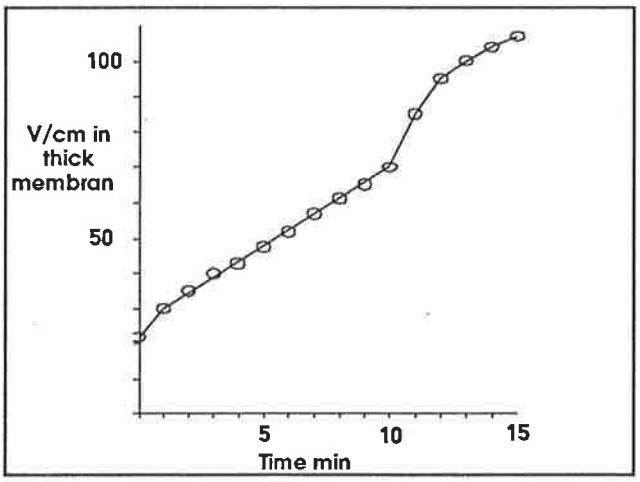

Figure 3-1. *VOLTAGE GRADIENT rise within the thick membrane upon establishment of an impermeable dynamic equilibrium. The apparatus was started with no applied voltage. When the apparatus was in equilibrium with respect to the flow, the voltage was applied (160V total). Within 15 min the Hb in the feed stream was being fully retained and the voltage gradient within the thick membrane had risen dramatically.*

minutes after application of the electric field the potential drop across the thick membrane had risen from 16% to 73% of the total applied voltage (of 150V). Figure 3.1 shows the rise in measured voltage as a function of time after application of the external voltage.

Initial separations trials, using a solution of 2.5g/l Hb and 2.5g/l BSA, were successful, although problems were experienced with precipitation of the retained Hb at very high concentrations. To avoid precipitation, feed concentrations of 0.25g/l were used for all further tests. Before application of the electric field, the apparatus was run until the outlet stream reached equilibrium as monitored by HPLC. The apparatus employed have significant dead volumes associated with each chamber, due to the plumbing involved with the recirculation pumps. Therefore 60 minutes or more elapsed, after applying the power, until complete separation of the Hb and BSA was observed. Figure 3.2 shows the separation in an apparatus of 28cm2 cross section at a flow of

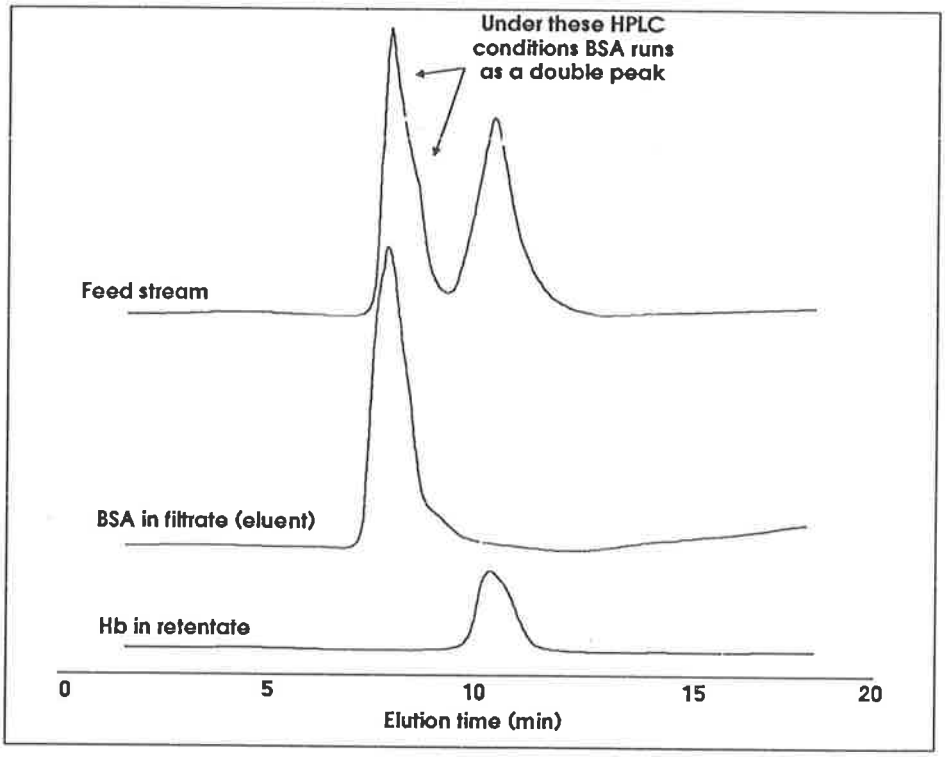

Figure 3.2 *The SEPARATION of BSA and Hb is shown. The upper HPLC trace shows the Hb and BSA in the feed stream. The lower two traces show that the Hb is being completely retained in the retentate while the BSA is passing through in the filtrate (eluent). The retentate and filtrate samples were taken at 4 hours (one hour after the apparatus had reached a steady state). The HPLC conditions were: Buffer A, water + 0.01% TFA; Buffer B, Acetonitrile + 0.05% TFA; Column Brownlee 4.6mm x 30mm RP-300 C8 cartridge; Flow 1ml/min; Temp 25 C. Gradient, linear segments between: 0 min, 0%B; 1 min, 30%B; 15 min 50%B. The retentate (Hb) was loaded at 5% concentration compared with the feed and filtrate streams.*

15ml/min (0.48cm/min); which is equivalent to a protein throughput of 0.45g/hour (27mg/cm2/hour).

Theory of operation of the CEF apparatus predicts a linear relationship between the bulk fluid velocity through the thick membrane, and the electric field strength required to retain an ion. In addition to the relatively long lag phase upon application of the electric field, a transient disruption in the field strength, within the thick membrane, was observed each time the external voltage was increased. Despite these interferences it was possible to determine flow velocity - electric field relationships for the retention of Hb and BSA and these are shown in figure 3.3.

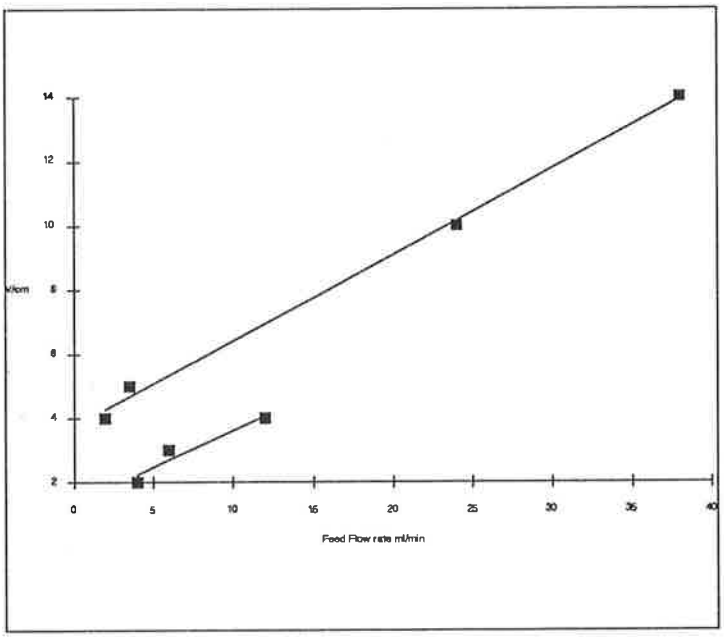

Figure 3.3 *The MINIMUM VOLTAGE GRADIENT in the thick membrane to retain BSA (blue) and Hb (red) for increasing feed flow rates. Over the range shown the potential gradient required to just retain an ion is linearly related to the feed flow rate. For the same flow rate Hb is more easily retained (requires a lower voltage) than BSA. Thus a voltage gradient and flow rate can be selected which will retain Hb but allow BSA to pass.*

Figure 3.4 shows the increase in the retained BSA concentration and concomitant decrease in eluting BSA after application of a blocking voltage.

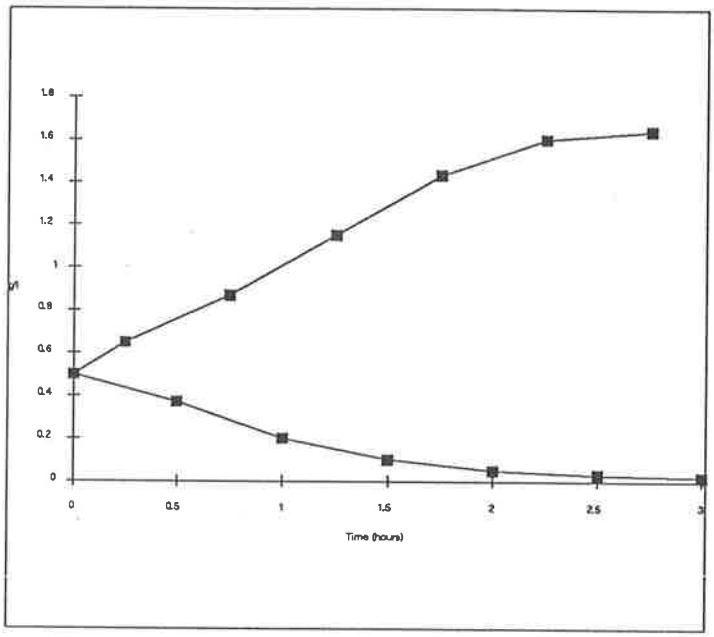

Figure 3.4 *THE RETENTATE (blue) CONCENTRATION RISES as the BSA is retained. Before the voltage was applied the apparatus was equilibrated with the flow (the concentration in the filtrate (red) stream equalled the feed). At time 0 the voltage was applied (and held constant). Steady state was reached after three hours in this case. This experiment used BSA only in 5mm Tris Acetate as the feed.*

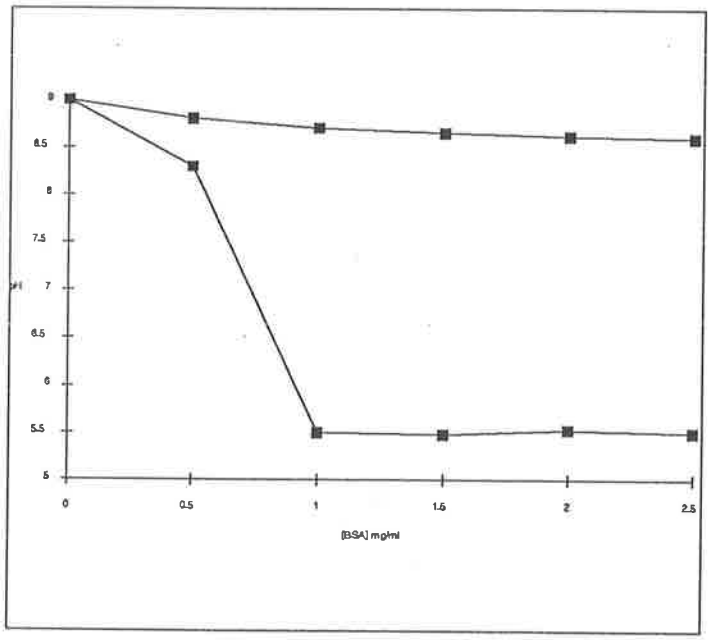

Figure 3.5 *pH FLUCTUATIONS in the retentate stream result from unstable operation when the external voltage gradient is held constant. Under this condition the operation of the CEF unit modifies the voltage gradient in the thick membrane and the buffer ion pumping effects alter correspondingly. The pH of the retentate at varying BSA (red) concentrations is shown. The small variation of the pH of the same BSA concentrations in the buffer used (5 mm tris Acetate) is shown in blue. This experiment used BSA only in 5mm Tris Acetate as the feed.*

To investigate the possibility of pH fluctuations within the apparatus, the feed solution (0.25g/l BSA & Hb in 5mm Tris Acetate pH 9.0) was doped with the pH indicator phenolphthalein. After equilibration, upon application or increment of the electric field, large transient fluctuations in pH throughout the apparatus were observed. An alkaline front was observed to progress from the inlet buffer chamber (anodic side of apparatus) through the thick membrane to the outlet buffer

chamber. An acidic front then traversed in the opposite direction, leaving the inlet, outlet and thick membrane acidic, and the electrode chambers (which are recirculated to each other) alkaline. The electric field within the thick membrane fluctuated dramatically as the pH varied. Phenolphthalein was removed for quantitative studies of the pH and electric field fluctuations and dependencies.

In tests using BSA alone the drop in retentate pH upon trapping of BSA was compared with the affect of varying BSA concentrations in the Tris Acetate buffer alone. As shown in figure 3.5 the retentate pH varies far more than that which can be accounted for by the influence of increasing BSA concentration alone.

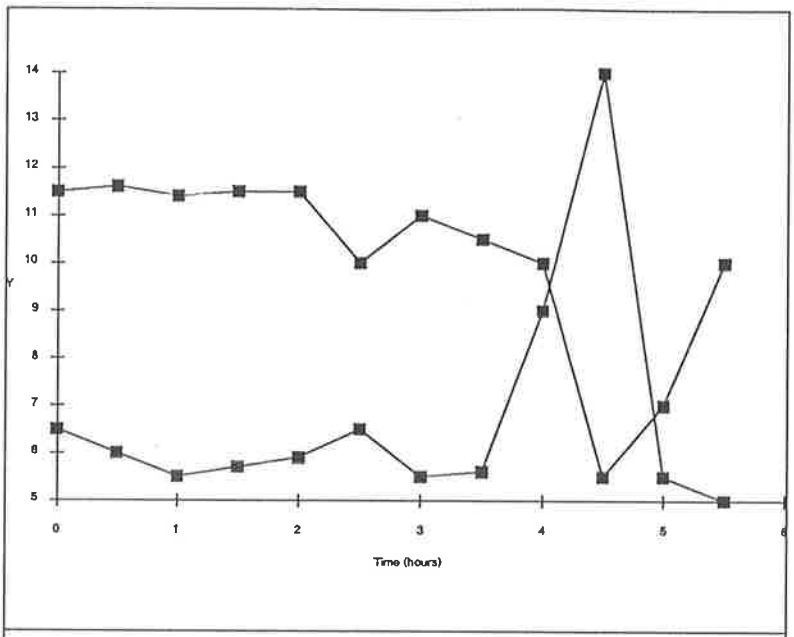

Figure 3.6 *RETENTATE pH (red) AND POTENTIAL GRADIENT (blue) in the thick membrane are linked to each other. Positive feedback mechanisms result in large fluctuations in both when no attempt is made to hold the potential gradient within the thick membrane constant. The Y axis represents pH and 6 x v/cm within the thick membrane. This experiment used BSA only in 5mm Tris Acetate as the feed.*

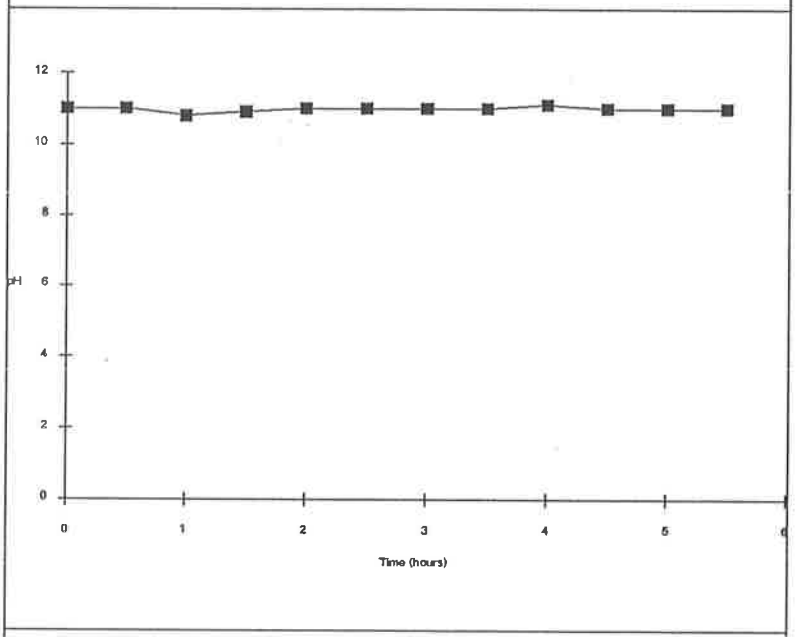

Figure 3.7 *STABLE OPERATION results when the potential gradient within the thick membrane is held constant. The pH of the retentate over a 4 hour period is shown. The external potential was varied manually over this period to maintain a constant potential gradient in the thick membrane. This experiment used BSA only in 5mm Tris Acetate as the feed.*

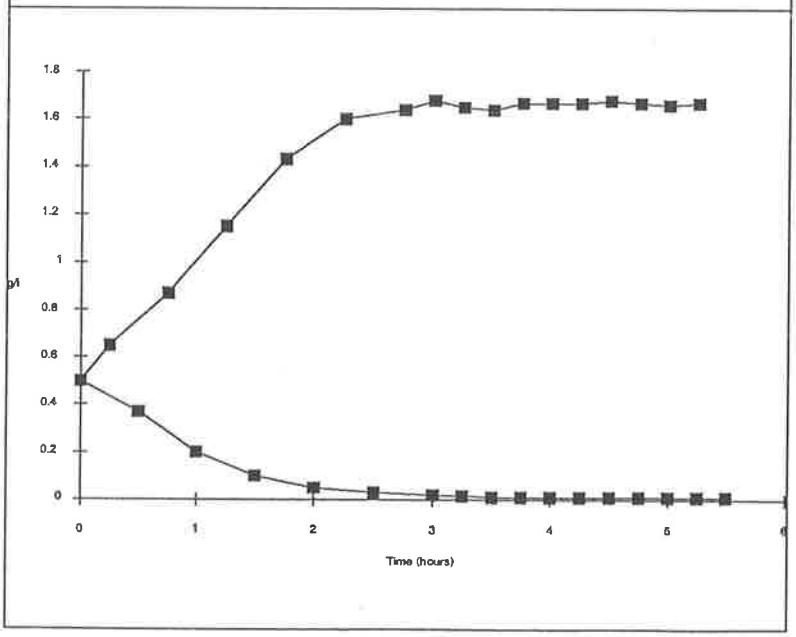

Figure 3.8 *THE CEF FILTER reached equilibrium after three hours running. This figure shows that the stable condition continued for up to 6 hours when the experiment was terminated. The stable operation required feedback control of the external voltage to keep the potential gradient in the thick membrane constant. Using BSA only the concentration in the retentate (red) and feed (blue) streams is shown.*

To examine the relationship of electric field strength within the thick membrane and the retentate pH, measurements were taken for a six hour period following application of a blocking voltage. The applied external voltage was held constant throughout all of these experiments. As shown in figure 3.6 the field strength and pH exhibit a mirror symmetry. To determine causality, the external voltage applied to the electrodes was manually varied to maintain a constant field strength within the thick membrane. Apart from a minor pH transient in the first hour, operation was stable, although the retentate pH stabilized a whole pH unit lower than the feed solution, this is shown in figure 3.7. In this experiment the BSA concentrations in the output streams had stabilised after 3 hours. This is shown in figure 3.8.

Although attempts to separate BSA and Hb in an apparatus with a thick membrane consisting of glass beads alone proved partially successful this was not pursued.

Discussion

The principal and practice of electrophoretic filtering has been demonstrated. Retention, concentration and separation of protein samples have been demonstrated, and although the overall performance was predicted, several operating parameters indicate a more complex interaction of forces than initially envisioned.

Certainly the permeability of a thick membrane for a given protein at constant buffer pH and fluid velocity can be uniquely determined by the applied counteracting electric field. The real challenge lies in technical aspects of predicting, measuring and maintaining predetermined pH and electric field strength within the inlet side of the thick membrane. The model for the thick membrane used in the described apparatus is a thin layer of gel filtration media. In such a gel it is known that the net fluid velocity within the gel beads is effectively zero. Also the penetration and residence time within the gel beads is inversely proportional to Stokes radius. It is also known that dispersion at right angles to the hydrodynamic gradient (ie pressure drop and bulk fluid flow) is minimal in gel beds packed with small particles. Although not experimentally determined, it is expected that uncharged gel beads do not significantly distort the electric field lines and therefore electromotive force acting on entrapped ions. Under such conditions even ions with the same charge to mass ratio but differing hydrodynamic radii can be separated.

It is expected that the apparatus described would perform adequately with a thick membrane which offered no selective modification of electric or hydrodynamic gradients experienced by entrapped ions. One such test performed with glass beads alone in the thick membrane yielded some separation but was hampered by the large size (0.5mm) beads used. Such a membrane would serve only as a region of laminar flow in which solution electrophoretic mobility would be the only criteria on which ions could be separated. This last example provides the clearest picture of the basic underlying principals and requirements of the CEF technique.

First, a thick membrane is required. Size exclusion filtering, where permeability through a membrane is determined by size alone, is best implemented with a thin membrane, with selection occurring at the surface.

Opposed to this CEF requires that an ion ENTER the membrane, which provides a characteristic environment (ie. laminar flow), where selectivity is determined by the interaction of electric and hydrodynamic gradients. Thus in CEF the membrane provides an environment in which the selection process takes place, and while the membrane may modify the selection process it is not the major determinant.

Second, although the selection process occurs within a matrix (thick membrane), collection of retained samples from within the matrix is not necessary. Removal of separated species from a matrix is the demise of half of all the possible electrophoretic purification methods. The second half of electrophoretic methods are of the 'free flow' category, their demise is turbulent flow and mixing.

The CEF technique suffers from no such drawbacks. The CEF method relies upon diffusive and active processes to expel retained ions from the high pressure (inlet) side of the membrane. Therefore high resolution separations are performed in a laminar flow region, within a matrix, and yet do not suffer from problems of sample recovery. The more finely tuned the CEF membrane to 'just' reject an ion, the further the ion will penetrate the membrane before being finally rejected. Also, as the throughput increases (increased flow rate accompanied by increasing electric field strength) the degree of penetration before complete rejection will increase. This is in a manner completely analogous to the criteria for good efficiency in gel chromatography; efficiency increases with decreasing flow and decreasing bead size.

The generation of heat and wasted power consumption are the nemesis of those who try to scale up electrophoretic processes. There are obvious ways to reduce power consumption:

minimizing unnecessary voltage drops (path length) outside the crucial separating component; and

reducing power loss to conduction of current by 'useless' ions such as buffer species.

There are practical limits to which path length and buffer concentration can be reduced. Ultimately, inherent efficiency and heat removal capacities of the core process are the determining factors. It is in this area where the CEF process has proven to be particularly successful. In direct contradiction to expectations, as the filter traps ions efficiency increases. Before experimenting, it was expected that retained ions would increase the conductivity within the thick membrane, requiring higher external applied voltages (and therefore current and power) to maintain a constant electric field strength within the membrane. Exactly the opposite was observed to occur. As retained ions increased

in concentration the potential gradient within the thick membrane increased! Therefore to maintain a constant electric field strength within the thick membrane the total external voltage must be reduced. Consequently a higher percentage of power goes directly into the separation zone within the thick membrane. This could explain the unstability observed when applying a constant external voltage. The increase of retained ions increases the electric field strength within the thick membrane which in turn increases the retention of ions. The same situation would apply in reverse: ie. should the electric field strength within the thick membrane start to fall (while some ion is being retained) the retention of ions will decrease and further reduce the electric field strength. This is a classical positive feedback loop. Positive feedback loops are characterized by extreme and unpredictable oscillations. As shown earlier the introduction of sufficient negative feedback into the loop (to stabilize the electric field strength within the thick membrane) stabilizes overall operation. A plausible explanation of the physical causes for such a surprising result are tied in with, and supported by, the observation of the selective ion pumping effect observed. The ion pumping effect manifested itself as a rise in combined electrode buffer pH (both cathodic and anodic electrode buffers are inter-recirculated) accompanied by a drop in retentate and eluent pH. The drop in retentate and eluent pH are simply explained. The elution of acidic buffer ion (Acetate) from the apparatus is retarded in the presence of the electric field, while the elution of the basic buffer ion (Tris) is facilitated. Therefore the pH, within the chambers experiencing a net fluid flow, is decreased. Due to simple charge attraction, the increased Acetate concentration attracts an increased concentration of Tris ions to the other side of the electrode buffer membranes (these low molecular weight (3500) membranes have significant boundary layers and ion and potential gradients across them). Conduction within the apparatus is predominated by the excess of anions, this includes the anions which are retained. As the retained ions increase in concentration they become the predominant species within and immediately above the thick membrane, excluding by charge repulsion other anions (ie. acetate). By the very action of the CEF apparatus, these ions exhibit no net migration through the thick membrane, therefore blocking the current and passage of other anions.

The initial results described here are sufficient that an apparatus capable of 10's to 100's of grams per hour throughput has been built. Also constant delta V feedback power supplies have been designed and constructed which will vary the electrode voltage to maintain a set potential drop across the thick membrane. To the best of the author's knowledge, the technique of CEF is the most efficient and highest resolution electrophoresis system which is practically scaleable.

Spectral Enhancement

Spectroscopy is amongst the more venerable of the analytical techniques that have been allied to the relatively new science of protein chemistry. The following chapters will introduce, describe, develop, analyse and discuss some methods of spectroscopy as applied to protein analysis. The techniques described permit the reliable extraction of more information than has been previously available from 'normal or derivative spectroscopy', and involves judicious employment of instrumental, data collection, algorithmic and computational procedures to this end.

I would like to dispel any misconceptions at the outset that the title "Spectral Enhancement" may conjure to mind. Information content is similar to Entropy: In a closed system order/information cannot increase. The methods to be described merely process the raw spectral data into a form where the human eye and brain can easily identify the information contained within the original data set. On the contrary, ALL of the methods described pay the price for any data manipulation by suffering from some degree of signal-to-noise degradation (entropy increase).

The methods described stem from three hypotheses that may be, and will be, subjected to rigourous testing. The thesis is structured around these hypotheses.

After a general introductory chapter, the three hypotheses and the methods stemming from them will be covered in separate chapters. In the final chapter I will discuss the work and its implications.

INTRODUCTION

The ultraviolet absorption spectra of proteins provides one of the easiest and most widely used sources of information obtainable on proteins. In their pure form all proteins have a characteristic Absorptivity at a given wavelength. Measurement of the optical Absorption at given wavelengths provides the easiest means for the determination of protein concentrations. As proteins cannot practically be obtained pure of all other molecular species (ie. bound water), it is not possible to accurately determine protein concentrations simply by dissolving a known weight of 'pure' protein in a known volume of liquid. Often if a protein is dried down too much, particularly in the absence of some salts, then the protein will undergo irreversible aggregation and conformational changes which render it insoluble. For this reason alone, accurate quantitation of proteins is best carried out by solution spectroscopy in the ultraviolet wavelength range. In fact, methods for determining the Molar Absorptivity (ε) of proteins entirely by solution procedures have been shown to be superior to other methods[1]

While the peptide bond itself absorbs light significantly below 210nm, there are too many other possible contaminants that absorb in this region, making solution spectroscopy impractical at these short wavelengths. For example, oxygen has a significant absorbance below 210nm and also many of the salts, buffers and solutions used in protein work absorb in this region. In the region above 210nm only three of the twenty normal amino acids found in proteins have significant absorbances. These are the aromatic amino acids; Phenylalanine (Phe), tyrosine (Tyr), and tryptophan (Trp). However, the Molar absorptivities in the 240 - 300nm range of these amino acids vary considerably. At 248nm the absorptivity of Phe peaks at $\varepsilon = 110.6$[2] determined for N-acetyl Phenylalanine which is representative of Phe residues incorporated into proteins[3]. The ε of tyrosine is quite sensitive to solvent effects[4] but can be accurately determined from the ε of a representative protein which has no tryptophan to interfere with the tyrosine absorbance (Phe does not significantly interfere[5]). Tyrosine incorporated into proteins has a peak $\varepsilon = 1330$ at 276nm[6]. The ε of tryptophan is also moderately sensitive to solvent effects but has been accurately determined in 6M GuHCl

1 Thomas A Bewley. Analytical Biochemistry 123, 55-65(1982).

2 Mihalyi,E.J. Chem.Eng.Data 13, 179-182.(1968)

3 Rodney L.Levine,M.Marcia Federici, Biochemistry 21, 2600-2606.(1982)

4 Soli,N.J,&Herskovits,T.T,Anal.Biochem.54,370-378.(1973)

5 Rodney L.Levine,M.Marcia Federici, Biochemistry 21, 2600-2606.(1982)

6 Mihalyi,E.J. Chem.Eng.Data 13, 179-182.(1968)

solutions and is representative of tryptophan incorporated in proteins. The ε of N-acetyl tryptophan in 6M GuHCl peaks at 281nm, ε = 5620. The relative differences in the Molar Absorptivities of the three aromatic amino acids can be seen graphically in figure 4.1.

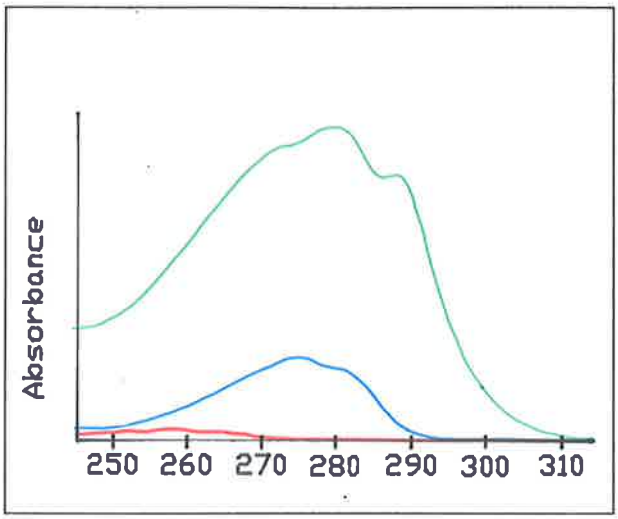

Figure 4.1 *THE RELATIVE ABSORPTIVITIES of the three aromatic amino acids are very different. Phenylalanine (red) has only one sixth the absorbance of tyrosine (blue), which has only one quarter the absorbance of tryptophan (green) at the same concentrations.*

Clearly, given roughly equal molar quantities of the three aromatic amino acids, tryptophan will dominate the spectrum between 240-310nm. In addition to being the bulkiest and most hydrophobic amino acid, tryptophan is the rarest of the normal amino acids with tyrosine and phenylalanine occurring three times as frequently[1]. Even so, in general the spectra of many proteins are dominated by tryptophan with a significant contribution from tyrosine and very little contribution from phenylalanine. This gives rise to the "average" protein having a maximum Molar Absorptivity in the region of 280nm.

In addition to absorption, light scattering has a significant contribution to the measured apparent absorption of proteins. The larger a particle, the more it will scatter light. This light scattering is a function of the inverse ratio of the wavelength of light to the particle (molecular weight) size and is quite significant at 280 nm for proteins of 1000Mw. The light scattering contribution to any protein spectrum can be determined by fitting a straight line on a log-log scale to the apparent absorbance of the protein above 320nm. In this region the only significant contribution to the apparent absorbance is light scattering. The light scattering contribution can then be extrapolated back into the wavelength region of interest (140-300nm usually)[2].

1 Handbook of Biochem and Mol Biol,3rd edn.Proteins, Vol 3.(G.D Fasman, ed.)C.R.C.Press, Clevland, Ohio.(1976)

2 Bewley,T.A,Anal.Biochem.106,49-54.(1980)

Absorptivities given for proteins in the 210-310nm range are therefore a summation of contributions from the absorbances of aromatic amino acids and of light scattering. Figure 4.2 demonstrates the significant contribution that light scattering makes to the spectrum of PGH.

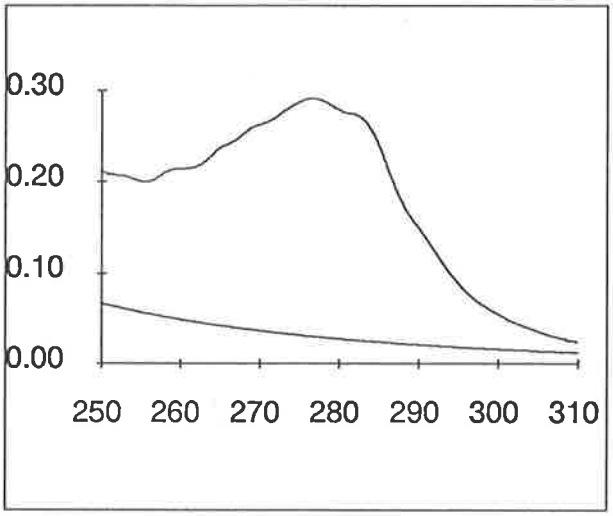

Figure 4.2 *LIGHT SCATTERING is significant for most proteins. In this typical spectra of PGH, light scattering contributes10% to the absorbance at 280nm. The light scattering is determined from a best fit on a log-log scale of the apparent absorbance between 320-350nm.*

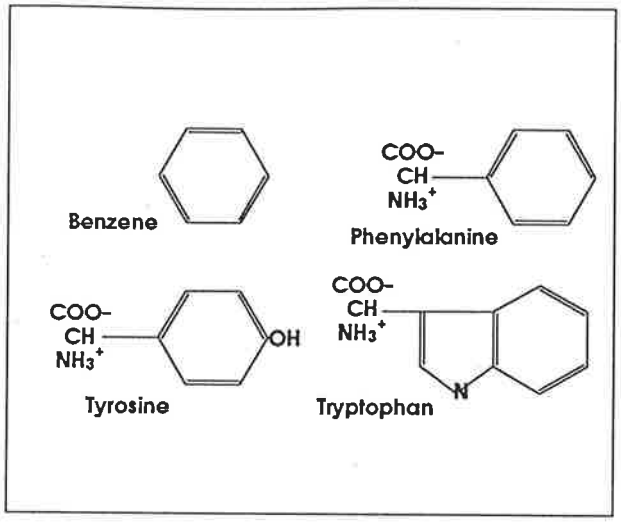

Figure 4.3 *THE AROMATIC AMINO ACIDS share the common six member ring and some spectral characteristics with Benzene.*

The absorbance of the three aromatic amino acids in proteins is based on their shared aromatic ring structures (figure 4.3) and is therefore similar. Phenylalanine exhibits a spectrum not vastly different from benzene, which corresponds to the side group of phenylalanine. The additional components in the structure of tyrosine and tryptophan have a net effect (apart from other structural differences) of donating electrons into the ring structure. In these cases this has the effect of narrowing the energy between the excited and ground states that determine the spectra in this region. The net effect is a general red shift of their spectra compared with phenylalanine. It is also because of these electron donating groups that the spectral properties of tyrosine and tryptophan are so solvent sensitive (tryptophan only to a minor degree). The more electron donating (proton withdrawing; basic) the environment, the greater the spectral changes. In the case of tyrosine, where the OH group can be ionised at moderate pH's(9-11), the spectrum exhibits a dramatic alteration with the ionised species having a spectrum red shifted by 10nm, as shown in figure 4.4.

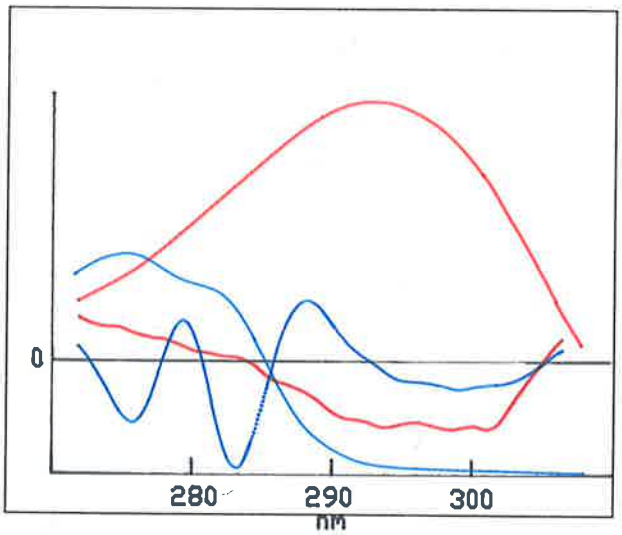

Figure 4.4 *ZERO (solid) AND SECOND DERIVATIVE (dashed) SPECTRA OF TYROSINE. At pH 8.0 (blue) tyrosine is not charged. At ph 12.8 (red) tyrosine is fully ionised and the spectra dramatically red shifted.*

Tryptophan exhibits a similar drastic shift in one of its minor absorption bands in the presence of an electron withdrawing (acidic) group. In the presence of a carboxylate ion in the hydrophobic interior of a

protein, the L^1a band of tryptophan undergoes a massive 12nm red shift[1].

Clearly, the spectrum of a given protein depends upon the conformation and environment of the protein. This creates both problems and opportunities. The problems arise when we want to quantitate the protein irrespective of conformational and environmental changes over which we may not always have complete control. Under these circumstances probable spectral changes add error and uncertainty to quantity measures if the exact effects of environment and conformation are not known. In contrast, opportunities arise when we analyse and interpret the spectral changes and correlate them to changes in conformation and environment.

The literature in this area is full of examples of ingenious methods of both difference and derivative spectroscopies to aid in the accurate quantitation and conformational analysis of proteins.

It is worthwhile to review this work as it has been applied to the analysis of proteins in the Growth Hormone Super Family.

As an example of the use of difference spectroscopy used for accurate quantitation of proteins, there is Bewley's elegant technique for determining em's for proteins of known amino acid structure[2]. After first removing all conformational effects by enzymatic digestion, the difference spectrum of high and low pH titrations is used to quantitate the exact molar quantity of tyrosine present. At 287nm, where the difference is measured, phenylalanine does not contribute at all. Although the spectrum of tryptophan does alter slightly with varying pH, it exhibits a well defined isosbestic point at 287 and therefore does not interfere with the measurement. As noted earlier, this method is the most accurate reported to date for the determination of em's of proteins with the restriction that the protein in question contains at least one tyrosine and its amino acid composition is known.

As an example of the use of derivative spectroscopy for the determination of aromatic amino acids, I refer to the work of Levine and Federici[3]. They report on the successful application of multi-component analysis to the determination of the aromatic amino acid composition of

1 Bewley,T.A,Choh Hao, Li. Arch of Biochem & Biophys. Vol 233, No 1.219-277(1984)

2 Bewley,T.A, Anal Biochem. 106, 49-54(1980)

3 Rodney L.Levine, M Marcia Federici, Biochemistry 21, 2600-2606(1982)

proteins. In multi-component analysis, a computer follows an optimisation algorithm which seeks the best match between some combination of model spectra to the spectrum of the protein. To work successfully, the spectra of the model compounds must be significantly different. However this is not the case for the aromatic amino acids and the problem was overcome by using the second derivatives of the protein and model compounds. While their spectra appear similar in many ways, the second derivatives of the model compounds differ significantly as can be seen in figure 4.5.

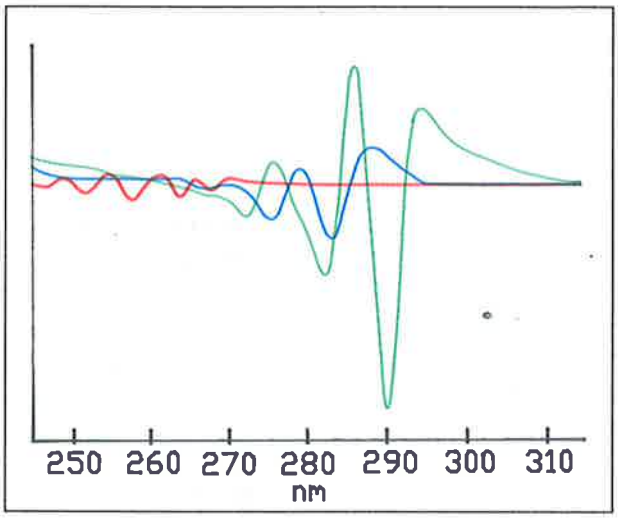

Figure 4.5 *SECOND DERIVATIVE SPECTRA of the three aromatic amino acids: 100uM each of the N-acetyl esters of phenylalanine (red), tyrosine (blue), and tryptophan (green).*

C h i r o Balestrieri *et al*[1] also use the second derivative spectra of denatured proteins to determine the composition of aromatic amino acids. They do this by quantitating the second derivative spectra in several regions where the derivatives of these amino acids do not strongly overlap. The use of second derivative fluorescence spectroscopy to quantitate tyrosine and tryptophan has also been reported[2] (phenylalanine does not exhibit any significant fluorescence).

Chiro Balestrieri was involved with the development of a very elegant procedure for the determination of tyrosine exposure (to the surrounding solvent) in proteins[3]. The essence of the work is based on the observation that while the tyrosine spectrum is heavily influenced by the hydrophobicity (and therefore exposure to polar solution) of its environment, the spectrum of tryptophan is relatively unaffected. Thus

1 Balestrerie.C, Colonna. G, Giovani. A, Irace. G, Servillo. L,.Eur. J. Biochem, 90 433-440(1978)

2 Garcia-Borron.J.C, Escribano.J, Jimenez.M, Ibora.J.L,. Analytical Biochem 125, 277-285(1982)

3 Ragone.R, Colonna.G, Balestreri.C, Servillo.L, Irace.G,. Biochemistry 23, 1871-1875(1984)

for proteins containing both tryptophan and tyrosine residues, the tryptophan second derivative serves as an internal reference. By examining the ratio of the major tryptophan and tyrosine peaks in the second derivative spectrum it is possible to calculate the exposure of the tyrosines to the surrounding solution.

More recently, Bewley has reported on the use of second derivative spectroscopy to demonstrate a hydrogen bonding between the single tryptophan of HGH and a carboxyl group buried inside the protein[1]. Careful examination of the derivative spectrum in the 300nm region revealed minor tryptophan transitions (higher vibrational levels) which can only be accounted for by tryptophan hydrogen bonding to a carboxyl group in a hydrophobic environment[2]. Bewley goes on to compare the spectra of HGH to HPL (Human Placental Lactogen) which have exactly the same structure with respect to the aromatic amino acids. Interestingly, HPL does not have its one tryptophan hydrogen bonded to a carboxyl group in its native conformation. These features are shown in figure4.6 taken from Bewley's paper. Bewley notes that there is a transitory hydrogen bond to tryptophan formed as the HPL is enzymatically digested. This study elegantly identifies not only the micro-enviroment inside the protein surrounding one particular residue but also that a very similar protein is slightly distorted with respect to the tryptophan environment in its native conformation, yet still retains the carboxyl group involved.

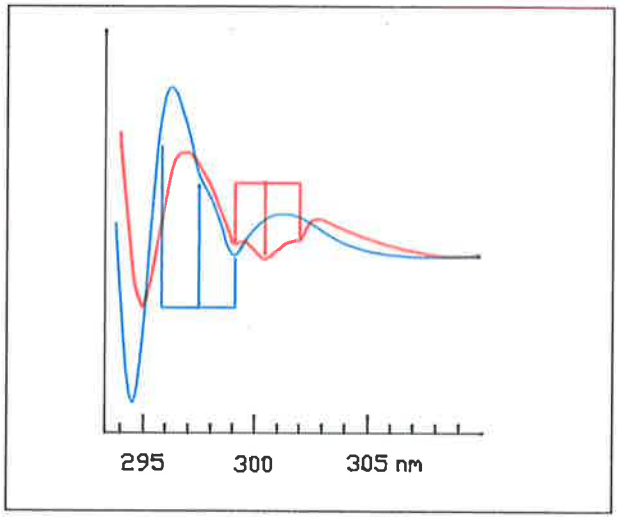

Figure 4.6 *SECOND DERIVATIVE spectra of HGH (red), and HPL (blue). The two sets of triple lines indicate the positions of the Trp-L1a bands. The red shift of these bands in HGH is due to the indole nitrogen of the Trp in HGH hydrogen bonding to a carboxyl group in the interior of the protein.*

1 Bewley.T.A, Cho Hao. L,. Arch of Biochem and Biophys. Vol 233, No 1. 219-227(1984)

2 Strickland.E.H, Billups.C, Kay.E,. Biochemistry 227, 618-625(1983)

This final example, more than the earlier examples, leads to the questions: How much information regarding structure of proteins can be obtained from their spectra?; and What is the best way, and limits, to extract information from the spectra.

Beyond the simple observation that more features are observable in the derivative spectrum (not just second derivative, but any derivative), previous authors have not addressed these questions. In 1988 when investigating the folding pathway of PGH (Porcine Growth Hormone) it became apparent that there was far more real information available in the spectrum than others had previously extracted. At that

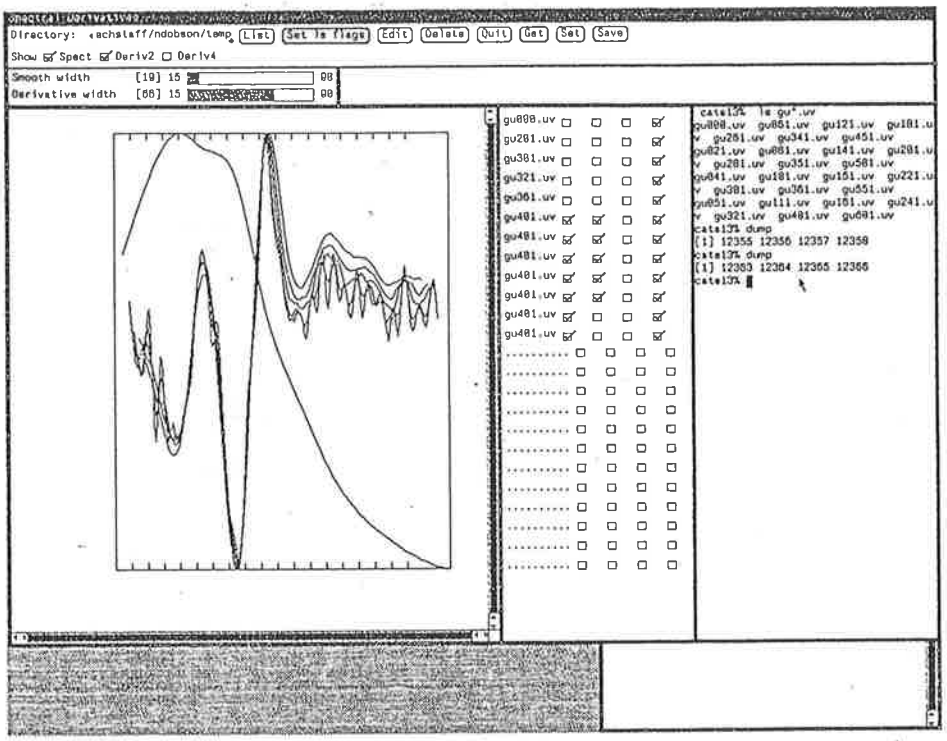

Figure 4.7 *SECOND DERIVATIVE SPECTRUM OF PGH at varying digital filter widths (1.0-3.5nm). Screen image from interactive spectral analysis software package developed by the author to run under SunWindows on Sun Workstations.*

stage I had just developed an interactive spectral analysis package to run on SUN workstations under SUN Windows. I had also just collected a series of very high resolution spectra of PGH in increasing Urea concentrations on a Cary 2400 spectrophotometer. The software package permitted very rapid comparison of the second derivatives of multiple spectra with varying smoothing and resolution. Upon analysis of the spectra two things became apparent immediately. 1. Although never stated, all previously published derivative spectra of proteins had used methods that resulted in generating a VERY smoothed derivative (effective smoothing widths between 2-7nm). 2. When the smoothing of the

derivative was reduced to below 2nm (0.5-2.0nm) the resulting 'noise' was not noise but instead reproducible features.

A representative screen dump is shown in figure4.7. In this particular session, resolution enhancement as effective smoothing width is reduced is demonstrated. As will be demonstrated in the subsequent chapters, the fine detail seen in the rightmost portion of the second derivative represents reproducible information.

It requires considerable instrumental and computational performance to permit the extraction of fine detail from protein spectra. As will be shown in the following chapters, it requires the highest spectral resolution from the best spectrophotometers available today, collecting spectra over extended times (over 3 hours for one spectra spanning 60nm) to yield data of sufficient quality to permit good high-resolution data extraction. In addition, many of the procedures require considerable amounts of raw computing power for the spectral enhancement procedures I will describe. Previous authors have employed very large amounts of signal smoothing, both instrumental (large band width, and low spectral resolution) and computationally (wide digital filter widths) to achieve reliable results. Many such efforts have also been limited by popular but low resolution instruments and the low power of readily available computers (mainframe, mini and personal). In some cases the instruments used are incapable of producing data of sufficient spectral resolution for subsequent high resolution enhancement. The more modern (and popular) diode array spectrophotometers are only capable of 1nm resolutions at best (normally only 2nm). Although these instruments have inherent design advantages with respect to signal-to-noise, the low spectral resolution precludes their use when high-resolution spectral enhancement is to be applied (where I will show that resolution of 0.1nm or better is desired).

In addition to the instrumental and computation power limitations, the application of many spectral enhancement techniques is plagued by poor computational application of even applicability. The spectral signal must be digitised before being processed by the computer. Only in recent times has the accuracy of the analogue to digital (A-D) converters risen to the point where they are capable of matching the maximum S/N ratio of the instrument's optics and analogue components. The best modern instruments are capable of S/N ratios of approximately 1,000,000:1 or better, which is close to 20 significant bits digital resolution. Unfortunately, many instruments capable of these S/N performances are fitted with A-D converters of lower resolution (typically 16 bits). This is because their designers could not see any improvement in the unprocessed signal with higher performance A-D converters. As I will show later (and is intuitively obvious) it is imperative

to collect the optical signal with as little distortion as possible. This requires A-D converters capable of representing the 'noise floor' of the instrument under optimum conditions. This is particularly true of most modern instruments that use chopper stabilised analogue and optical systems to rapidly output a series of values (most modern research grade dual beam spectrophotometers have a chopper frequency of 10-100Hz). When long signal averaging times are employed, the advantage of averaging successive data points may be limited by the resolution of the A-D converter, which is perfectly adequate for single (or small numbers of averaged) data points. For instance: If an instrument has a S/N ratio of 1,000,000:1 ($\sim 2^{19}$) and is fitted with a 24 bit A-D converter, then it will have 5 bits of 'excess' resolution relative to a single point reading. Such an instrument would be suitable for allowing averaging of up to 32 (2^5 = 0.32 s at 100Hz data rate) data samples. Beyond that, additional averaging is limited by the resolution of the A-D converter and the S/N will not improve for longer averaging times.

In addition to all of these problems are computational constraints. As the spacing of the spectral data decreases (increasing spectral resolution) the number of points within a set window size (set nm width filter window) increases. Therefore performing derivative and other analysis on higher resolution data requires increasing digital filter widths. Many authors have employed integer sets of weights to perform various spectral analysis functions. Working entirely with integers speeds up computing times. The problem is that as the digital filter widths increase so do the integers and the normalisers. This is best seen in the tables for least squares best fit to various polynomials and their derivatives first published by Savitkzy and Golay[1]. While an overflow (over range) calculation will flag an error in computers an underflow (a division of a non-zero value reduces to 0; ie. the result is below the smallest resolution of the number format employed) calculation does not flag an error. This can unknowingly lead to significant errors and limit the accuracy of such implementations. For many of the procedures described in the following chapters, it is necessary to perform all calculations in the real domain with at least 64 bit long (20 digit resolution) numbers. Using the shorter (and normal for microcomputers) 32 bit real format can be a limiting factor.

Finally there is the 'differential noise amplification factor' to contend with. That is: When any transform is applied to a data set with the net effect of narrowing/enhancing bands, the high frequency components (including noise) are dis-proportionately increased. (This will be dealt with fully in the following chapters and discussion but warrants a

1 Savitkzy. A, Golay. J, Analytical Chemistry, Vol 36, No 8, July 1964, 1672-1639

brief explanation here.) This is most evident when the transforms are applied or modelled in the Fourier (frequency) domain. Any band narrowing (this includes all derivatives and derivative based functions) requires an increasing high frequency component in the Fourier domain. The converse is also true: Any smoothing (band broadening) function requires a falling response in the Fourier domain. Since normal spectral data is 'contaminated' with noise of equal and higher frequency than the signal then the derivatives and other band narrowed transforms of the data will be noisier than the original data. This is intuitively obvious although the consequences are not so obvious.

Experimental change: The signal-to-noise ratio in the original data is improved two fold by averaging for four times longer.

Analytical consequence: The signal-to-noise ratio in the band narrowed data will be improved by a factor of 2 x 'differential high frequency amplification'.

The 'differential high frequency amplification' for typical band narrowing and derivative analysis can range from 10's to 10's of thousands.

The practical consequence of this is that it appears that high resolution band narrowing suddenly becomes possible with very high S/N data. Below a threshold S/N of the source data (usually corresponding to a S/N of 2:1 in the processed data where the signal just becomes discernible above the noise), no useful analysis is possible but as the S/N (of the source data) improves the S/N of the processed data improves at a faster rate. The visible changes in source S/N are undetectable by eye and yet the changes in the enhanced data are quite dramatic. This is not a case of getting something for nothing and does not persist for higher and higher S/N or greater band narrowing. In both cases there is convergence between the frequency profile of the noise and signal (in the processed data not the source data) which limits the effect. Unfortunately the S/N threshold in the source data for permitting high resolution enhancement is very high, requiring data collection times in the order of 1 hour/30nm on the very best instruments available. With no obvious improvement in the source data or VERY smoothed derivatives it is little wonder that other researchers have not previously collected data suitable for the high resolution enhancement techniques I will describe. But once having passed the S/N 'threshold' where analysis becomes possible, very small (almost insignificant seeming) improvements will dramatically improve the S/N of the enhanced data.

Many of the concepts and procedures I will describe appear obvious and intuitive in hindsight. But all of the above problems have been contributing factors to the past ignorance of the procedures to be given. In addition, it is often difficult to develop new fields and procedures

where strong understanding of the underlying principles from diverse fields is required. The work I report on here unites significant principles from Biochemistry, Physical and Organic Chemistry, Applied Mathematics, Numerical Analysis, Computing, Electrical Engineering, Optics and Instrument Design.

I commenced the work reported on in the following chapters on the basis of three hypotheses as follows:

The First Hypothesis:

"The equal information hypothesis".

It is possible to extract from/enhance the spectra of molecules in a liquid phase, detail/information approximating closely that available from non-enhanced gas phase spectra of the same molecules.

The Second Hypothesis:

The amount of detail/information that can be extracted as a consequence of the "equal information hypothesis" is sufficient to identify individual tyrosine and tryptophan residues and their environments in complex proteins.

The Third Hypothesis:

The contribution to the spectra of proteins from phenylalanine residues can be extracted and quantified with sufficient accuracy to provide a method for the accurate quantitation of protein concentrations irrespective of normal conformational and environmental variations.

As they must be, all three hypotheses are testable for truth and failure.

The first hypothesis would be supported utilising molecules whose spectra can be collected in both the liquid and gas phases. If enhancement of the liquid phase spectra yields spectra not significantly different from the gas phase spectra then the hypothesis is supported. Conversely, if it could be shown mathematically that it is not possible to narrow a spectral peak (and thus enhance resolution) then the hypothesis would be proven false.

It is important to note that the Equal Information Hypothesis does not claim to enhance Information. All the information and detail is available in the unprocessed spectrum. It is impossible to increase the information content of the original isolated data set just as it is impossible to increase order in a closed system.

The second hypothesis would be supported if a single tyrosine or tryptophan residue could be identified in a protein containing several such residues. If it could be shown that the spectra of tyrosine and tryptophan were identical under all conditions then the hypothesis would be proven false. It is important to note that the second hypothesis does not claim that all tyrosine and tryptophan residues in a complex protein can be individually identified. This may be possible in some cases but certainly not in all cases.

The third hypothesis would be supported if the concentration of a protein solution was invariant as calculated from the enhanced phenylalanine spectrum when the pH was varied over a wide range and also as the protein was denatured with guanidine. Both of these conditions are known to change the conformation and spectra of proteins. 'Normal environmental changes' are defined as those conditions commonly encountered in protein chemistry and include: pH(1-13); Denaturant concentration (GuHCl 0-6M); Reducing agents (DTT); DNA contamination (0-2.5%). The third hypothesis would be proven false if any of these conditions/contaminants significantly affected the ability to quantitate the phenylalanine second derivative spectrum.

MATERIALS and METHODS DEVELOPMENT

Introduction.

The human eye is extremely good at identifying peaks and valleys, even in very noisy data. Unfortunately the eye does not have similar abilities in identifying subtle changes in the second derivative (rate of change of the slope) of a line. Spectral analysis ultimately reduces to a human observer examining a spectrum and observing the location and magnitude of peaks. Having ascertained that peaks are observable, the observer may employ tools of varying sophistication to locate and quantitate the peaks.

The computer has no requirement to "see" peaks to identify spectral components. None-the-less, humans still program computers to first generate the familiar looking peaks and then analyse them. This is because of our native ability to crudely describe the process and features to use in identifying a "peak". This can then be described in the form of an algorithm and programmed. We do not possess a similar native ability or familiarity with the identification and characterisation of subtle line shape changes, such as an inflection point in the second derivative. While such identification and familiarity can be learned and programmed into a computer, it remains a more desirable goal to first recast the data into the intuitively familiar form of peaks, and then analyse the peaks. Unfortunately raw spectral data from molecules in the liquid phase do not often exhibit many discrete peaks. As I will show, the vast majority of the data is represented as subtle line shape changes. The reason for this is that the spectra are composed of very many overlapping peaks, usually grouped in discrete regions. If a molecule is volatile then a gas phase spectrum will reveal much more detail because the component peaks are much narrower and do not overlap as strongly. The amount of apparent degradation in the information content is demonstrated in the two spectra of benzene in gas and liquid phases. I say "apparent" because in the liquid phase the component peaks are blended together making it harder for the untrained observer to identify them and extract all the information the spectrum encodes.

The goal of the methods described in this thesis is to extract spectral features to the extent that they appear as peaks. Further quantitation and analysis of the extracted peaks is not discussed here and it is left to the reader to choose among the already available methods for this purpose.

Spectroscopy basics

Absorption of radiation

The energy levels of molecules are quantised; they may have discrete values only as determined by quantum mechanical principles and rules. The absorption of light by a molecular species can occur only when the energy of the quantum of light, the photon, is matched by an equivalent energy difference within the molecule. As a result of the absorption of the photon, the molecule will be converted from a low energy state, the "ground" state in thermodynamic equilibrium with the surroundings, to a higher energy, "excited", state. The absorption of visible-ultraviolet radiation produces a molecule in an electronic excited state. However, simultaneously with the electronic energy change the molecule may also alter its vibrational and rotational energy states, which would involve only a fraction of the total energy of the photon absorbed. Indeed, undergraduate texts dealing with spectroscopy generally write the total molecular energy change, ΔE_{total}, in the uv-visible range as

$$\Delta E_{total} = \Delta E_{elec} + \Delta E_{vib} + \Delta E_{rot} \qquad ..5.1$$

showing that such spectra involve simultaneous changes in the molecular electronic, ΔE_{elec}, vibrational, ΔE_{vib}, and rotational, ΔE_{rot}, energies. More specifically, a given electronic transition consists of bands due to the simultaneous vibrational transitions and each one of these vibronic bands, in turn, has a rotational fine structure.

Except for relatively small molecules in the gas phase, the rotational structure is not resolved in general - it just merges into a continuous band. Thus molecular uv-visible spectra, even those that appear to an observer as completely structureless, are, nevertheless, composed of a collection of vibronic bands belonging to the same electronic transition.

Diatomic molecules

The simplest electronic-vibrational or vibronic band structures occur with diatomic molecules which possess just one fundamental mode of vibration: bond stretching. A convenient way of classifying bands is by defining progressions; in a progression the

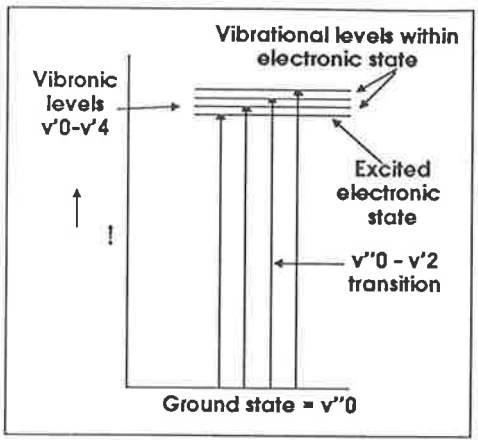

Figure 5.1 *Absorption occurs when the energy of a photon matches an energy difference in the molecule. As a consequence the molecule is converted from the low energy 'ground state' to an energised vibronic state.*

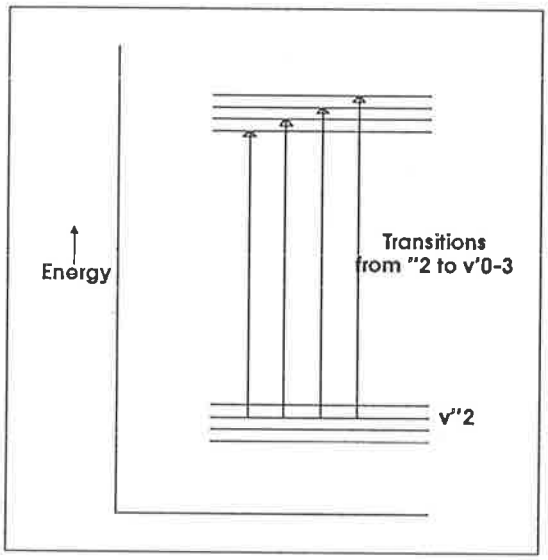

Figure 5.2 *The 'ground state' is determined by the average thermal energy of a molecule and is not zero (for temperatures above absolute zero). The ground state that most closely matches the mean thermal energy will be the most populated in the absence of any exciting energy (other than thermal). A decreasing percentage of molecules will be in ground states increasingly further away from the most populous state as predicted by the Boltzmann distribution of thermal energies about the mean temperature.*

vibrational quantum number of one of the electronic states is constant while that of the other state progressively varies. As an example, in a (v',0) progression the quantum number of the lower state, v", is zero and that of the upper state, v', varies by unit increments starting from zero. The spectral transitions that belong to the (v',0) and (v',2) progressions are shown, respectively, in Figures 5.1 and 5.2.

The amount of light absorbed by each band, the intensity of absorption, is not uniform. Given that the electronic transition of the diatomic molecule considered is allowed by the quantum mechanical "selection rules", there are two factors that govern the relative intensities of the vibronic bands of that transition.

The first factor is the relative population of the vibrational levels in the ground electronic state of the molecule; clearly the larger the population the more light is absorbed. The population of the levels, in turn, is determined by the Boltzmann distribution from which one concludes that at room temperature, for the majority of molecules of interest to biochemists, (v',0) progressions dominate.

The second factor, often referred to as the Franck-Condon principle, affects the relative intensity distribution of bands within a progression. In Figure 5.3 are shown two electronic states of a diatomic molecule together with their respective vibrational levels. In this figure the ordinate is energy and the abscissa corresponds to the internuclear distance between the two atoms of the molecule. Thus the horizontal lines depict the complete change in internuclear separation for the vibrations of various energies; it should be noted that the equilibrium internuclear separations (the minima of the potential energy curves) do not, in general, coincide for the various electronic energy states. We now observe that the most probable internuclear distance for a v = 0 state corresponds very nearly to the minimum of the potential energy curve, while for v > 0 the vibrating molecule will spend the greatest amount of time at the extremes of the vibrational displacement. Next, we recognise that, due to their relative masses, electrons move several orders of magnitude faster than atomic nuclei so that during an electronic transition the internuclear distances remain sensibly the same; expressed in another way, electronic transitions are vertical. Thus, as shown by the thick vertical line in Figure 5.3, the most probable transition and therefore the most intense absorption band in a (v',0) progression in this case is (2,0) with intensities rapidly decreasing for both v' > 2 and v' < 2 as shown by the two dashed lines.

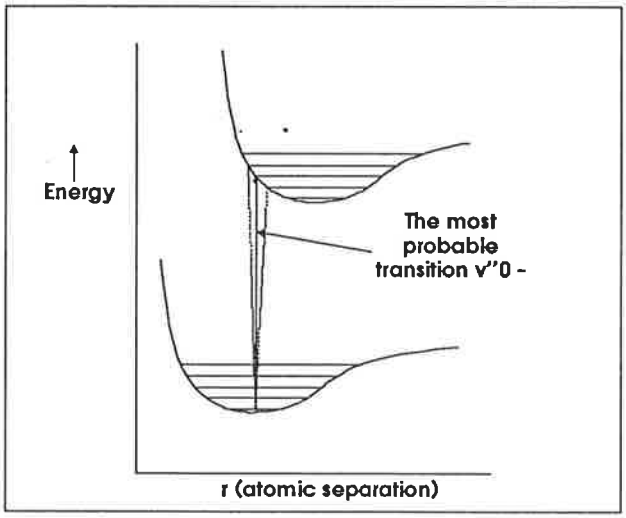

Figure 5.3 *The Franck-Condon principle predicts the probability of a transition (absorption band) occurring. The most probable transitions are vertically, involving rearrangement of electronic states only. For any vibronic level the most populated positions are represented by the line ends for v > 0 states and the line centre for v = 0 states. The r axis represents increasing diatomic separation, with increasing energy represented by the e axis.*

Polyatomics

The uv-visible spectra of polyatomic molecules are also vibronic, consisting of series of superimposed bands. The principles that govern distribution of the intensity of the bands of diatomic molecules apply here as well. However, since polyatomic molecules possess many different fundamental modes of vibration, the number of possible progressions that could contribute potentially to their absorption spectra may be quite large. Fortunately, additional principles related to the symmetry of the molecular framework and its distortion by certain modes of vibration prohibit any substantial absorption of light by a great many of the potential progressions and the spectra of polyatomic molecules often remain manageable in complexity.

Band shapes

The vibronic bands of an electronic transition of the molecule are generated by a common underlying mechanism; for this reason the observed bands will generally differ in amplitude and in energy (position) but not in shape. This has two important analytical consequences:

> it becomes possible to formulate an optimum extraction/enhancement procedure that will apply to most spectra of like molecules and, with minor modifications, to other spectra as well; and
>
> such a procedure may be developed on the basis of a single band with either an assumed or experimentally determined shape.

These statements apply to procedures involving deconvolution/convolution functions whose effect is to increase the number of observable high frequency components of the spectrum. Moreover, such procedures, whether applied in the normal (time or wavelength) domain or in the Fourier (frequency) domain, should work equally well in principle on both single and overlapping bands. It follows that knowing the band shape and being able to accurately model it is of prime importance in the development and evaluation of techniques of spectral enhancement.

Of the various phenomena contributing to band broadening in the uv-visible region there are just two of particular relevance in liquids and solutions. First, the frequent collisions between molecules with consequent exchange of energy lead to an uncertainty in the precise values of energy levels resulting in bandwidths at half maximal intensity ("halfband widths") of the order of 50 cm^{-1} (1500 GHz). The theoretically predicted shape of such a "collision broadened" band is Lorenzian (or Cauchy); the explicit form of such a function is given further below. However, experimentally determined band shapes in

the uv-visible region are much closer to a Gaussian function also given further below. This is attributed to further broadening arising from Van der Waals interactions between the molecules in the liquid phase. Such interactions modify molecular energy levels (in a semi-continuous fashion about the mean) and the superposition of the consequential family of Lorenzian bands produce the Gaussian resultant[1]. The explicit forms of the two bandshape functions normalised to unit area are given by the formulae:

..5.2

Lorenzian $$Y(x) = \frac{1}{\pi b} \frac{1}{1+\left(\frac{x-a}{b}\right)^2}$$

..5.3

Gaussian $$Z(x) = \frac{1}{\sigma\sqrt{2\pi}} e^{-\frac{1}{2}\left(\frac{x-a}{\sigma}\right)^2}$$

In these formulae 'a' refers to the position of the maximum of a band and 'σ' and 'b' are referred to respectively as the Gaussian and Lorenzian band width parameters. The functions are described graphically in figure 5.4 with a=0.

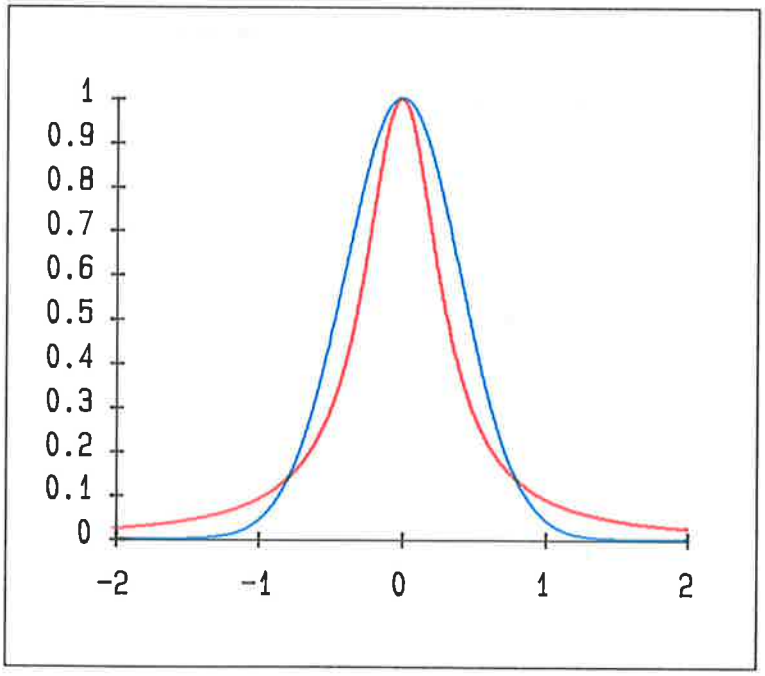

Figure 5.4 *The Gaussian (broad blue band) and Cauchy (narrower red band) functions normalised to unity height and area are shown. The broader Gaussian band shape is the most commonly encountered in UV-VIS spectroscopy. The narrower Cauchy (also known as Lorenz) band is only seen in some vapour phase spectra and never in solution spectra.*

1 R.N. Bracewell, The Fourier Transform and its Applications, 2nd ed., 1978, McGraw-Hill, New York, p.

The degree of band broadening typical of the liquid versus vapour phase can be seen in figure 5.5.

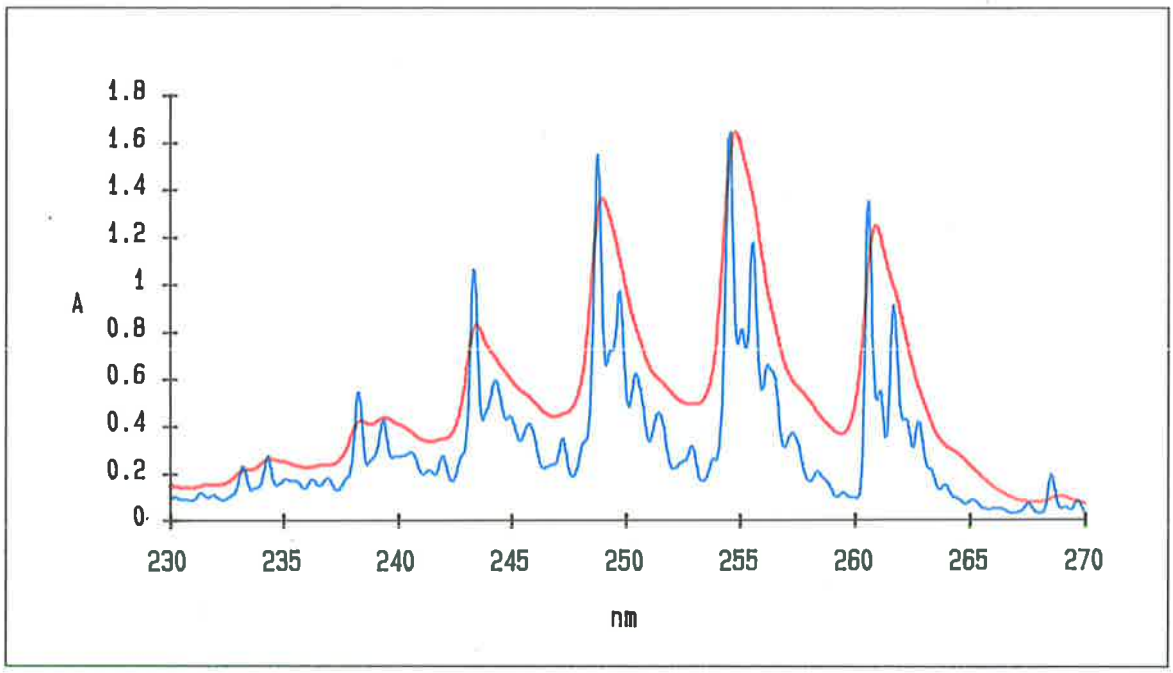

Figure 5.5 *Vapour phase (blue) and solution (red) spectra of benzene demonstrates the dramatic band broadening going from gas to liquid phases. The spectra were collected on a Varian Cary 3 spectrophotometer: slit band width 0.6 nm (solution spectra) and 0.2 nm (vapour phase spectra); resolution 0.02 nm; samples averaged 33 (vapour phase, 1 second) and 198 (solution, 6 seconds / wavelength step). The solution spectrum was recorded with a larger slit bandwidth and more points averaged to increase the S/N to a level where spectral enhancement is possible.*

Methods Development

A spectrum is, in principle, the measured absorbance, A, the dependent variable, given as a function of the wavelength, λ, the independent variable. However, in practice the spectrum consists of the discrete set: $\{ A_i , \lambda_i \}$ so that, in contrast to the ideal, the independent variable is not continuous, it is granular. Thus, the maximum spectral resolution of the spectrophotometers used for this study was 0.02 nm and this value sets the lower limit for the wavelength- or time-granularity in this work. Having allowed for their granularity it will be assumed, however, that the precision of the λ_i is high and their standard deviations are negligibly small.

Similarly, it will also be necessary to take into account the possible magnitude-granularity of the measured values of the absorbance as well as the precision of the A_i.

In order to address the problems associated with the enhancement of the spectra expressed as a set of granular and imprecise pairs of numbers, a model for the bandshape must be selected. In view of its prevalence in uv-visible spectroscopy this will be taken to be Gaussian. The Gaussian form given by eqn (5.3) which is normalised to unit area contains just 2 parameters, the position of the band maximum, a, and the bandwidth parameter, σ. If the normalisation of the area is relaxed an additional parameter, I, the maximal intensity, needs to be introduced. In this work an additional quantity, referred to as the bandlimit parameter, θ, will also be used. The need for such a parameter arises from the practical limitation of measuring a band between finite boundary limits specified by θ even though theoretically these limits are at infinity.

As a further parameter we shall need to specify the convolution width parameter, denoted here by β, that defines the limits of the convolution function to be used.

Given that λ is granular, the numbers of steps, $n\sigma$, $n\theta$ and $n\beta$, that will span the distances σ, θ and β, respectively, provide an equivalent description of the bandwidth, bandlimit, and convolution width parameters. Note that granularity bears an inverse relationship to these numbers; thus, for example, the smaller $n\sigma$ the less points are collected for a given σ and the larger the granularity. We also note that the convolution width is expressed alternately in terms of the integer, m, with $n\beta = (2m + 1)$.

The first step in developing optimum enhancement techniques is to address the computational constraints to determine what is possible and best, utilising suitable models, before tackling experimental data. I will commence the description of the computational methods by first characterising the most widely used current methods; second derivatives obtained by convolution.

As has been pointed out earlier, the second derivative of the spectrum has been extensively utilised in the analysis of proteins and other molecules. The methods most commonly used to generate the second derivatives have been electronic (simple RC (resistor capacitor) circuits). Unfortunately this approach leads to many errors and will not be considered here. (Major among the errors is the time polarised nature of all RC circuits (they cannot look into the future), whereas digital filtering post data collection can implement symmetrical filters.) The favoured approach is to collect the data with no analogue smoothing or other processing and then to apply all smoothing, derivative and other functions digitally. The most popular form of generating derivatives and smoothing the data has been the application of convolution functions such as those first described by Savitsky and Golay[1]. Henceforth I will describe these procedures and all others of the same type as Least Squares Polynomial Procedures (LSPP). They have in common the premise that over a set window size (2m +1) the input data (X(i), a set of discreet values) can be fitted to a polynomial function (of order i : P_i (x)) by least squares criteria. Savitsky and Golay demonstrated that sets of convolution coefficients (C_j j=-m..+m) could be generated, for any order polynomial or its derivative, and these would yield the least squares solution for the centre point. That is, the output set of integers (Y(i), the output set on values) is related to the source data by a convolution

..5.4

$$Y_i = \sum_{j=-m}^{m} X_{(i+j)} C_j \quad i = m..n - m.$$

Where the set of input values is $X(i)$ $i = 0..n$

The next most common method for manipulating the spectral data is to transform the data into the Fourier domain, where simple band narrowing and smoothing functions can be applied before performing the inverse transform to yield the enhanced spectrum. The Fourier transform translates data from the time domain into the frequency domain and back. There are a number of advantages to performing spectral enhancements in the Fourier domain, not the least of which is the intuitively simple nature of the band narrowing and smoothing

1 Savitkzy. A, Golay. J, Analytical Chemistry, Vol 36, No. 8, July 1964, 1627-1639.

functions. Band narrowing involves emphasising the higher frequencies by simply multiplying the Fourier data by some increasing function. Conversely, smoothing involves attenuating the higher frequencies by simply multiplying the Fourier data by some decreasing function. Numerically there are a number of problems encountered when implementing the Fast Fourier Transform (FFT), although computational demand is not one of the problems and often LSPP take longer to perform similar tasks. The major problem with the FFT is that it assumes that the input data set is one cycle of a cyclic function. This means that the FFT is well behaved only if the data 'wraps around'. This is demonstrated in figures 5.6 and 5.7. In the case of the 'non-cyclic' data, such as shown in figure 5.7, an FFT followed by an inverse FFT does not return the original' data. The data are contaminated with very large amounts of

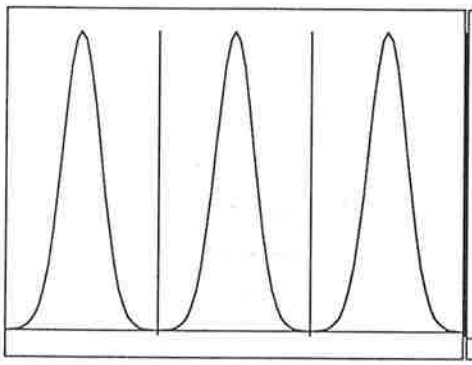

Figure 5.6 *The FFT assumes that it is given one cycle of a cyclic waveform that 'wraps around' smoothly to the next cycle. If the source data is limited in frequency response to s and the data has been sampled at intervals less than 1/(2s) and the data set smoothly wraps around then the discreet FFT introduces no errors at all.*

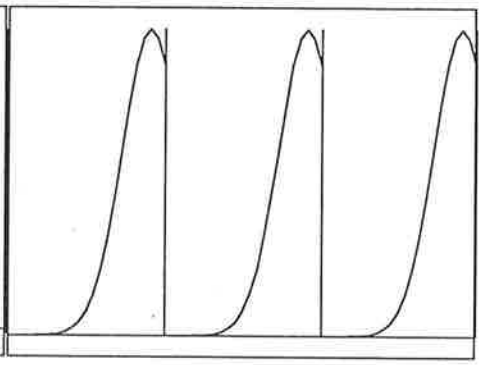

Figure 5.7 *The FFT will introduce large amounts of high frequency noise when presented with a data set that does not wrap around smoothly. The large amounts of high frequency noise represent a large discontinuity when the input set is considered cyclic. The solution is to fit some polynomial to the end points (eg. the first and last 3 points) and subtract this from the source data. If necessary the FFT of the polynomial can be extracted to yield a 'correct' Fourier transform of the initial source data.*

spurious high frequency noise.

LSPP is by far the more common method applied to spectral analysis at present. I have found it useful to combine the two techniques by generating Fourier transforms of both the spectral data and the LSPP convolution function and then performing the convolution in the Fourier domain. Often this is faster than LSPP alone when large window sizes are involved and it has the distinct advantage of allowing one to see the frequency response of the LSPP convolution function.

All of the possible procedures for performing spectral enhancement share common goals and limitations imposed when using experimentally derived data. The primary goal is 'band narrowing' to the degree that the majority of bands in a spectrum are resolved; and the primary limitations in the source data are granularity in both time and magnitude domains.

Computing.

All code fragments are given in AT&T V2.0 C++ compatible code. Code has been principally written in Pascal, C and C++. The most recent code for validating the analysis reported in this thesis was written in C++. The compilers used were (in chronological order) Compass Pascal (CP/M version by Polydata), VAX Pascal (VMS version by DEC), Turbo Pascal V1.x through 5.x(MS DOS version by Borland), Definicon C (Green Hills C for DSI 32032), Turbo C V2.0 (MS DOS version by Borland), UNIX C (SUN 3/60 and 4/10 versions by SUN under Sunwindows), and Turbo C++ V1.0 (MS DOS version by Borland).

The computers employed were (in chronological order) Apple IIc, Medfly (Apple IIc and CP/M compatible), VAX 750 and 780's, Aquarius (IBM PC XT compatible,8 MHz 8086 CPU), Olivetti M24 (IBM PC XT compatible, 10 MHz V30 CPU), Definicon DSI32 (processor board for IBM PC, 10MHz national 32032 CPU), SUN 3/60 and 4/10 workstations, various Microbits workstations (IBM PC compatible, 12MHz 80286 through 33 MHz 80486 CPU).

The bulk of the work was performed on a Microbits PC compatible (20MHz 80386, 20MHz 80387, 8Mb RAM), programmed in Turbo C V2.0.

Precision.

Wherever possible a long double real number representation was utilised. The real number formats available were:

Type	Bits	Digits precision	Range
float	32	8	3.4×10^{-38} to 3.4×10^{38}
double	64	16	1.7×10^{-308} to 1.7×10^{308}
long double	80	20	3.4×10^{-4932} to 1.1×10^{4932}

The float format was never used due to its low precision. The double format was only rarely used for input and output when the compiler did not adequately support I/O of long double. All internal

calculations utilised the long double format and were carried out by a floating point processor.

The int and long int integer formats were never used other than as index counters. Early experimentation showed that using integer based algorithms led to unacceptable errors mainly due to underflow errors which were not detected.

Generating Gaussian and Derivative bands.

The second derivative of the Gaussian function has the form:

$$\frac{d^2Z}{dx^2} = \left(\left(\frac{x-a}{\sigma}\right) - 1\right) \frac{I}{\sigma^3\sqrt{2\pi}} e^{-\frac{1}{2}\left(\frac{x-a}{\sigma}\right)^2} \quad ..5.5$$

The algorithm for generating a Gaussian band is:

```
#define REAL long double
#define LONG long int
#define PI 3.14159265358979323846
void peak(REAL data[], REAL tr, REAL sigma, REAL height, int data_points)
{
REAL area = height / (sigma * sqrt(2 * PI));
REAL t = 0 - tr;

 for(int j = 0; j < data_points; ++j)
  data[j] = area * exp(-0.5 * sqr(t++ / sigma));
}
```

Optimising by strength reduction yields the algorithm actually used:

```
void peak(REAL data[], REAL tr, REAL sigma, REAL height, int data_points)
{
REAL area = height / (sigma * sqrt(2 * PI));
REAL t = 0 - tr;
REAL a = (sqrt(0.5) * t) / sigma;
REAL a_step = sqrt(0.5) / sigma;

 for(int j = 0; j < data_points; ++j)
 {
  data[j] = area * exp(-sqr(a));
  a += a_step;
 }
}
```

Similarly, strength reduction yields the function used to generate the second derivative:

```
void dpeak(REAL data[], REAL tr, REAL sigma, REAL height, int data_points)
{
REAL area = height / sqr(sigma);
REAL t = 0 - tr;
REAL a = t / sigma;
REAL a_step = 1 / sigma;
 t = 0 - tr;

 for(j = 0; j < data_points; ++j)
 {
  REAL a_sqr = sqr(a);
  data[j] = area * exp(-0.5 * a_sqr) * (a_sqr - 1);
  a += a_step;
 }
}
```

RMS ERRORS

Let $D_t(x)$ denote the true derivative described by eqn 5.5 and $D_e(x)$ denote the derived derivative determined experimentally.

In those cases where the goal is to derive the second derivative of a Gaussian peak, accuracy can be assessed by comparison with the true derivative.

The measure of relative error between the true and derived derivatives must be independent of the three parameters, σ, a and the maximal band intensity, which describe the Gaussian peak. It would be convenient if it were possible to determine the error based on the ratio of the derived and true derivatives. The RMS sum:

$$s^2 = \frac{1}{(\beta - 1)} \sum_{i=-0.5\beta}^{+0.5\beta} \left(\frac{1 - D_{t(i)}}{D_{d(i)}} \right)^2$$

Unfortunately the Gaussian second derivative passes through zero once. Due to noise and resolution constraints the derivatives may fall to, or very close to, zero several times near the zero crossing thus invalidating the $\frac{D_{t(i)}}{D_{d(i)}}$ term.

A robust method for determining the relative error is to normalise the difference of the sum of squared deviations:

$$s^2 = \frac{1}{(\beta - 1)} \quad \frac{\sigma^2}{I} \sum_{i=-0.5\beta}^{+0.5\beta} \left(D_{t(i)} - D_{d(i)} \right)^2$$

```
REAL rms_error(REAL data1[], REAL data2[], REAL height, REAL sigma, int data_points)
{
REAL s = 0;

 for(j = 0; j < data_points; ++j)
 {
  REAL temp = data1[j] - data2[j];
  s += sqr(temp);
 }
 s = sqrt(s / (REAL)data_points);
 return(sqr(sigma) / height * s);
}
```

Convolution.

The convolutions described in the chapter on derivative methods were based on a third order polynomial as described by Savitzky and Golay[1]. These authors tabulate these convolution integers in their Table VI for m = 2..12, where we recall the relationship $n\beta = 2m + 1$. Convolution widths were required for m up to several hundred. The sets of convolution integers are symmetrical and are therefore fully described by C_j, j = 0..m and the normaliser C_n. For increasing m the following algorithm returns the convolution set:

```
#define DERIV2_CENTRE_BASE -2
#define DERIV2_CENTRE_STEP 2
#define DERIV2_CI_STEP 6
#define DERIV2_CI_BASE -3
REAL gen_2deriv_ci(int m,  REAL ci[])
{
 int j;     /* general counter     */
 REAL s = 0;     /* cumulative counter  */

 /** generate centre coefficient **/
 j = m;
 while(j > 1) s += j—;
 ci[0] = DERIV2_CENTRE_BASE - s * DERIV2_CENTRE_STEP;

 /** generate remaining coefficients **/
 REAL step = DERIV2_CI_BASE;
 for(j = 1; j < m; ++j)
  ci[j] = ci[j-1] + (step += DERIV2_CI_STEP);

 /** generate normaliser **/
 s = sqr((REAL)ci[0]);
 for(j = 1; j < m; ++j) s += (2 * sqr(ci[j]));
 return(s / 6.0);
}
```

No attempt was made to determine the derivative for the m end points at the start and end of the source data set. The size of the source data set was always larger by 2m points than required to allow for the loss of m points from each end. To avoid problems when graphing, the end m points were set equal to the m+1th point in from each end

1 Savitkzy. A, Golay. J, Analytical Chemistry, Vol 36, No. 8, July 1964, 1627-1639.

respectively. The diagrams presented in this thesis do not display the m end points where convolutions were involved.

In those cases where smoothing was required, a third order polynomial model was used as tabulated by Savitzky and Golay[1] in their Table 1. As for the derivative coefficients, the following function generates sets of coefficients for any m:

```
#define SMOOTH_CENTRE_BASE 5
#define SMOOTH_CENTRE_STEP 6
#define SMOOTH_CI_STEP 10
#define SMOOTH_CI_BASE -5
REAL gen_smooth_ci(int m,  REAL ci[])
{
 int j;
 REAL s = 0;

 /** generate centre coefficient **/
 j = m;
 while(j > 1) s += j—;
 ci[0] = m * SMOOTH_CENTRE_STEP + SMOOTH_CENTRE_BASE;

 /** generate remaining coefficients **/
 REAL step = SMOOTH_CI_BASE;
 for(j = 1; j < m; ++j)
  ci[j] = ci[j-1] + (step += SMOOTH_CI_STEP);

 /** generate normaliser **/
 s = 0;
 for(j = 1; j < i; ++j) s += ci[j];
 return(s * (LONG)2 + (LONG)ci[0]);
}
```

1 Savitkzy. A, Golay. J, Analytical Chemistry, Vol 36, No. 8, July 1964, 1627-1639.

The function for the convolution is:

```
void convolute(REAL source[], REAL dest[], int points, REAL ci[], REAL normaliser, int m)
{
 int x;

 for(x = m+1; x < (points - i); ++x)
 {
  REAL sum = 0;
  for(int j = 1; j < m; ++j)
    sum += (source[x+j] + source[x-j]) * ci[j];
  sum += source[x] * ci[0];
  if(bn) then sum /= norm;
  dest[x] = sum;
 }

 for(x = 0; x < m; ++x) dest[x] = source[m+1];
 for(x = points; x > points - m; ++x) dest[x] = source[points-m-1];
}
```

FFT.

The FFT was implemented as described by Press et al[1]. The only modification made was to subtract 1 from all array indexes. This is because an n element array in C is indexed 0..n-1 whereas in Pascal and

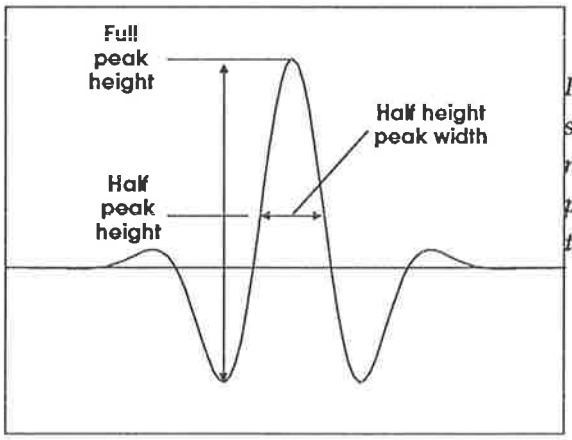

Figure 5.8 THE HALF-HEIGHT BANDWIDTH measurement is shown. This measure is fast end easily applied to any peak shape no matter how distorted.

Fortran the indexing is from 1..n.

Band Narrowing Assessment.

Before examining the band narrowing ability of a proposed filter we must define the measures by which the performance of the filter can be assessed.

There are three factors to consider:

Band narrowing.

1 Press. H, *et al*. Numerical Recipes, The art of Scientific Computing. Cambridge University Press, 1987.

Band distortion.

S/N degradation.

Band narrowing is the desired effect while both band distortion and S/N degradation are detrimental side effects which limit the degree of useful band narrowing that can be achieved.

Because of the distortion of the band shape as a result of the band narrowing procedures, it becomes necessary to introduce a practical measure of narrowing. I have used the width at half height to monitor narrowing which will be expressed as % narrowing relative to the input band, referred to as the "relative band width", and denoted by δ. The full height is taken as the band peak down to the first minimum as depicted in figure 5.8. The accuracy of the half width measure is refined by interpolation as shown in the following code fragment.

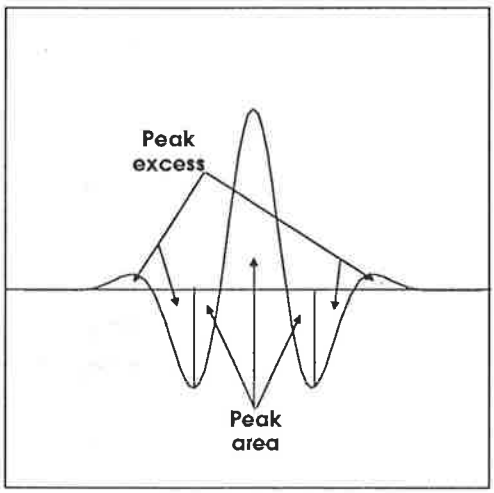

Figure 5.9 PEAK DISTORTION is measured as a peak excess %. This parameter, which is the percentage of the absolute area beyond the first minima, is easily measured and independent of band shape.

```
REAL half_height_width(REAL data[],
LONG points)
{
LONG j;
REAL half_height;
REAL hhw;

 points /= 2;

 //find bottom of peak
 j = points;
 while((data[j] > data[j-1]) and j) j--;
 if(j) half_height = data[points] - (data[points] - data[j])/2;
 else half_height = data[points]/2;

 //refine half height width by interpolation
 j = points;
 while(data[--j] > half_height);
 hhw = points-j-1;
 hhw += (data[j+1] - half_height) / (data[j+1] - data[j]);
 return(2*hhw);
}
```

Noise degradation is expressed as a S/N degradation factor. Although simple sounding, the S/N degradation factor is not trivial in its determination. The procedure employed was:

Two data sets were generated: First the noise free gaussian band; Second the noise.

The RMS of the noise was determined and a S/N ratio relative to the band maximum determined.

FFT's were performed on both data sets separately.

The two data sets were convoluted with a band narrowing filter and transformed back to the time domain.

The RMS of the noise was determined and a S/N ratio relative to the narrowed band maximum determined.

The S/N degradation is the ratio of the original and final S/N ratios.

The noise generator used is part of the Turbo C compiler and uses a multiplicative congruential random number generator with a period of 2^{32} to return successive pseudorandom numbers between 0 and a specified maximum. The random number generator was seeded with a number determined from the processor clock. A large sample of random sets were transformed to the Fourier domain and checked for random phase and power spectra. The random number generator performed well with no evident order in the phase or power spectra.

For quantitation of the peak distortion I have introduced a new parameter, peak excess. As described in the chapter on Band narrowing, the form of peak distortion on band narrowing is oscillating side lobes. Clearly the relative area in these side lobes adds complexity and detracts from the goal of band narrowing. The peak excess is defined as the percentage of total absolute area included in these side lobes. For computational simplicity the definition is refined to: The percentage of total alsolute area beyond the first minimum (central band extent) from the band centre. This is depicted in figure 5.9 and explained fully in the following code fragment.

```
REAL peak_excess(REAL data[], LONG points)
{
REAL peak = 0;
REAL excess = 0;
LONG j;

 points /= 2;

 j = points;
 while((data[j] > data[j-1]) and j) peak += fabs(data[j--]);
 if(!j) return(1.0); //100% peak
 while(--j) excess += fabs(data[j]);

 return(1 - (peak / (peak+excess)));
}
```

The overall procedure for analysing the performance of a given filter is best described by the following code fragment.

```
REAL rms(REAL data[], LONG points);
void noise(REAL amplitude, REAL data[], LONG points);
void peak(REAL data[], REAL tr, REAL sigma, REAL height);
void real_fft(REAL data[], LONG n, LONG isign);
void fft_gaus(REAL data[], REAL tr, REAL gamma, LONG points);
void fft_gaus_sqr(REAL data[], REAL tr, REAL gamma, LONG points);
void fft_exp(REAL data[], REAL tr, REAL g, LONG points);
void fft_e_sqx(REAL data[], REAL tr, REAL g, LONG points);
REAL half_height_width(REAL data[], LONG points);
REAL peak_excess(REAL data[], LONG points);

main(int argc, char *argv[])
{

LONG points = 256;
LONG fpoints = points / 2;            // number of complex points for FFT
REAL *p1 = new REAL[points];          // noise free gaussian peak
REAL *p = new REAL[points];           // gaussian peak
REAL *temp = new REAL[points];
REAL sigma = 20;                      // gaussian variance
REAL tr = 128;                        // gaussian mean
REAL height = 1;                      // gaussian height
REAL gamma = 2 * M_PI / sigma;        // fourrier variance of gaussian
LONG j;                               // general counters
REAL t = 20;                          // filter parameter
REAL g = 20;                          // filter parameter
REAL phw;                             // gaussian half width
REAL h_w;                             // half width of filtered peak
REAL pp;                              // % valid peak
REAL rms_noise;                       // unfiltered noise
REAL rms_fn;                          // rms filtered noise
void (*filter)(REAL data[], REAL tr, REAL gamma, LONG points);
```

```
// select filter to be tested here
filter = fft_gaus;

for(j=0; j  < points; ++j) p[j] = 0;
for(j=0; j  < points; ++j) p1[j] = 0;
peak(p, tr, sigma, height);
phw = half_height_width(p, points);

noise(1.0, p1, points);
rms_noise = rms(p1, points) / p[fpoints];
t = 10;

// nested loop for testing two parameter filters
for(g = 2; g  < 1000000; g *= 10) {
 cout < g < "\n";

 for (t = 5; t < 20; t += 1) {
  memcpy(temp, p, points * sizeof(REAL));  // get copy of noise free band

  real_fft(temp, fpoints, 1);          // FFT into Fourier domain
  filter(temp, t, g, points);          // convolute with filter
  real_fft(temp, fpoints, -1);         // Inverse FFT back to time domain

  h_w = half_height_width(temp, points);   // determine half height width
  pp = peak_excess(temp, points);          // determine band excess
  REAL height = temp[fpoints];             // height of narrowed band

  memcpy(temp, p1, points * sizeof(REAL)); // get copy of noise
  real_fft(temp, fpoints, 1);          // FFT
  filter(temp, t, g, points);          // filter
  real_fft(temp, fpoints, -1);         // Inverse FFT

  rms_fn = rms(temp, points) / height;     // determine S/N

  REAL nr = h_w / phw;                 // determine narrowing as %
  rms_fn = rms_fn / rms_noise;             // determine S/N degradation
  cout < t < "\t" < nr < "\t"< rms_fn < "\t"< pp < "\n";
 }//t
}//g

}
```

Spectroscopy.

Spectra were collected on either a Varian Cary 2200 or a Cary 3 spectrophotometer. Unless otherwise noted, temperature control was used and set to 25 C. The benzene vapour phase spectrum was collected at 90 C in a nitrogen atmosphere with 0.2 nm slit width, 0.02 nm resolution and signal averaging time of 1 s (33 samples on Cary 3). Solutions of proteins were always centrifuged and filtered through a 0.22 μ filter immediately prior to analysis. Unless otherwise noted, cuvets were capped, matched 1 ml quartz with a 1cm path length. Other nominal settings for solution spectra were: 0.6 nm slit band width (triangular slit); 0.02 nm step; 6.0 s averaging time (198 samples on Cary 3). All data were exported as ASCI pairs of x and y data. All protein refolding solutions were allowed to equilibrate for at least 1 hour prior to analysis.

Reagents.

All solutions and reagents were of analytical grade unless otherwise noted. Solvents were of spectroscopic grade.

Analysis and Graphing.

All results were output as 19 digit ASCII numbers in a format suitable for direct import into Excel (Microsoft spreadsheet). All charting, statistical and other final analysis were then carried out in Excel. Any non-trivial reduction or merging of results was performed by co-ordinating programs written in C prior to the results being imported into Excel.

SECOND DERIVATIVES

This, and the next chapter will deal with the first hypothesis.

The First Hypothesis: "Equal Information Hypothesis"

It is possible to extract from/enhance the spectra of molecules in a liquid phase most of the detail/information that would be available from a non-enhanced gas phase spectrum of that molecule.

Tests:

The first hypothesis would be supported utilising a molecule whose spectrum can be collected in both gas and liquid phases. If enhancement of the liquid phase spectrum yielded a spectrum closely resembling its gas phase spectrum, the hypothesis would be supported. If it could be shown mathematically that it is not possible to narrow a spectral band (and thus increase resolution) then the hypothesis would be proven false.

The basis for this hypothesis is that while the environment (gas vs. liquid) may change, the causal factor generating the spectrum (absorption of photons by a molecule) does not change. The environment may distort (band broaden) all of the absorption bands and may even shift some bands, never-the-less the great majority of bands will still be present. Same molecule, same information, at least in principle. Due to band broadening in solutions, the casual observer may think the information content is considerably less than in the vapor phase but this is not the case. The information is there, but it is smeared out, with many bands which would be resolved in the gas phase now overlapping. There is no question of retention of all the information in going from the gas phase to a solution, but rather a question of to what degree the smearing effects can be reversed, given experimental data contaminated with noise from various sources.

Result:

The hypothesis is supported and demonstrations are given of enhanced liquid phase spectra which closely match the corresponding vapour phase spectra. The penalty for the resolution enhancement is degradation of the signal to noise ratio (S/N). The liquid phase spectrum requires data collection times some 200 times longer to reduce the S/N to a level where, after enhancement, the spectrum looks similar (and has a similar S/N ratio) to the corresponding vapour phase spectrum.

The figure 6.1 demonstrates the ability of the enhancement techniques developed in resolving the liquid phase spectrum of benzene.

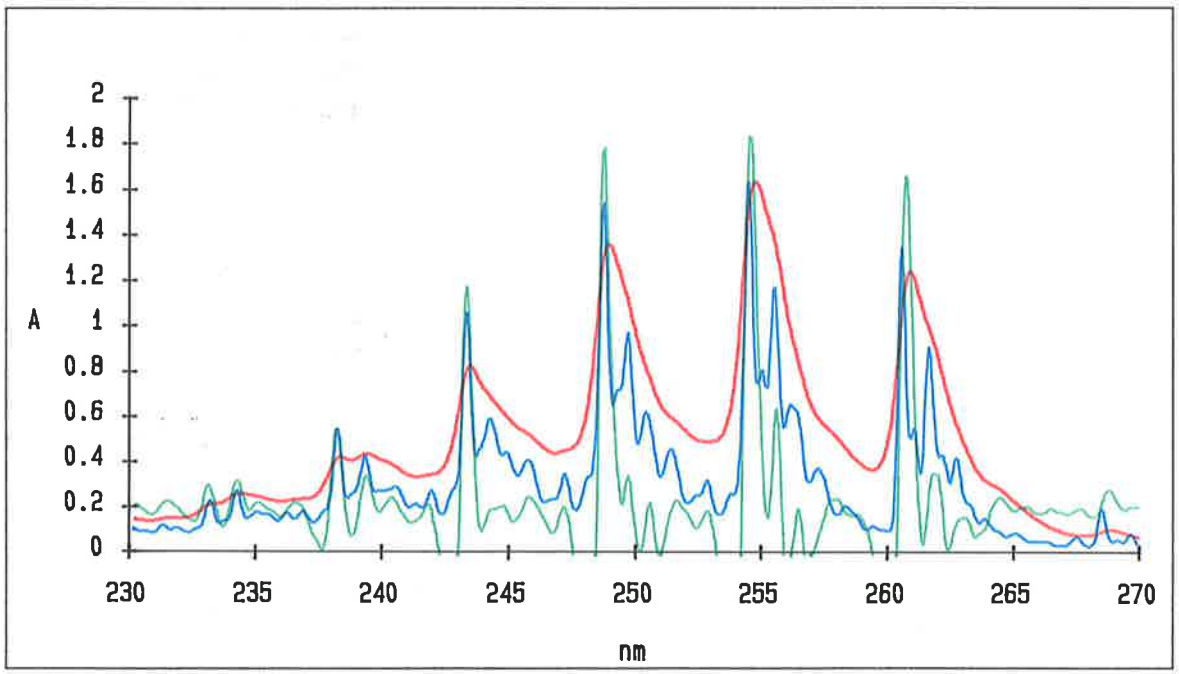

Figure 6.1 *The enhanced spectrum (green), derived from the solution spectrum (red), closely matches the vapour phase spectrum (blue). The enhanced spectrum was generated with a 1.0 nm (51 point) cubic second derivative convolution as described in the text. The vapour phase spectrum was measured under nitrogen against a nitrogen reference at 90 C. Benzene was dissolved in ethanol for the solution spectrum which was referenced against ethanol at 25 C. The spectra were collected on a Varian Cary 3 spectrophotometer: slit band width 0.6 nm (solution spectra) and 0.2 nm (vapour phase spectra); resolution 0.02 nm; samples averaged 33 (vapour phase, 1 second) and 198 (solution, 6 seconds/wavelength step). The solution spectrum was recorded with a larger slit bandwidth and more points averaged to increase the S/N to a level where spectral enhancement is possible.*

Why second derivatives?

Figure 6.2 shows a Gaussian band and the second, fourth and sixth derivatives of the band all normalised to the same height. The desired feature of the even derivatives is the narrower central peak. The odd derivatives are also band narrowed except that they are non-symmetrical, making visual interpretation of odd derivative spectra difficult.

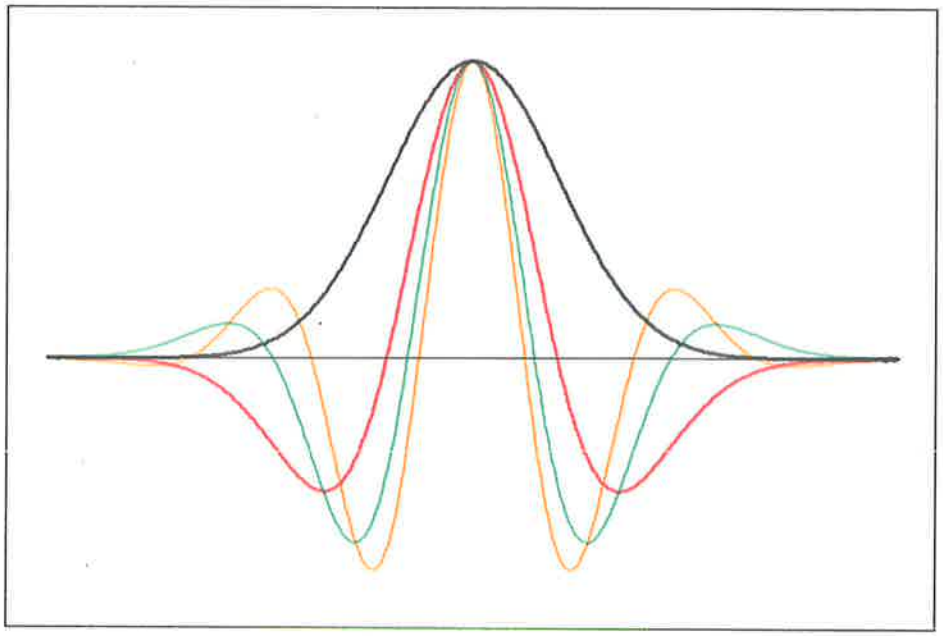

Figure 6.2 *Second (red), fourth (green) and sixth (orange) normalised derivatives of a Gaussian (black) band. Each successive higher even derivative adds one more side lobe and narrows the central band.*

As can be seen, the higher the order of the derivative the greater the degree of band narrowing. The drawback to derivatives is the generation of the negative [oscillating] side lobes. The higher the derivative order; the larger the magnitude and number of side lobes. These computer generated and normalised derivatives do not show the relative amplification of noise as the derivative order increases. This amplification is proportional to the rate at which the peak amplitude of the derivatives falls off, which is $\frac{1}{s^n}$ where n is the order of the derivative. Taking all of these factors into account, it is not beneficial to go beyond the second derivative. Going from the second to fourth derivative introduces far more noise than the slight improvement in band narrowing warrants.

Figures 6.3 and 6.4 demonstrate the resolution enhancement for simple two band overlaps gained from the second derivative.

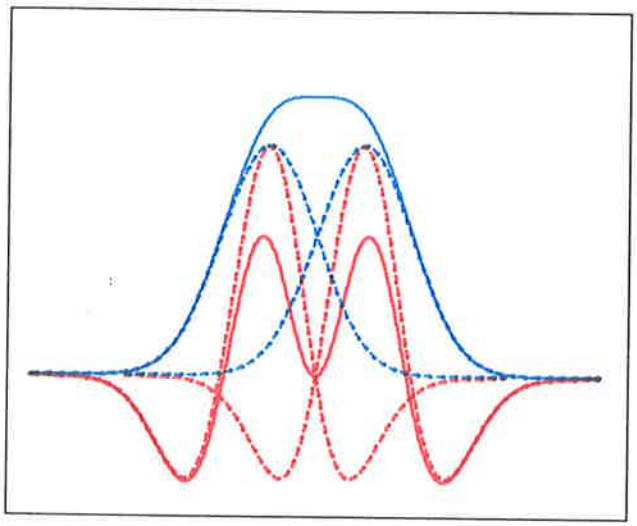

Figure 6.3 *The second derivative (solid red) resolves two overlapping Gaussian bands (solid blue). The individual Gaussian bands (blue dots) and individual derivatives (red dots) are also shown.*

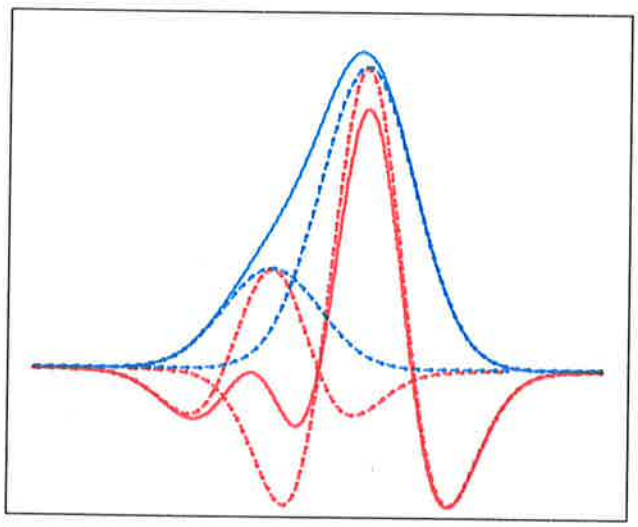

Figure 6.4 *The resolution of two Gaussian bands of unequal area is quite dramatic. The two Gaussian bands are separated by the same distance as in the accompanying figure. The second derivative (solid red) resolves two overlapping Gaussian bands (solid blue). The individual Gaussian bands (blue dots) and individual derivatives (red dots) are also shown.*

Granularity

What is the effect of granularity in the x and y axes (time and magnitude)? How does this limit the ability and extent to which the data may be enhanced?

Time granularity

It is possible to eliminate (in practical terms) the granularity in the magnitude by dealing wholly in real numbers (20 significant digits). It is not practical to reduce the granularity in the time axis to the same degree (this would require a θ (band limit parameter) of 10^{20} points). Therefore the relationship between the ability to accurately extract the second derivative from a computer generated (real numbers) band for a varying number of points (time granularity) in a band provides an absolute best baseline to compare all subsequent performances to. Figure 6.5 shows the experimentally determined relationship between the number of points in such a band and the accuracy with which the second derivative can be extracted. In this experiment an optimal convolution width parameter to band width parameter ($\frac{n\beta}{n\sigma}$) ratio (determination of the optimum ratio will be demonstrated shortly) was maintained while the band width parameter, σ, was increased. The relationship was determined to be

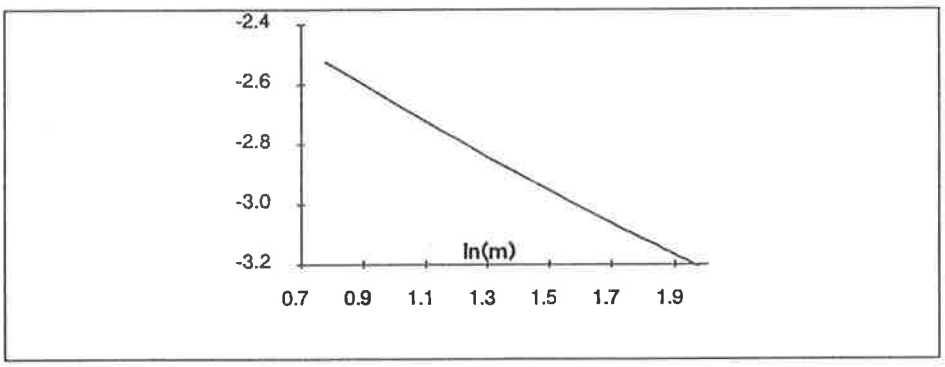

Figure 6.5 *The accuracy of the second derivative extraction by LSPP increases (decreasing error) as the number of data points used to represent the band increases. This figure shows experimentally determined error, ln(s), in the second derivative as a function of ln(m) (the convolution width, β = 2m+1). The ratio of $m/n\sigma$ was held constant at 1. In spectral terms this means that once an optimum convolution width parameter (β, expressed in nm) has been determined, the higher the resolution (more points/nm) the better the LSPP will work.*

..6.1

$$s_{(\sigma)} = e^{(-0.56\ ln(n\sigma) - 2.11)}$$

where $s_{(\sigma)}$ is the RMS error in the extracted second derivative. A band limit parameter of $\theta = 6\ \sigma$ describes the entire band for practical purposes.

It is important to consider the case of bands represented with very few points. It is impossible to reduce the convolution width parameter of a third order LSPP derivative convolution below 5 points (m=2). The effect of reducing the β/σ ratio to beyond certain limits can be seen by comparing figures 6.6 and 6.7. For a constant band width, as the convolution width increases so the derivative will be smoothed out more and more to the point depicted in figure 6.7, where the derivative is actually broader than the band! Therefore if the data are too coarse (very granular) in the time domain then band narrowing by derivative procedures is not possible. This also applies to all of the other procedures I have studied: There is an absolute minimum requirement of spectral resolution below which no band narrowing (spectral enhancement) is possible. For the present it is clear that the absolute minimum for some band narrowing using LSPP is 7 points per band (figure 6.6 $n\beta$=7).

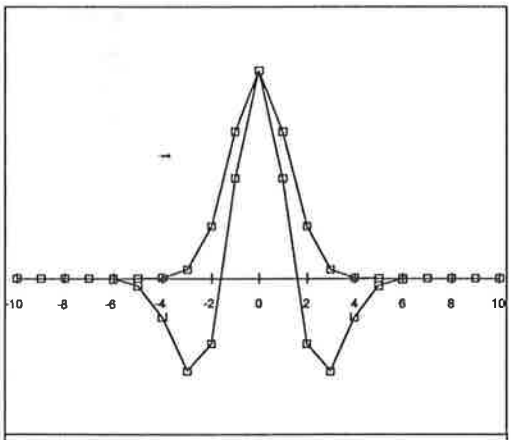

Figure 6.6 *A band with a width of $n\sigma$ = 1.33can just be narrowed by LSPP differentiation. The convolution width used here ($n\beta$ = 5) is the minimum possible for a third order second derivative polynomial.*

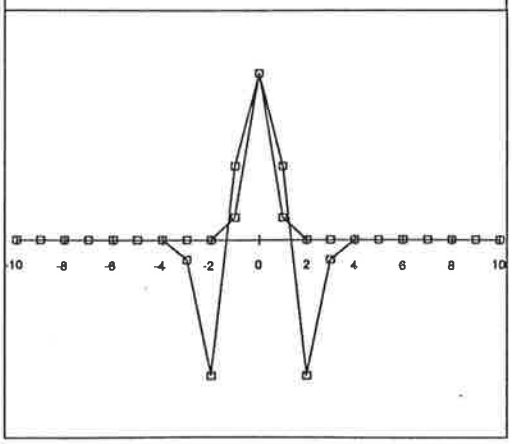

Figure 6.7 *For very narrow bands, the derivative generated by the procedures described in this chapter is actually broader than the original band. This band shown has a $n\sigma$ = 0.5.*

In the next experiment the band width was fixed and the convolution width was varied. The error in the derived derivative is plotted against the width ratio defined as $wr = \frac{m}{n\sigma}$. As the ratio increases much above 1 (the convolution width is wider than the band width), the derivative becomes smoother. This smoothing introduces an error and as figure 6.8 shows, it is better to use the narrowest convolution width possible. The error due to smoothing depicted in figure 6.8 is

$$E(wr) = e^{(2.1\ ln(wr) - 2.9)} \quad ..6.2$$

Combining these equations we can arrive at an equation which given band and convolution widths predicts the RMS error due to smoothing alone (no magnitude granularity yet).

Magnitude granularity

Magnitude granularity is a much more serious problem than time granularity. In the time domain (wavelength or wavenumber for spectra) there are discrete points, and a minimum interval at which data may be collected. Nevertheless the location of these points is accurately defined with little error associated with their position (the spectral accuracy always significantly exceeds the minimum selectable interval between data points). This is not the case for the response (magnitude). Given an accurately selected wavelength the possible response (absorbance) is continuous. Therefore the granularity introduced by the A/D conversion introduces a considerably larger error than the error in the selected wavelengths. In essence, although the time domain is granular it is not in error whereas the response domain granularity represents an error.

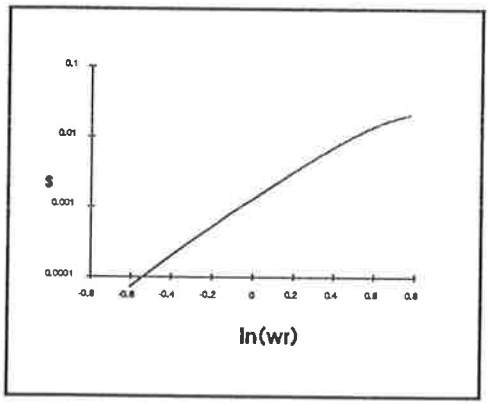

Figure 6.8 *As the convolution width parameter, β, increases for a fixed band width, nσ, so the error in the derivative increases. These results were obtained with a band width, nσ = 20, using a noise free band. The error introduced as β increases is due to smoothing and is accompanied by a decrease in S/N of the derivative for noisy data as shown in figure 6.10.*

Described more formally: A spectrum is described by two variables. Experimentally either variable can be very accurately defined for some set of equally spaced but fixed values. With only

one degree of freedom only one variable can be accurately known (set) so that the second variable will only be approximated within the resolution for that variable.

All spectrophotometers use wavelength as the input variable and the absorbance as the output variable. It would be quite easy to construct a spectrophotometer with the absorbance as the input variable and the wavelength as the output variable. However this would not improve the overall performance or quality of experimental spectra.

Given the high accuracy (20 bit resolution) of modern research instruments, it is worth considering the reasons why the spectral bands recorded may have a significantly lower resolution. Firstly the full resolution is scaled to cover the maximum absorbance range of the instrument. On most high quality research instruments this will be an absorbance of -0.5 to 4. This means that an instrument with an absorbance maximum of 4.0 and a 20 bit A/D converter will only have 18- bit resolution for a peak absorbance of 1.0. In any relatively complex spectra (in a liquid phase), the spectral envelope will be the summation of many overlapping spectral bands. Typically a single isolated band may only have an absorbance maximum of 5% of the envelope. This now reduces the resolution for that single band by another 4+ bits to 14- bits. It is quite likely that for any number of reasons it may not be possible or desirable for the absorbance to exceede 0.1, which now means that our average spectral band has approximately only 10 bits resolution. Should we be interested in a minor band or if the instrument does not employ the highest quality 20 bit A/D (some older machines have as low as 12 bit A/D's, although 16 bits is common) then the number of bits resolution per spectral band may drop to 5-9 bits.

Clearly it is sensible to consider the performance of band narrowing techniques for resolutions of 5 bits upwards to cover all eventualities.

Figure 6.9 and 6.10 show the error in deriving the second derivative for varying magnitude (number of bits) granularity as a function of *ln(wr)*. Figure 6.9 is a log:log version of figure 6.10 and demonstrates the superposition of the time and magnitude granularity effects which have approximately equal slopes of opposite signs.

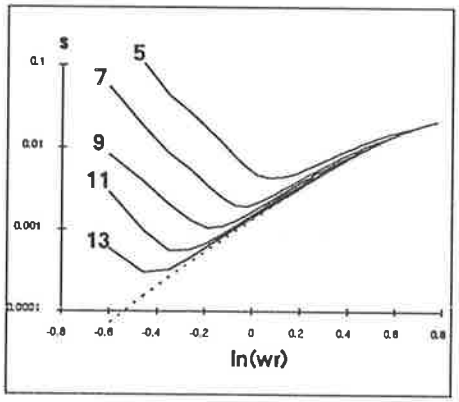

Figure 6.10 *The error in the derivative is determined by two factors. One is the error due to smoothing, shown by the dashed line, which is the same as in figure 6.8. The second is due to noise, represented here by decreasing bits resolution. The results obtained here (and elsewhere) are the same when random noise of equivalent peak-peak (p-p) excursion is used instead of significant bits resolution (ie 5 bits resolution = p-p S/N of 32). All other parameters were identical to those used to generate figure 6.8.*

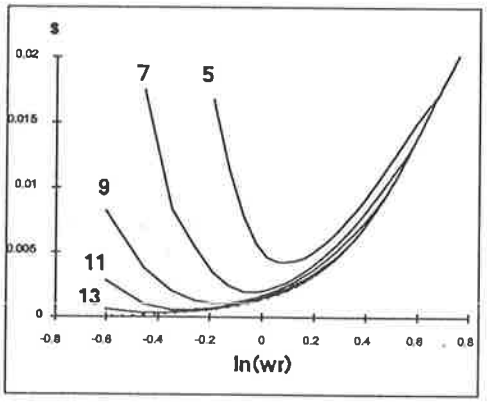

Figure 6.9 *This figure is the same as figure 6.10 with a linear y axis (error). It serves to highlight the VERY rapid degradation of the derivative away from the optimum* $(\frac{\sigma}{m} = 1)$ *at lower resolutions (higher S/N).*

Extrapolating the error contours in figure 6.9 from the left (small convolution width) gives a set of zero intercepts plotted in figure 6.11. The average slope of these extrapolations is -2.7. The expression describing figure 6.11 is

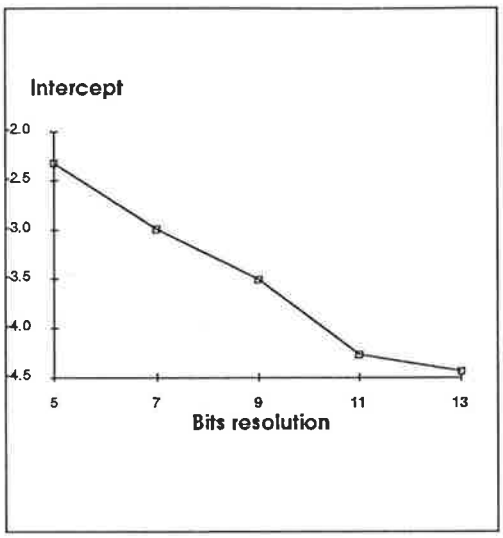

Figure 6.11 *The $ln(m/\sigma) = 1$ intercepts of the data (extrapolations of the resolution error from smaller ln(wr)) depicted in figure 6.10 are plotted here. As described in the text this figure demonstrates the relationship between the increasing error and the reducing S/N (increasing bits resolution) for any given ratio of* $\frac{m}{n\sigma}$.

..6.3

$$E(\text{intercept}) = e^{(-0.33\ \text{intercept} - 0.65)}.$$

From this equation it can be seen that the error contribution from magnitude granularity alone (ignoring the effects of smoothing; convolution width) is proportional to $e^{N/3}$ where N = the number of bits resolution.

For any given number of significant bits resolution the error is proportional to $e^{-2.7\ ln(wr)}$ for (convolution width < band variance), and $e^{2.1\ ln(wr)}$ for (convolution width > band width).

The exact form of these relationships is not as important as the trends and their practical impact. The net conclusion is that there is an optimum *wr* ratio of 1 for the best results over a wide range of band & convolution widths, and significant bit resolution. Furthermore the lower the number of significant bits (lower S/N) the more critical is to select the correct convolution width. Finally as the number of significant bits exceeds 12, the convolution width selection becomes less critical, with smaller widths being better.

Using a convolution width of 1.0 nm: Figure 6.1 at the begining of the chapter depicts the spectral enhancement of the solution spectrum of benzene in ethanol, and compares it with the vapour phase spectrum.

BAND NARROWING

Introduction

There are fundamental differences between LSPP and FFT procedures which render any attempt to compare the two techniques directly difficult. Both techniques are applied here to the enhancement of spectra and yield similar results. However the LSPP are designed to extract a well defined function of spectral bands (the second derivative) while (practical) FFT methods are designed to narrow the bands only, without predetermining the output band function. Both methods are constrained by noise gain and smoothing errors. However, while the accuracy of the LSPP methods can be assessed by comparison with a known band function, the FFT procedures developed here have no single output band function as a goal. Some initial trial comparisons of LSPP and FFT methods both performing second derivatives proved futile (an FFT based approach to second derivative generation fares very badly compared to LSPP procedures).

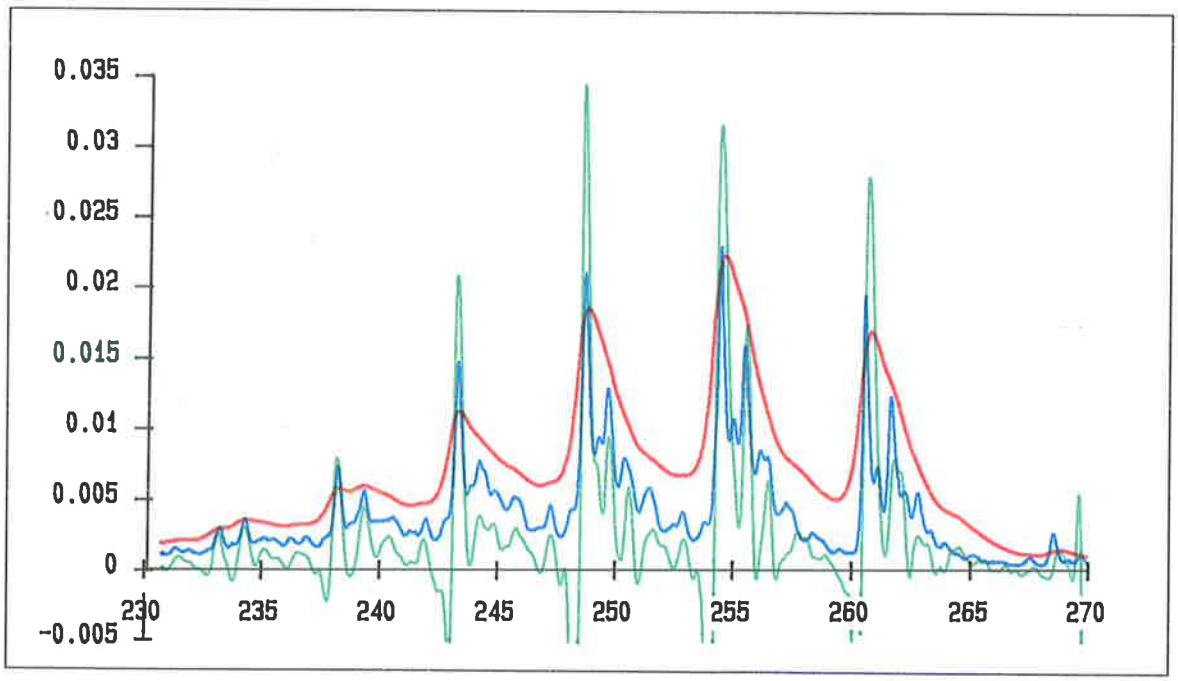

Figure 7.1 *The enhanced spectrum (green), derived from the solution spectrum (red), closely matches the vapour phase (blue) spectrum. The enhanced spectrum was generated with a Gaussian filter nf = 75, nγ = 23 as described in the text. The vapour phase spectrum was measured under nitrogen against a nitrogen reference at 90 C. Benzene was dissolved in ethanol for the solution spectrum which was referenced against ethanol at 25 C. The spectra were collected on a Varian Cary 3 spectrophotometer: slit band width 0.6 nm (solution spectra) and 0.2 nm (vapour phase spectra); resolution 0.02 nm; samples averaged 33 (vapour phase, 1 second) and 198 (solution, 6 seconds / wavelength step). The solution spectrum was recorded with a larger slit bandwidth and more points averaged to increase the S/N to a level where spectral enhancement is possible.*

It is a decidedly non-trivial task to design and carry out meaningful tests of the relative performance of the various FFT filters developed. This chapter chronicles two major tasks: First the development of the concept of, and practical approaches to, ideal band narrowing; and Second the implementation and evaluation of the filters developed.

The net result is shown in figure 7.1. Close comparison with the equivalent figure illustrating the LSPP method and shown at the beginning of the last chapter reveals a significant improvement. What is not obvious from this figure is the robust nature of the filter used and its excellent performance with respect to S/N maintenance for a given degree of spectral enhancement.

Fourier methods

Ideal smoothing and band narrowing.

As noted earlier, convolution and deconvolution in the Fourier domain simply involves the multiplication or division of the successive members of each function. With this simple fact in mind I will address the next question.

What is the ideal (gaol) in spectral enhancement, given that the source spectrum consists of overlapping Gaussian bands?

The answer is: To narrow the band widths, without distorting their shape or area, to an extent that the majority of the bands no longer overlap.

The LSPP covered in the previous section distort the band shapes and areas. In addition any derivative method will introduce extra peaks in the form of side lobes.

Using Fourier methods I have devised a way of narrowing the bands without changing their form or area. Unfortunately the method is not applicable in its pure form to real data as it is very sensitive to high frequency noise. However the approach does provide a general method for smoothing any data of known function without distorting the function form or area.

Let $f(x)$ be the source function of some known form. Let $f_n(x)$ be a function of the same form and area as $f(x)$ but with a narrower bandwidth.

We seek a transforming function which, by convolution, relates $f_n(x)$ to $f(x)$.

If the Fourier transforms $F_n(\alpha)$ and $F(\alpha)$ of the function exist then the problem is solved in the form [1]

$$F_n(\alpha) = F(\alpha) \cdot T(\alpha) \qquad ..7.1$$

where $T(\alpha)$ is the transforming function sought in the Fourier domain.

We now consider $f(x)$ and $f_n(x)$ to represent Gaussian bands of the same area differing only in bandwidth. Centred at x=0 and normalised to unit area the functions are given explicitly as

$$f(x) = \frac{1}{\sigma\sqrt{2\pi}} e^{-\frac{1}{2}\left(\frac{x}{\sigma}\right)^2} \qquad ..7.2$$

$$f_n(x) = \frac{1}{\sigma_n\sqrt{2\pi}} e^{-\frac{1}{2}\left(\frac{x}{\sigma_n}\right)^2} \qquad ..7.3$$

Here the parameters σ and σ_n define the bandwidths. For example, the bandwidths at half maximal intensity are given by $\sigma\sqrt{(8ln(2))}$ and $\sigma_n\sqrt{(8ln(2))}$, respectively.

The corresponding Fourier transforms are evaluated (appendix A) as

$$F(\alpha) = e^{-\frac{1}{2}\left(\frac{\alpha}{\gamma}\right)^2} \qquad ..7.4$$

$$F_n(\alpha) = e^{-\frac{1}{2}\left(\frac{\alpha}{\gamma_n}\right)^2} \qquad ..7.5$$

with $\gamma = \sigma^{-1}$ and $\gamma_n = \sigma_n^{-1}$. The independent variables in the two domains are related by

1 R.N. Bracewell, The Fourier Transform and its Applications, 2nd ed., 1978, McGraw-Hill, New York, p. 108

..7.6

$$x = \frac{2\pi}{\alpha}$$

Thus the Gaussian function has the important property of having the same form in both the Fourier and time domains. As the Gaussian function is always non-zero in both domains, a transforming function must exist and is given by

..7.7

$$T(\alpha) = e^{-\frac{1}{2}\alpha^2\left(\frac{1}{\gamma_n^2} - \frac{1}{\gamma^2}\right)}$$

..7.8

$$= e^{\frac{-1}{2}\alpha^2\left(\sigma_n^2 - \sigma^2\right)}$$

For smoothing (band broadening), $\sigma_n > \sigma$ and $T(\alpha)$ has the form of

..7.9

$$e^{-\alpha^2}$$

For enhancing (band narrowing), $\sigma_n < \sigma$ and $T(\alpha)$ has the form of

..7.10

$$e^{\alpha^2}$$

For $\sigma_n = \sigma$, as required, $T(\alpha) = 1$.

Since a Gaussian function retains its form in both the time and frequency domains, it is evident that convolution of a Gaussian function with another (unity area) Gaussian function results in ideal smoothing. That is: with no distortion of shape or area; the only parameter affected is the band width, σ, which increases. This method is practical and works well on real world data.

Unfortunately the converse process of ideal band narrowing, as given above, is not practically applicable for any significant narrowing. The reason for this is the exponentially increasing frequency response required for ideal band narrowing. If left unchecked, an exponentially increasing frequency response results in an output of effectively pure noise. However, accepting that we live in a real world where the source data are already compromised, there is a way to closely approach ideal band narrowing. The question that requires answering is: Can the high frequency response be attenuated in a way that does not significantly detract from ideal band narrowing, and is this practical to implement? The answer is almost; but there is a complex trade-off between S/N, band narrowing and band distortion (side lobes). To achieve band narrowing of noisy data some combination of S/N degradation and band distortion must be accepted. A choice between S/N degradation or band distortion can be selected at will. It is even possible to band narrow and

increase S/N at the same time, but the trade off is significant band distortion (side lobes).

Practical band narrowing.

Consider smoothing first: While the signal (Gaussian) in the Fourier domain falls off with increasing frequency, the noise spectrum remains flat (for white noise) at all frequencies. Beyond some upper limit the Fourier power spectrum effectively contains only noise. Clearly we can ignore this noise using a cutoff filter to limit the frequency response. If the cutoff is set at a frequency where the S/N is below 2 then there will be no significant loss of information at the same time as the noise is reduced. Even with such a cutoff filter it is not possible to implement an exponentially increasing frequency response. The reason is that the last points just before the cutoff are given the most weight and also contain the most noise. This results in an unacceptable degradation of the overall noise content.

Briefly then the problems caused by sharp cutoff filters are: the greatest weight is given to the frequency just below the cutoff; this one frequency may now dominate the entire filtered spectrum. In the extreme we end up with a notch filter (the ultimate bandpass filter) which passes only one frequency. Unless the source data was a pure sinusoid of this frequency then this filter is useless.

Clearly the frequency response must be attenuated smoothly to reach zero response at the cutoff point. Ideally attenuation should match the rate at which the S/N falls off. Obviously the S/N will decrease at the same rate as the function decreases. Thus for a Gaussian band we arrive at an attenuation filter which we demonstrated earlier is the ideal smoothing filter: the Gaussian itself of the general form given by equation 7.2.

Turning next to band narrowing, the ideal response to narrowing a Gaussian is given by equation 7.9. However, if one combines the real smoothing function with the ideal narrowing function the two cancel; for a Gaussian band it is not possible to implement ideal smoothing and ideal band narrowing simultaneously. One is obliged, therefore, to consider non-ideal filter functions.

The ideal smoothing and narrowing functions do not alter the shape of a Gaussian band. This is no longer true for any other filter function; relative to the ideal there will be an increased frequency response centred at some frequency, f, say, in the Fourier domain. On convolution with a Gaussian band, and transformation back to the time domain, this will have introduced a cyclic modulation, of frequency f in

the Gaussian band. This modulation will generate side lobes, such as those seen in the even derivatives of the band.

Filter Functions.

In this work I compared the effect of three distinct filter functions (which approach the ideal in different ways) on band narrowing of Gaussian bands.

The first filter function to be considered here is based on requiring the optimum form of band narrowing, equation 7.9, at low frequencies; the optimum form for smoothing, equation 7.10, at high frequencies and a gentle transition between the two forms. A filter function fitting these requirements is a Gaussian band, denoted by $FG(\alpha)$, centred at some non-zero frequency, f, referred to as the peak location.

Explicitly, the filter function is

$$FG(\alpha) = \exp\frac{-1}{2}\left(\frac{\alpha - f}{\gamma_f}\right)^2 \qquad ..7.11$$

Instead of the band width parameter, γ_f, it is more convenient for the computations to use a "gain factor", g, defined by

$$g = \frac{FG(f)}{FG(0)} \qquad ..7.12$$

and related to the band width parameter of the filter function by

$$\gamma^2_f = \frac{f^2}{2\ln(g)} \qquad ..7.13$$

The effect of the filter, in addition to smoothing and band narrowing, is the superposition of a cosine function on the Gaussian; if the original Gaussian is the function $Z(x)$ then, as shown in appendix B, the resultant function will be of the form:

$$Z(x) \,.\, \cos f(x) \qquad ..7.14$$

The second filter function may be called the Fourier derivative filter and has the form similar to that recommended by Cameron and Moffatt[1].

..7.15

$$FD(\alpha) = \alpha^{\pi}\, sinc^{2}\left(\frac{\pi\alpha}{C}\right)$$

where the smoothing function is defined by $sinc(x) = \sin(x)/x$, C is the cutoff points for smoothing and p is the EVEN derivative power (for example, p=5 is a smoothed 6th derivative).

The third filter function is a combination of the ideal smoothing form, equation 7.10, with a band narrowing form of a lower power than the ideal according to equation 7.9:

..7.16

$$FE(\alpha) = \exp^{\alpha - \left(\frac{1}{2}\left(\frac{\alpha}{\gamma f}\right)^{2}\right)}$$

In the following sections the results using the three filter functions on band narrowing of a Gaussian band will be described. The Gaussian band used for the comparisons was of unit height with $n\sigma = 20$ in a 256 point data set; all points were used in calculating the Fourier transforms.

The Gaussian filter, $FG(\alpha)$, and the derivative filter, $FD(\alpha)$, each require the choice of two parameters. These filters were first examined independently in order to find the optimum values of the parameter f, the optimum Gaussian filter peak location and C, the derivative cutoff point. Subsequently the parameters f and C were kept fixed at their optimum values and the three filters compared by varying only one parameter in each case: gain, g, for the Gaussian, power, p, for the derivative and smoothing, γf for the exponential filters respectively.

1 D.G.Cameron and D.J.Moffatt, Applied Spectroscopy, 1987, Vol. 41,539-544

Gaussian filter.

Initial tests to determine the valid extents over which the parameters should be varied indicated the following ranges:

Gain factors, g, of 10 to 100,000,000.

Filter peak location, f, of 5 to 20 units.

Figure 7.2 shows the relationship of band narrowing to filter peak location, f, for decreasing gain, a. It can be seen that the minimum reduced band width decreases with increasing gain and that there is an optimum filter peak location for any given gain factor. The minimum achievable reduced band width goes from 0.8 to 0.4 for gains of 10 to 100,000,000. The relationship between the minimum band width reduction possible and gain is shown in figure 7.3. Clearly it is extremely difficult to achieve 50% or better reduced band width.

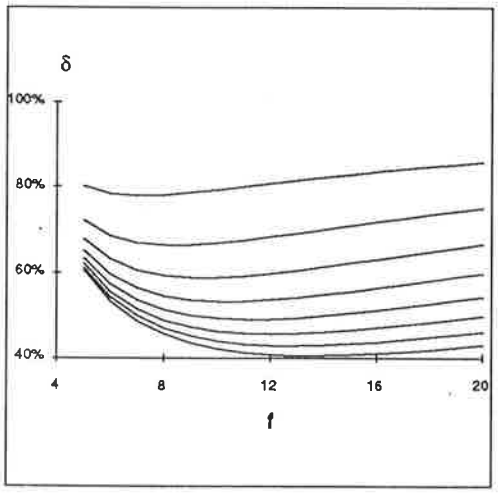

Figure 7.2 The reduced band width decreases as the amplification increases. From bottom to top the lines depict the reduced band width for decreasing log amplification of 8..1. For any given amplification there is an optimum (minimum reduced band width) filter position (f). As the amplification increases this optimum occurs at increasing filter position (f).

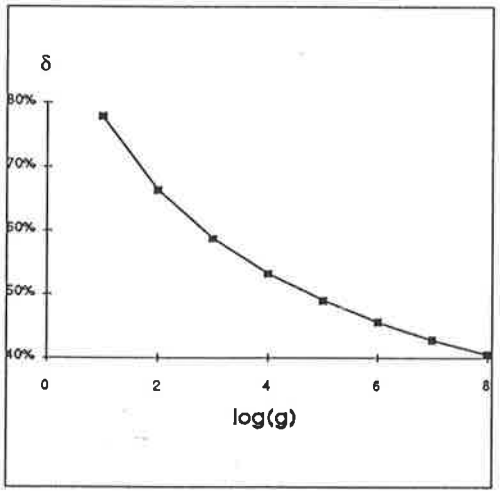

Figure 7.3 The minimum reduced band width for each amplification is shown. The values shown correspond to the minima for each amplification shown in the previous figure.

Figure 7.4 shows the relationship of band excess to filter peak location, f, for decreasing gain, g. It can be seen that the band excess decreases as the filter location increases for a given gain. For a given filter location the band excess increases as the gain increases.

Figure 7.5 superimposes the band excess at the specified gain values obtained from figure 7.4, on the band narrowing graph of figure 7.2.

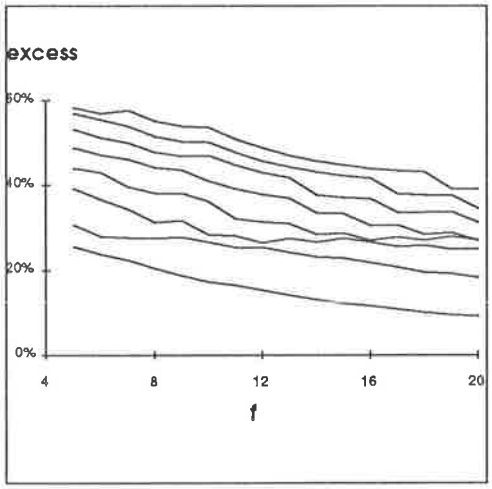

Figure 7.4 *The narrowed band excess falls off with increasing filter maximum and decreasing amplification. In increasing order the lines depict the peak excess for log amplifications of 1..8.*

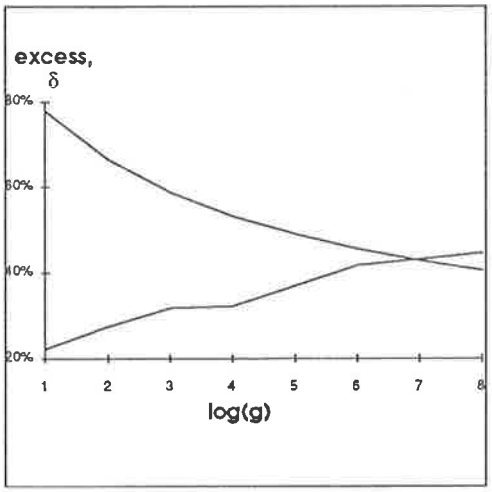

Figure 7.5 *This graph combines the reduced band widths (upper line) from the previous figure with the corresponding band excess (lower line). It can be seen that a reduced band width of 55% can be achieved before the band excess exceeds 40%.*

Figure 7.6 shows the relationship of S/N degradation to filter peak location, f, for increasing gain, g. As expected the noise increases with increasing filter location and gain.

For the parameters shown in figures 7.3 and 7.5, the S/N reduction is shown in figure 7.7.

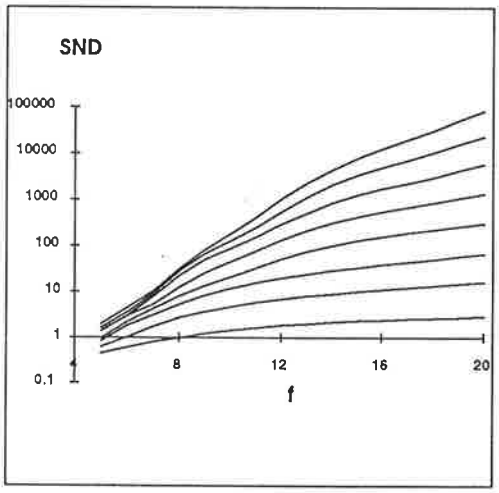

Figure 7.6 The S/N degradation, SND, increases as both amplification and filter location increase. From bottom to top the lines depict the SND for log amplifications of 1..8.

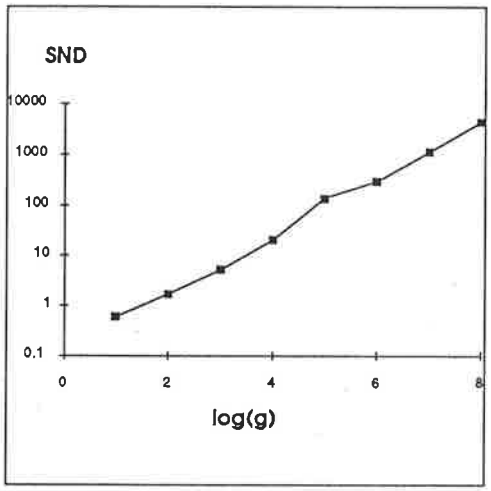

Figure 7.7 The log(SND) increases linearly with the log(amplification) for the optimal filter locations.

Derivative filter.

Initial tests to determine the valid extents over which the parameters should be varied indicated the following ranges:

Derivative powers, p, of 2 to 6 and $sinc^2$ cutoff points of 10 to 20 units.

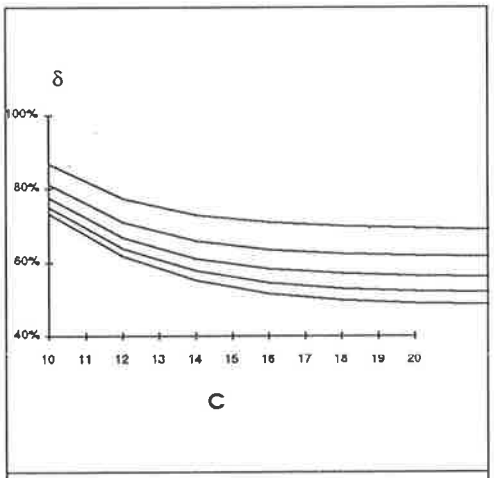

Figure 7.8 *The reduced band width continues to decrease as the $sinc^2$ smoothing cutoff point increases for any of the derivative powers shown. From bottom to top the reduced band width is shown for decreasing powers, p=6..2.*

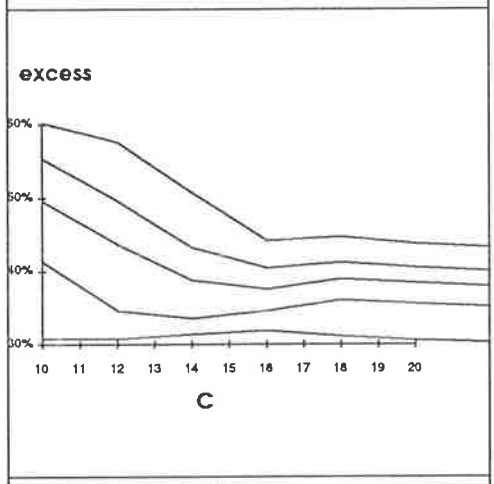

Figure 7.9 *The band excess decreases up to a smoothing cutoff of 16, after which the excess remains relatively constant. From bottom to top the lines represent increasing powers, p=2..6.*

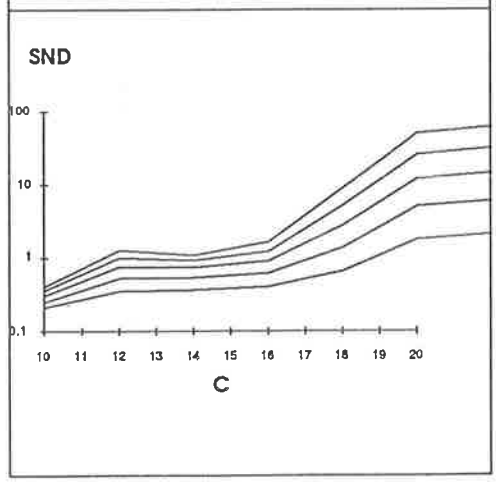

Figure 7.10 *Between filter cutoffs of 12..16, the S/N degradation remains relatively constant for all power derivatives. From bottom to top the lines represent increasing powers, p=2..6.*

The three figures 7.8, 7.9 and 7.10 depict the reduced band width, band excess and S/N degradation respectively. Of particular note is the relative flat region in the S/N degradation below a cutoff of 16 and band excess above a cutoff 16. Very clearly for a Gaussian band with $n\sigma = 20$ there is a optimum cutoff of 16.

Fixing the cutoff at 16, the results of this filter are summarised in figures 7.11 and 7.12.

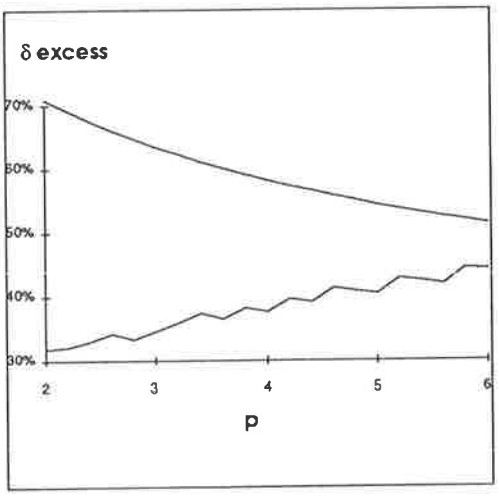

Figure 7.11 *Selecting a cutoff of 16 as optimal, the reduced band width (upper line) and band excess (lower line) are shown relative to derivative power.*

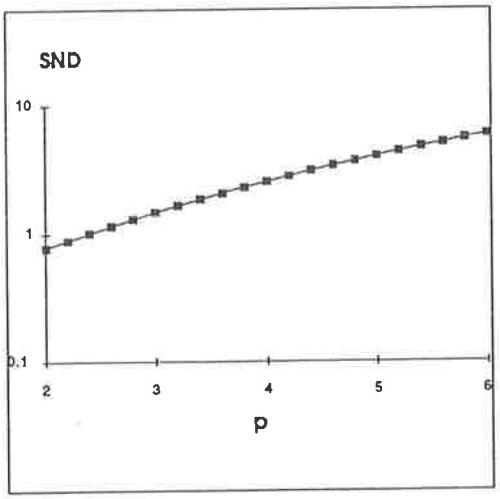

Figure 7.12 *For an optimal smoothing cutoff of 16, the S/N degradation rises logarithmically with linearly increasing derivative power.*

Exponential filter.

Initial tests to determine the valid extents over which the parameters should be varied indicated the following ranges:

Gaussian band width term, γ_f, of 2 to 5.5.

The larger value means less smoothing.

Figures 7.13 and 7.14 depict the reduced band width & band excess and S/N degradation respectively.

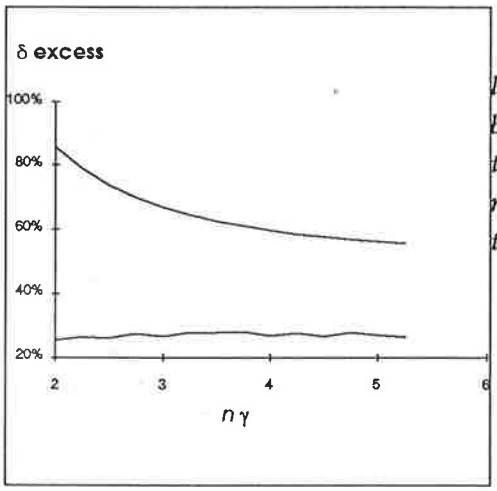

Figure 7.13 *The band excess (lower line) is independent (and low) of reduced band width (upper line) plotted against the Gaussian smoothing width, nγ. It is not practical to use this filter to reduce the band width below 70%.*

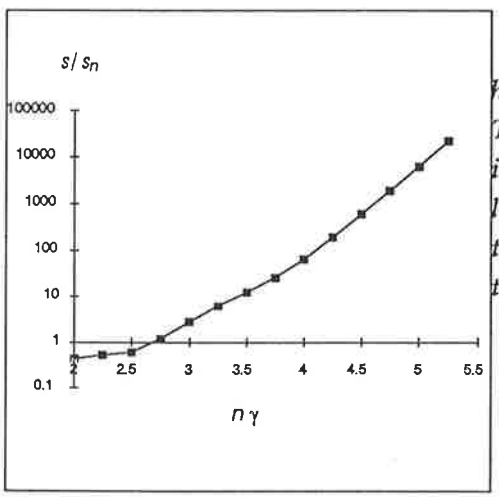

Figure 7.14 *The exponential filter has an extremely poor S/N performance. The increase of the log(S/N degradation) is roughly linearly proportional to the linear increase of the Gaussian smoothing width (increasing nγ = less smoothing).*

We know that a filter of the form e^{α^2} would not distort the band shape. As figure 7.13 shows, a filter of the form e^{α} slightly distorts the band. When the ideal smoothing function (the Gaussian) is applied, we find that the band distortion is independent of the degree of smoothing. Unfortunately the price to pay for the minor band distortion is a large degradation in S/N performance.

Comparative performances.

Figures 7.15 and 7.16 compare the performances of the three functions. For the derivative and exponential filters, the x axis represents derivative order and $n\gamma$ respectively. For the Gaussian filter the x axis represents 1.4log(g) + 0.25. This linear scaling of the log[g] term maps the band narrowing of the Gaussian filter almost exactly onto the band narrowing of the derivative filter making visual comparison of the two filters easier. No simple mapping relationship could be found for the exponential filter.

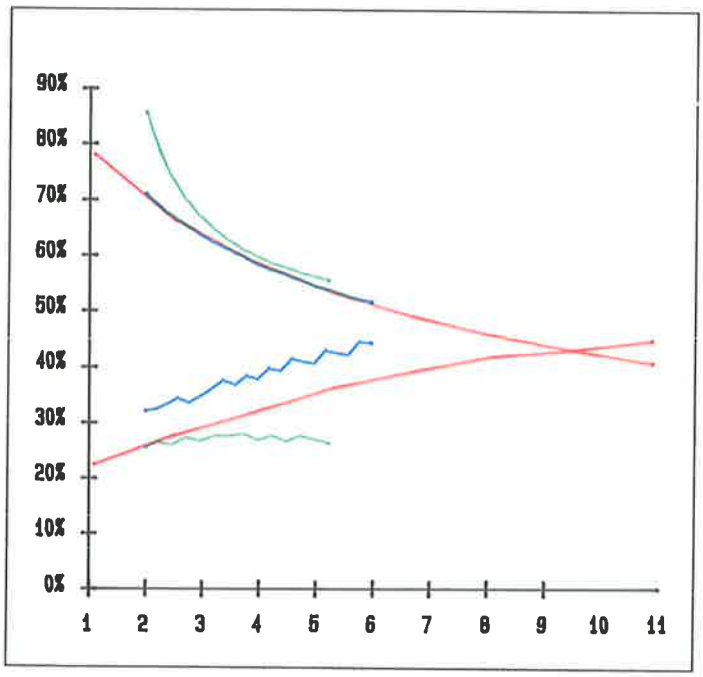

Figure 7.15 *The performance of the three filter types is compared; Gaussian (red), derivative (blue) and exponential (green). The upper curves in each case are the reduced band widths and the lower curves are the band excess. As noted in the text, there exists a linear relationship between amplification factor of the Gaussian filter and the power of the derivative filter for the same reduced band width. For each filter the x axis represents: exponential, $n\gamma$; derivative, power; Gaussian,* 1.4log(g) + 0.25

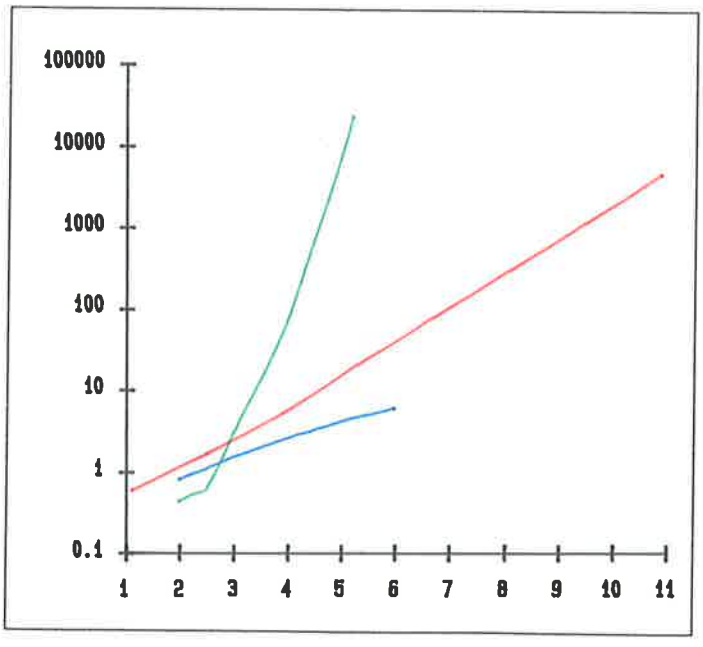

Figure 7.16 *The S/N degradation is shown in the same colour scheme and axis as for the previous figure.*

If S/N is not a problem and moderate amounts of band narrowing with minimum band distortion are required then the exponential filter is the best. However it would be extremely seldom that the amount of S/N degradation that this filter introduces could be tolerated.

The Gaussian and derivative filters appear to follow the same trends, the major difference being the trade-off between better band shape and greater S/N degradation in the Gaussian filter. It is important to note that the S/N of the source data can nearly always be improved while the band distortion cannot be changed for a given filter. Empirical tests indicate that a band excess of greater than 40% is intolerable. As the band excess rises above this point the side lobes become so large that for multi band data (real spectra) they become indistinguishable from true centre bands. Experience also indicates that a S/N degradation of just over 100 can be accommodated for spectra recorded on state-of-the-art instruments (with integration times of 2 to 8 seconds per point). This means that the exponential filter can be used to achieve reduced band widths down to 65%. Further band width reduction down to 50% can be achieved with the Gaussian filter. Due to severe band distortion, the derivative filter should not be used to achieve any more than 60% reduced band width. Where S/N is a limiting factor the derivative filter is generally best, although the trade-off is poorer band shape.

Discussion

The exponential filter is not practical because of its poor noise performance (very large S/N degradation). However it is interesting to note that an exponential combined with the ideal smoothing function gives a constant band shape regardless of the degree of band narrowing.

The Gaussian and derivative filters perform similarly, with the Gaussian trading band narrowing ability for S/N degradation relative to the derivative filter. Since there exists a simple linear relationship between the order of the derivative filter and the gain of the Gaussian filter, and also between the gain of the Gaussian filter and its optimum location, then: A single filter function can be constructed that is a weighted sum of the two filter types. Recalling the notations for filter parameters:

..7.17

γ = Gaussian filter band width.

..7.18

f = Gaussian peak location.

..7.19

C = Derivative filter $sinc^2$ cutoff.

..7.20

p = Derivative filter power.

..7.21

g = gain = $e\frac{1}{2}\left(\frac{f}{\gamma f}\right)^2$

and the input parameters defined as:

..7.22

σ = Gaussian band width.

..7.23

δ = reduced band width.

The following optima have been found for a Gaussian band with $n\sigma = 20$:

The optimum cutoff, C, for the derivative filter is 16 which is related to $n\sigma$ by:

..7.24

$$C = \frac{320}{n\sigma}$$

For a given gain, g, the optimum peak location, *nf*, of the Gaussian filter with *nsigma*=!20 is, by figure 7.2 approximately:

..7.25

$$g = 10^{(nf-6)}$$

so that, in general,

..7.26

$$nf = \left(\frac{20}{n\sigma}\right) * (log10(g)+6);$$

The relationship between the band narrowing, δ, and p, shown in figure 7.15 may be approximated by:

..7.27

$$log(\delta - 0.35) = -0.0886p - 0.28$$

so that,

$$p = \frac{log(\delta - 0.35) + 0.28}{-0.0886}$$

As shown in figure 7.15, the relationship between the derivative power, p, and the Gaussian gain factor, g, for the same band narrowing is:

..7.28

$$p = 1.4\ log10(g) + 0.25$$

Given all of these relationships we can now write all the necessary parameters entirely in terms of the two imput parameters $n\sigma$ and $n\delta$.

For the derivative filter:

..7.29

$$C = \frac{320}{n\sigma}$$

$$p = \frac{log(\delta - 0.35) + 0.28}{-0.0886}$$

For the Gaussian filter:

..7.30

$$nf = \frac{20}{n\sigma}\left(\frac{p}{1.4} + 5.8\right) = \frac{20}{n\sigma}\,(log10(g) + 6)$$

$$n\gamma f = \frac{f}{\sqrt{2log(e)(f+6)}}$$

Introducing an additional parameter, a weighting factor, τ, we can combine the Gaussian and derivative filters and write the equation describing "the general enhancing filter", $GF(\tau, n\delta, n\sigma; \alpha)$:

..7.31

$$GF(\tau, n\delta, n\sigma; \alpha) = FD(\alpha)\tau + FG(\alpha)(1 - \tau)$$

$$= \tau\alpha^p\, sinc^2\,(\pi\, \alpha/x) + (1 - \tau)\exp\frac{-1}{2}\left(\frac{\alpha - f}{\gamma f}\right)^2$$

Figure 7.17 shows the enhanced benzene spectra generated by applying the above general enhancement equation in conjunction with a windowed FFT algorithm. A significant number of spectra of differing samples have been analysed with this algorithm. In all cases a 100% Gaussian filter was found to be best. In general a reduced band width of 61% was optimum. With the reduced band width set at 61%, σ can be varied to include more high frequency components (smaller σ : larger γ = higher frequency) which increases the effective band narrowing. The optimum FFT window size was found to be the smallest available (64) with the current algorithm. This coresponded to 1 - 3 nm for the data sets examined to date.

The vapour phase spectrum of benzene was also enhanced and found to contain much fine detail not observed in the vapour phase spectrum (not shown here). The vapour phase spectrum shown in figure 7.17 is very moderately enhanced to aid in the comparison with the enhanced solution spectrum.

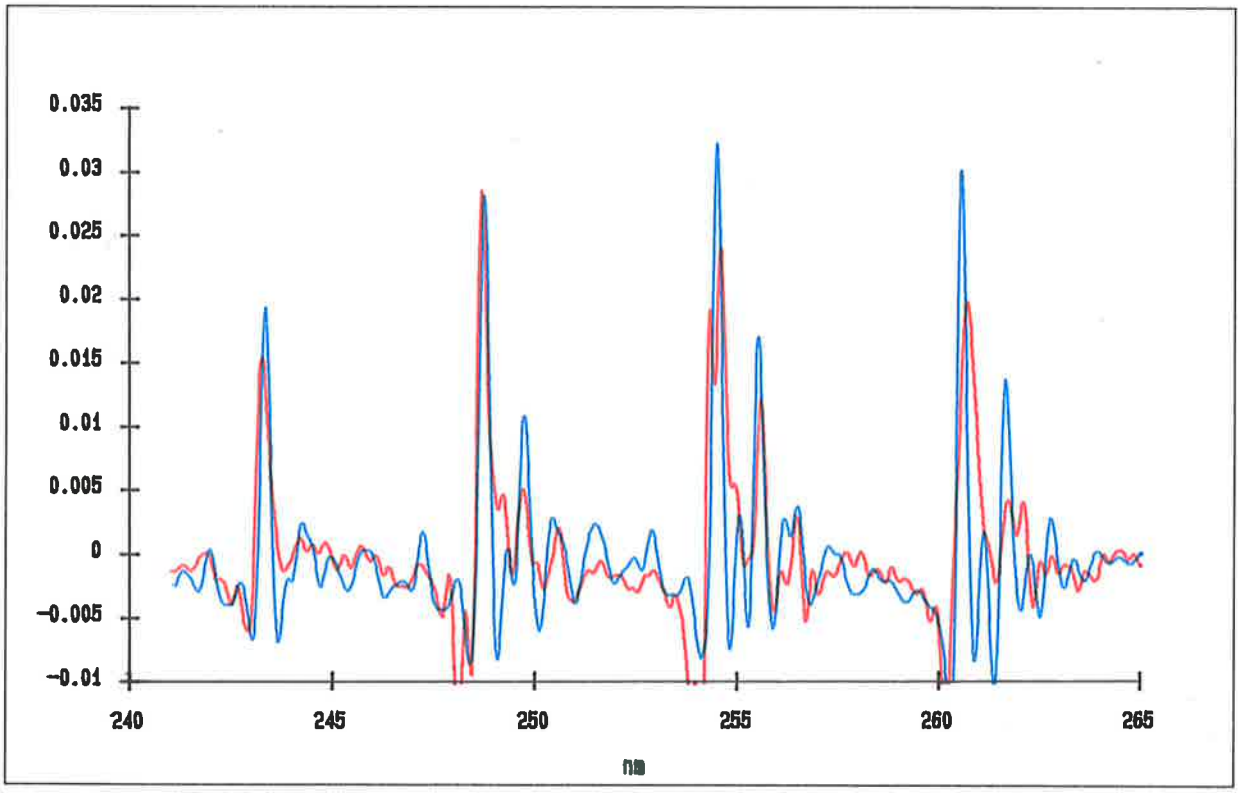

Figure 7.17 *THE ENHANCED LIQUID PHASE SPECTRUM closely matches the vapour phase spectrum. The vapour phase (blue) spectrum was moderately enhanced (FFT window=256, δ=0.75), while the liquid phase spectrum (red) was significantly enhanced (FFT window=256, δ=0.61).*

APPENDIX

(a)

We seek the Fourier transform $F(s)$ of the unit area Gaussian band centered at x = 0.

..7.32

$$F(s) = \int_{-\infty}^{+\infty} \frac{1}{\sigma\sqrt{2\pi}} e^{-\frac{1}{2}\left(\frac{x}{\sigma}\right)^2} e^{-2i\pi xs} \quad dx$$

$$= \frac{1}{\sigma\sqrt{2\pi}} \int_{-\infty}^{+\infty} e^{-\left(\frac{1}{2}(x/\sigma)^2 + 2i\pi xs\right)} \quad dx$$

If we put $r = \left(\frac{1}{\sqrt{2}}\frac{x}{\sigma} + i\sqrt{2}\sigma\pi s\right)$ with $dr = \frac{1}{\sigma\sqrt{2}}\,dx$, the integral becomes

..7.33

$$F(s) = \frac{1}{\sqrt{\pi}} e^{-2(\pi\sigma s)^2} \int_{-\infty}^{+\infty} e^{-r^2} \, dr = e^{-2(\pi\sigma s)^2}$$

This result may also be written, by defining $\alpha = 2\pi s$ and $\gamma^2 = \sigma^{-2}$, as

..7.34

$$F(\alpha) = e^{-\frac{1}{2}\left(\frac{\alpha}{\gamma}\right)^2}$$

(b)

We seek the inverse transform $Z(x)$ of a Gaussian function centered at $s = a$ in the Fourier domain

..7.35

$$Z(x) = \int_{-\infty}^{+\infty} e^{-2\pi^2\sigma^2(s-a)^2} e^{-2i\pi sx} \quad ds$$

$$= \int_{-\infty}^{+\infty} e^{-(2\pi^2\sigma^2(s-a)^2 - 2i\pi sx)} \quad ds$$

putting $r = \left(\sigma\pi\sqrt{2}(s-a) - \frac{i}{\sigma\sqrt{2}}x\right)$ with $dr = \sigma\pi\sqrt{2}\,ds$, we now have:

..7.36

$$Z(x) = e^{-\frac{1}{2}(x/\sigma)^2} e^{2i\pi ax} \frac{1}{\sigma\pi\sqrt{2}} \int_{-\infty}^{+inf} e^{-r^2} \quad dr$$

$$= \frac{1}{\sigma\sqrt{2\pi}} e^{-\frac{1}{2}(x/\sigma)^2} \cos(2\pi ax) \qquad \text{for real } Z(x)$$

PROTEIN ANALYSIS

The methods developed in the previous chapters have been applied to the analysis of the unfolding and purification of PGH. These reported analyses address the second and third hypotheses which are restated here.

The Second Hypothesis:

The amount of detail/information that can be extracted as a consequence of the "equal information hypothesis" is sufficient to identify individual tyrosine and tryptophan residues and their environments in complex proteins.

The Third Hypothesis:

The contribution to the spectra of proteins from phenylalanine residues can be extracted and quantified with sufficient accuracy to provide a method for the accurate quantitation of protein concentrations irrespective of normal conformational and environmental variations.

The second hypothesis would be supported if a single tyrosine or tryptophan residue could be identified in a protein containing several such residues. If it could be shown that the spectra of tyrosine and tryptophan were identical under all conditions then the hypothesis would be proven false. It is important to note that the second hypothesis does not claim that all tyrosine and tryptophan residues in a complex protein can be individually identified. This may be possible in some cases but certainly not in all cases.

The third hypothesis would be supported if the concentration of a protein solution was invariant as calculated from the enhanced phenylalanine spectrum when the pH was varied over a wide range and also as the protein was denatured with guanidine. Both of these conditions are known to change the conformation and spectra of proteins. 'Normal environmental changes' are defined as those conditions commonly encountered in protein chemistry and include: pH(1-13); Denaturant concentration (GuHCl 0-6M); Reducing agents (DTT); DNA contamination (0-2.5%). The third hypothesis would be proven false if any of these conditions/contaminants significantly affected the ability to quantitate the phenylalanine second derivative spectrum.

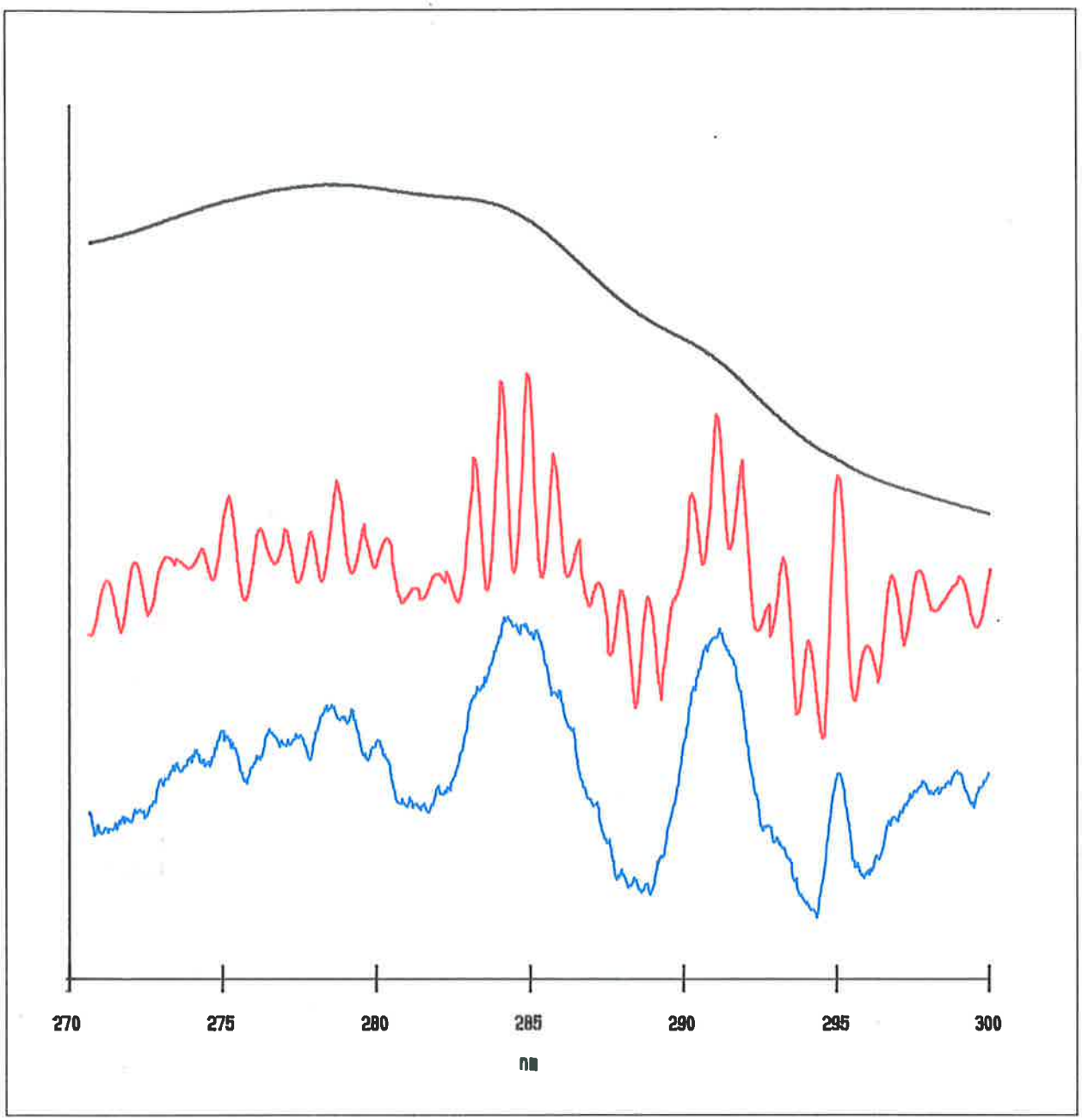

Figure 8.1 *THE NORMAL (black), ENHANCED (red), AND SECOND DERIVATIVE (blue) SPECTRA OF PGH. The derivative and enhanced spectra are optimised and constrained primarily by the S/N of the source data. Comparing with the enhanced spectrum, many of the bands can be seen as very minor features (inflections) in the derivative spectrum. The derivative spectrum was generated by LSPP methods; narrower convolution widths would provide greater resolution of bands but cannot be used due to unacceptable degradation in the S/N. The enhanced spectrum was generated using FFT methods with a pure Gaussian filter function and an FFT window of 64 points (0.04nm/point). The groups of bands seen in the enhanced spectrum coincide with the minor features ('bumps') in the normal spectrum.*

Results summary

Both hypotheses are amply supported by the data and analysis presented here. Using enhanced UV spectra I have demonstrated that at least two distinct steps are involved in the unfolding of PGH and that these two unfolding steps possibly involve separate (but overlapping) domains of the PGH.

Using the enhanced phenylalanine spectra it has proven possible to quantitate the protein irrespective of pH (1-13), denaturant (GuHCl 0-6M), DNA contamination (0-2.5%) and reducing agent contamination (0-10mm oxidised DTT).

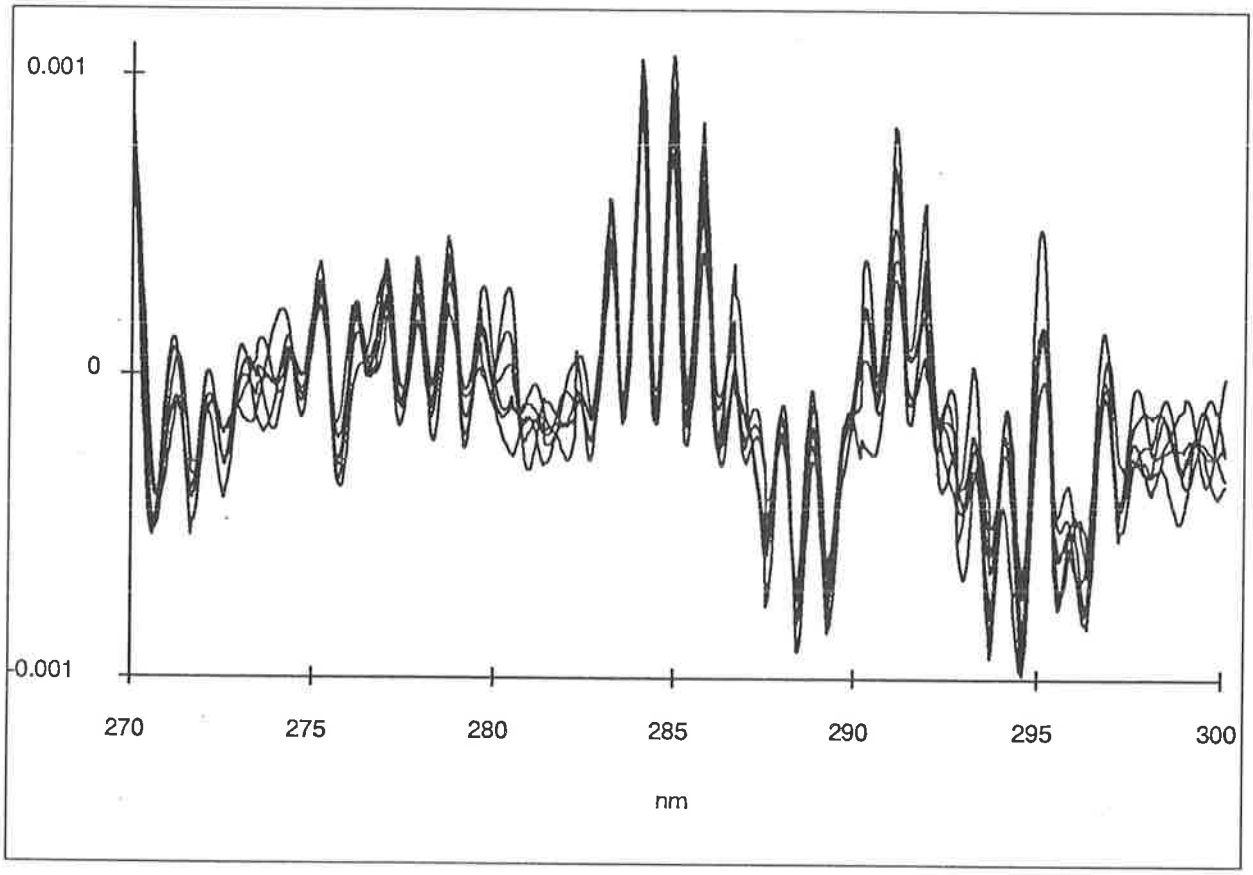

Figure 8.2 *ENHANCED SPECTRA OF SIX DIFFERENT PREPARATIONS show the reliability of the method. The spectra are of PGH (1mg/ml, 20mm Na Borate buffer pH9.1, 25 C) in varying [GuHCl] (0.25M, 0.5M, 1.0M, 1.25M, 2.0M, 2.1M). It is vital to demonstrate that this degree of enhancement yields reliable high S/N spectra which can be used for further analysis. Note the group of four peaks centred at 285nm. These peaks are not significantly affected by the denaturation of PGH and their peak locations are constant within 0.04nm (the resolution of the data) in all preparations from 0 to 6M GuHCl.*

Figure 8.1 shows a PGH spectrum, the second derivative and enhanced spectra. The amount of detail revealed in the enhanced spectrum exceeded all expectations. It is important to confirm that this degree of enhancement is reliably achievable and not prone to artifacts or poor S/N performance. Figure 8 .2 shows enhanced spectra of PGH in varying concentrations of GuHCl. Clearly the S/N is good and the enhanced spectra highly consistent. The important feature is the repeatability of these spectra and the reliability and precision with the 30+ bands can be identified. Many regions of the spectrum can be seen to be changing while others are unchanging. Over 30 individual bands can be observed between 270 - 300 nm. Detailed analysis of several regions within this part of the spectrum have shown that bands separated by as little as 0.8nm (figure 8.13) can be easily resolved. In addition, shifts of these bands by only 0.5nm are significant and easily detected (figure 8.13). In fact the four major bands between 284 - 287nm (whose position is not affected by denaturation) demonstrate a positional accuracy which equals (and may exceed) the resolution of the source data, 0.04nm.

Introduction

Measuring the conformational stability of proteins, and more specifically the unfolding/re-folding pathway, is of practical concern for two main reasons: First, because stability is usually the factor that most limits their usefulness [1] and Second, because very high level intracellular production of recombinant protein often results in the protein accumulating in a denatured form requiring subsequent refolding for activity. Commercial application of recombinant proteins often requires both of these problems to be addressed. In the case of PGH manufacture, the dissolution of insoluble inclusion bodies and the subsequent refolding are crucial for an economic process. Following refolding, long term stability in the form of slow release formulations is also vital for commercial acceptance.

Denaturation curves, such as figure 8.3, are used to determine the ΔG. Determination of the conformational stability requires measurement of the free energy change ,ΔG, upon denaturation. For a two state

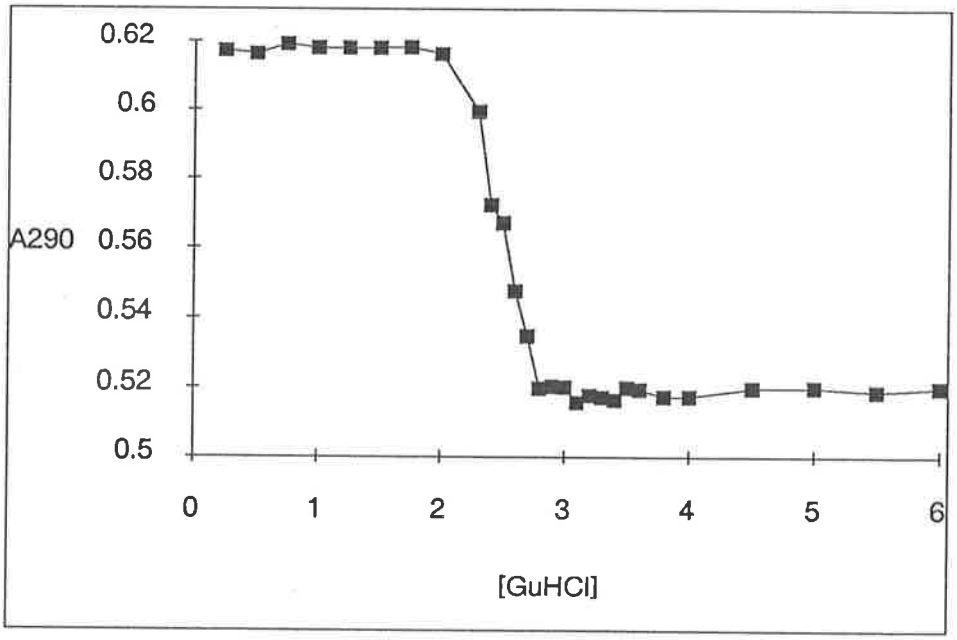

Figure 8.3 *THE ABSORBANCE OF PGH AT 290nm vs [GuHCl] shows a sharp hypochromic transition between 2.4 and 2.8M GuHCl. This crude measurement hides a complex interaction involving a number of different bands and transitions (both hyper/hypo-chromic, and wavelength shifts) occurring in this*

1 O'Sullivan, C. & Tompson, F. W. (1980) J.Chem.Soc.,57,834.

mechanism involving only folded and unfolded states Pace *et al* define ΔG as:

$$\Delta G = -RT \ln(K) = F_u / F_f \quad ..8.1$$

Where K is the equilibrium constant, F_u is the fraction unfolded (denatured), F_f is the fraction folded and $F_u + F_f = 1$. It can be seen in figure 8.3 that ΔG varies linearly with denaturant concentration over a short range. The simplest method of estimating the stability in the absence of denaturant is to assume that this linear dependence continues to zero concentrations and to use a least squares analysis and extrapolate from this linear region back to zero denaturant concentration.

Referring to denaturation studies, workers in the field often state something similar to this: "These experiments sometimes reveal additional features of a protein such as the existence of domains or the presence of stable folding intermediates" [2]. While this is true, it implies a general limitation in the data that often does not exist. A more accurate statement would be: With appropriate analysis and good quality data, denaturation studies nearly always reveal additional features of a protein, such as multiple unfolding events and domains. Let us consider this, and the ramifications for spectral enhancement further.

Proteins are complex molecules, with biologically active species varying in size from as few as several amino acid residues to thousands of residues. Of particular current commercial and research interest are extracellular hormones. These proteins tend to fall into the 5,000 to 50,000 Mw (50-500 amino acid residues) range; are often globular; and may have more than one domain.

The number of widely employed spectroscopic techniques that are applied to the analysis of such proteins is mercifully short. Most widely applied are the spectral techniques involving: UV absorbance, fluorescence, circular dichroism, light scattering and refractive index. The last two of these measurements (light scattering and refractive index) are typical of "bulk phenomena" which involve the behaviour of the entire protein as essentially a single entity. (Other similar examples of bulk phenomenon techniques would be settling velocity & hydrodynamic radii measurements and chromatographic or electrophoretic migration patterns.) In contrast, the techniques of UV absorption, fluorescence and circular dichroism are capable of giving information regarding the fine structure within a protein. This is because these techniques detect single amino acids and their summed result within any protein. Sometimes, with the right protein and technique, it may be possible, with fluores-

2 N Pace *et al*. Protein Structure: A Practical Approach". ed T.E Creighton (1989) IRL Press, Oxford. ch 13, p 311

cence for example, to tune into a unique amino acid (such as tryptophan). Even in such circumstances, this type of technique is still providing "fine detail" in the respect that even if only one chemical group is targeted this does not necessarily reflect the state of the entire protein but only the local microenviroment of the group being detected.

I have chosen a Guanidine Hydrochloride denaturation study to explore the amount of information the new spectral enhancement techniques, developed in the preceding chapters, can yield. Figure 8.3 shows the absorbance at 290nm for varying GuHCl concentrations. This figure is typical of the extent of information gained from absorption spectroscopy in denaturation studies to date. It conveys no information whatsoever about the underlying phenomenon. In particular it does not indicate whether a single or multiple site phenomenon is being observed. The next section of this chapter will examine the fine detail obtainable from the enhanced spectra. While preliminary and general conclusions regarding the unfolding of PGH are given, the main intent is to demonstrate the amount and quality of detailed information available from enhanced spectra.

PGH has 12 phenylalanine, 7 tyrosine and 1 tryptophan residues which make up for the vast majority of the UV absorbance (240-300 nm). As noted in the introduction to this section of the thesis, the contribution from phenylalanine was expected (and was found to be) independent of conformation. The 265-305nm region of the spectrum is dominated by the tyrosine and tryptophan contributions and, as expected, contained bands that were highly dependent on conformation.

PGH unfolding.

Brems et al. and others have published a considerable number of papers describing the use of UV absorbance and second derivative spectra in denaturation/refolding studies of BGH. In all these reports the most detailed information extracted from this and supporting data was the presence of a single 'associated' intermediate. The absorbance of PGH at 290nm (figure 8.3) indicates a single unfolding phenomenon with a mid point at 2.7-2.8 M GuHCl. This is similar to BGH, which Brems demonstrates has a mid point of 3.5 M GuHCl.

In the following table the column headings denote: Variable = indicates if the band changes in some way as the PGH in denatured; λ_n = the band position in native PGH (0M GuHCl); λ_i = the shifted band position at intermediate [GuHCl]; T1 = the [GuHCl] of the first transition seen for that band; T2 = the [GuHCl] of the second transition seen for that band; Group = grouping of bands by proximity.

As an initial step in the analysis of the enhanced spectra, the spectral band positions (from data shown in figure 8.1) from 270 to 300 nm were tabulated. With the data set used here, above 300nm the S/N ratio is too poor to confidently locate specific bands. The region below 270 is dominated by phenylalanine and is relatively unchanging. Of the 43 bands identified, 21 were found to change significantly as the PGH was denatured (variable bands). I have grouped most of the bands into 4 groups, A-D, based simply on proximity initially. Groups C and D were clearly observed to shift (wavelength) as the PGH is denatured. All other bands exhibit changes in intensity as the PGH is denatured. There appear to be several hyper variable regions which, due to rapid changes and perhaps poor S/N, defied attempts to reliably identify specific bands and their movement (mean band locations are given in the table). The accompanying table identifies the bands (in native PGH), their shifted positions and whether they change (variable bands) as the PGH is denatured (asterisked bands). Of the 21 variable bands, the intensities of 17 (vs. changing [GuHCl]) were examined closely and the transition points ([GuHCl]) annotated in the table. Of these 17 bands, 7 exhibit 2 transitions; or, expressed alternatively, 7 exhibit involvement in a three state unfolding with an observable intermediate state between native and denatured states.

Number	Variable	λ n	λ i	T 1	T 2	Group	Comments
1		271.2					
2		273.3					Hyper variable.
3		274.3					Hyper Variable.
4	*	275.2		2.4-2.7	3.4-3.7	A	
5	*	276.1		2.4-2.8	2.8-3.1	A	
6	*	276.9		2.7-3.1	3.4-4.0	A	
7		277.8				A	
8	*	278.7		2.2-2.8		A	
9	*	279.6		2.3-2.8		A	
10	*	280.2		0.0-1.5	2.5-2.8	A	
11		280.8					Hyper variable.
12		281.4					Hyper variable.
13	*	282.3		1.8-3.6			
14	*	283.3		2.4-2.8	2.8-3.0	B	
15		284.0				B	
16		284.4				B	
17	*	285.7		3.6-3.8		B	
18	*	286.3	287.0	3.6-4.0		C	Shifts once.
19	*	286.6	287.3	3.6-4.0		C	Shifts once.
20	*	287.5		3.5-3.8			
21		287.9					
22		288.8					
23	*	290.2	289.7	2.4-2.6		D	Shifts twice.
24	*	291.0	290.5	2.4-2.6		D	Shifts twice.
25	*	291.8	291.3	2.4-2.6		D	Shifts twice.
26	*	292.9					Variable: S/N low.
27	*	293.7		2.3-2.8	3.2-3.6		
28	*	294.5		2.3-2.7			
29		295.0					
30	*	296.0					Variable: S/N low.
31	*	292.8					Variable: S/N low.
32	*	297.7					Variable: S/N low.

Table 8.1 *32 BANDS have been documented in the 270 - 300nm region of the PGH spectrum. The bands have been numbered from 1 - 32 by increasing wavelength. The second column (Variable) indicates those bands which are observed to change as the [GuHCl] is increased. The columns titled λ n, and λ i record the band locations in the native (0M GuHCl) and intermediate states (0 M GuHCl) of PGH respectively. Columns T1 and T2 record the [GuHCl] ranges over which distinct transitions in the bands are observed. The 'Group' assignments are arbitrary and largely based on physical proximity and uniformity of intensity of bands.*

All of the observed transitions are listed in the following table in order of increasing [GuHCL]. The first pair of concentrations indicate the start and finish of a transition, and the third concentration the mid point of the transition. There are six distinct sharp transitions and two slower transitions. The sharp transitions span no more than 0.3 M variation in [GuHCl]. There are two major (both sharp) transitions: the first centred at 2.5 M GuHCl (10 instances); the second centred at 3.8 M GuHCl (6 instances). There are no significant transitions observed above 4 M GuHCl, although many of the variable bands exhibit a gentle transition in the 4-6 M region which taken as an average is significant.

Number	Start	Finish	Mid point	Transition
1	0.0	2.6	1.3	A
2	1.8	3.8	broad	B
3	2.0	3.0	broad	C
4	2.3	2.9	2.5	D
5	2.4	2.6	2.5	D
6	2.4	2.6	2.5	D
7	2.4	2.6	2.5	D
8	2.4	2.6	2.5	D
9	2.4	2.6	2.5	D
10	2.4	2.6	2.5	D
11	2.4	2.7	2.5	D
12	2.4	2.8	2.6	D
13	2.4	2.9	2.6	D
14	2.8	3.1	2.9	E
15	3.1	3.5	3.3	F
16	3.2	3.6	3.3	F
17	3.4	3.7	3.5	G
18	3.5	4.0	3.7	H
19	3.5	4.0	3.7	H
20	3.6	3.8	3.7	H
21	3.7	4.0	3.8	H
22	3.7	4.0	3.8	
23	3.7	4.0	3.8	

I have chosen 7 examples of variable bands whose intensity changes with [GuHCl]. In the order presented in figures 8.4 to 8.10, these will be the bands located at 278.7nm (2.5M sharp transition), 282.3nm (2-4M slow transition), 287.5nm (3.5M sharp transition), 276.1nm, 283.3, 293.7, 276.9 (3 state transitions centred at 2.9, 2.9, 3.0 & 3.2M). All of these figures show the intensity change normalised to a scale of 1, with 1 representing the native state at 0M GuHCl.

***Table 8.2** THE [GuHCl] FOR TRANSITIONS of the 23 variable bands listed in table 8.1 are listed in increasing [GuHCl]. The [GuHCl] for the start, finish and midpoint of the transitions are documented. Based on similarity of transitions eight (A-H) transition groups are proposed.*

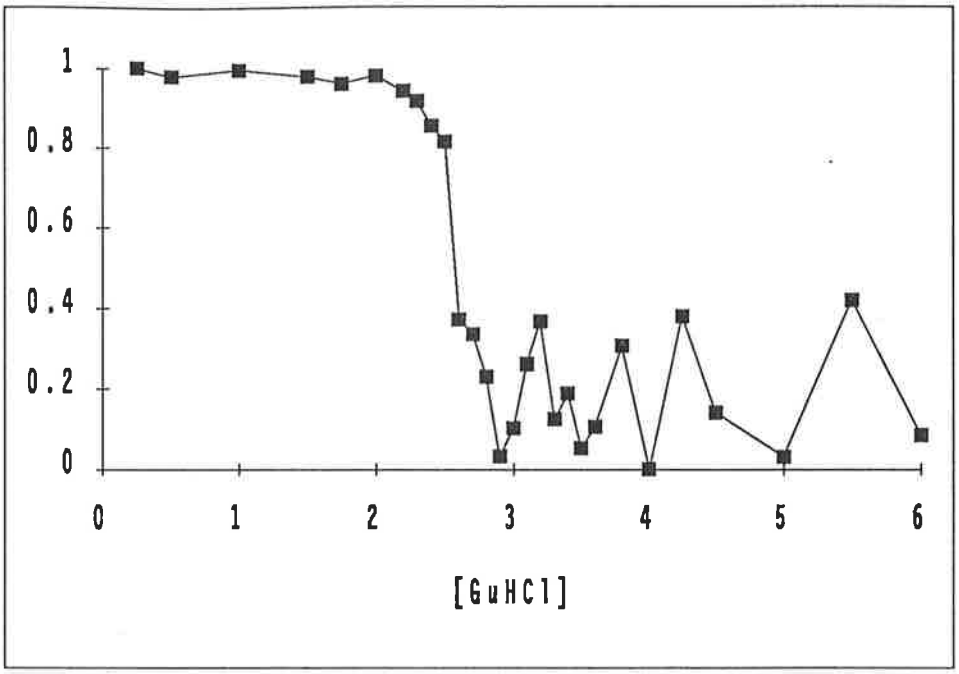

Figure 8.4 *THE 278.7nm BAND TRANSITION undergoes a sharp transition centred at 2.5M GuHCl. Transitions at this GuHCl concentration are the most common.*

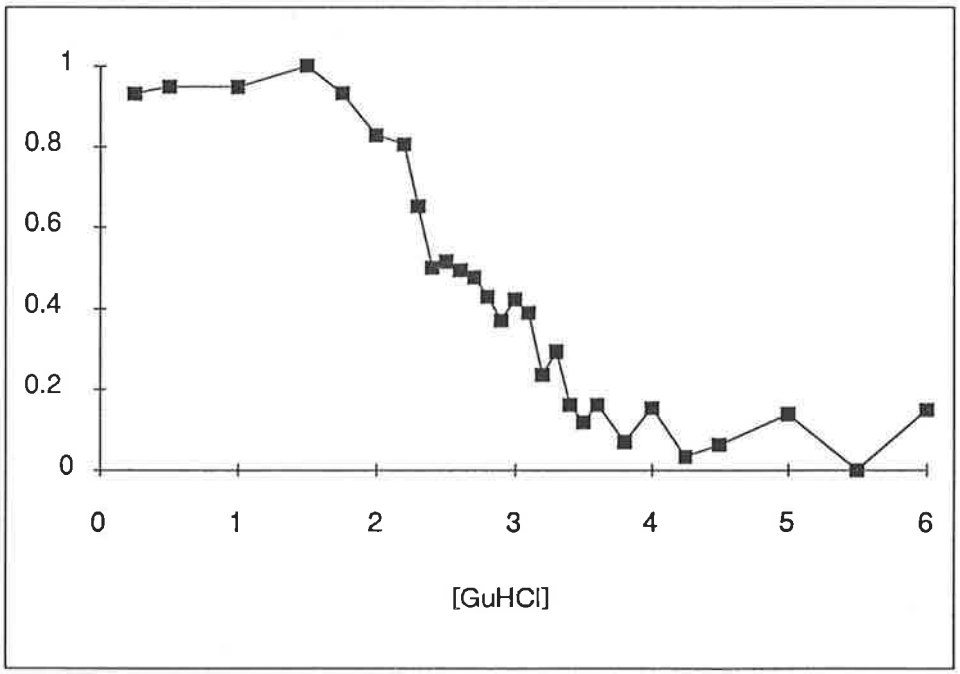

Figure 8.5 *THE 282.2nm BAND TRANSITION undergoes a gentle transition between 2 to 4M GuHCl.*

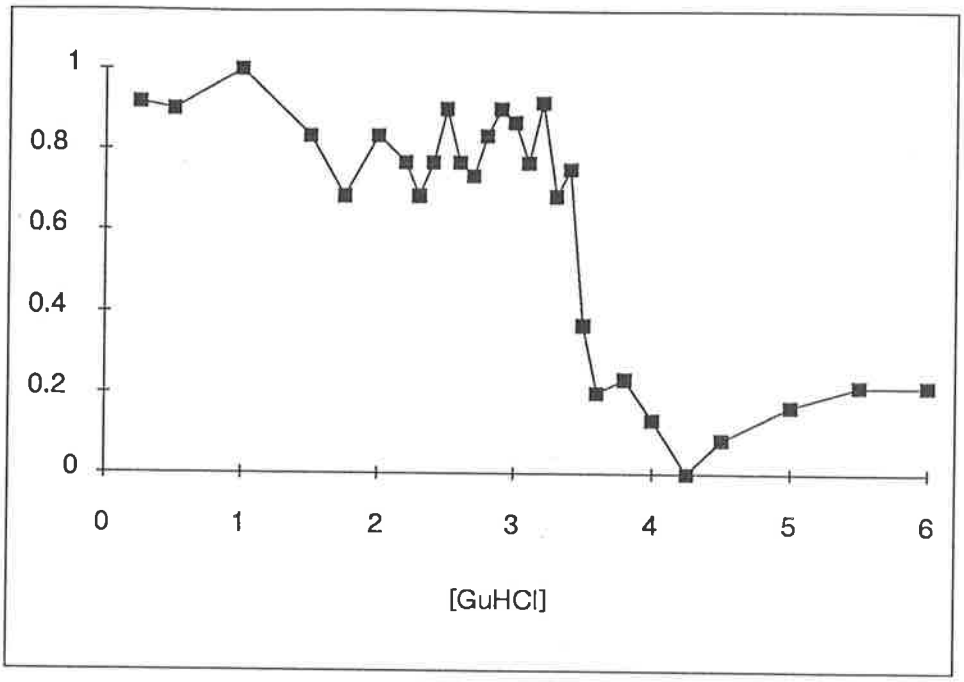

Figure 8.6 *THE 287.5nm BAND TRANSITION undergoes a sharp transition centred at 3.5M GuHCl. Transitions at this GuHCl concentration are the second most common.*

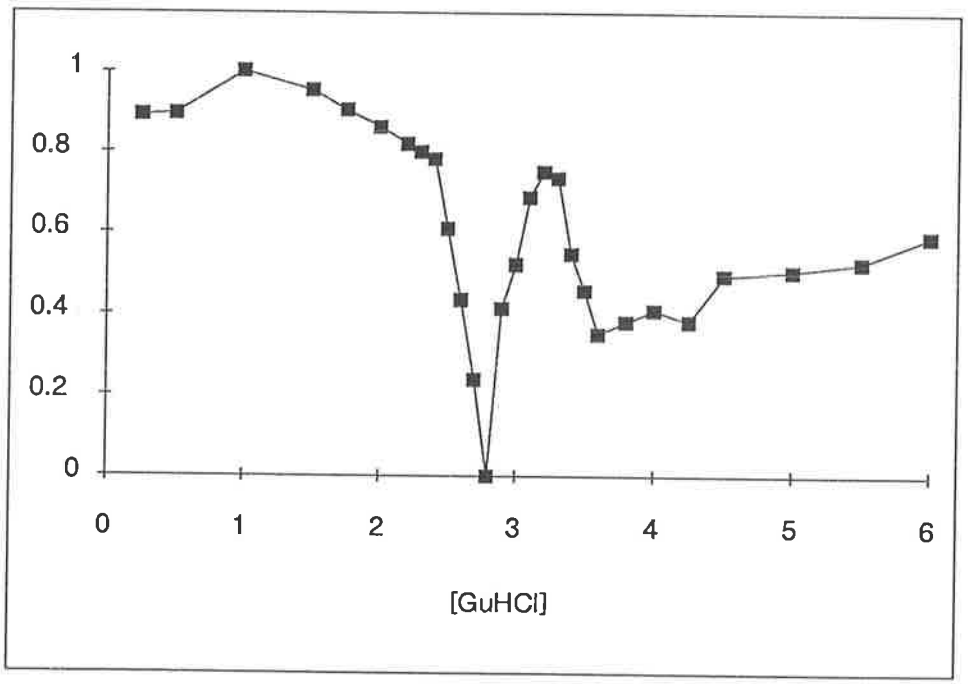

Figure 8.7 *THE 276.1nm BAND TRANSITION undergoes a number of transitions, including transitions centred at 2.5 and 3.5M GuHCl. This band exhibits significant transition states at 2.8 and 3.2M GuHCl.*

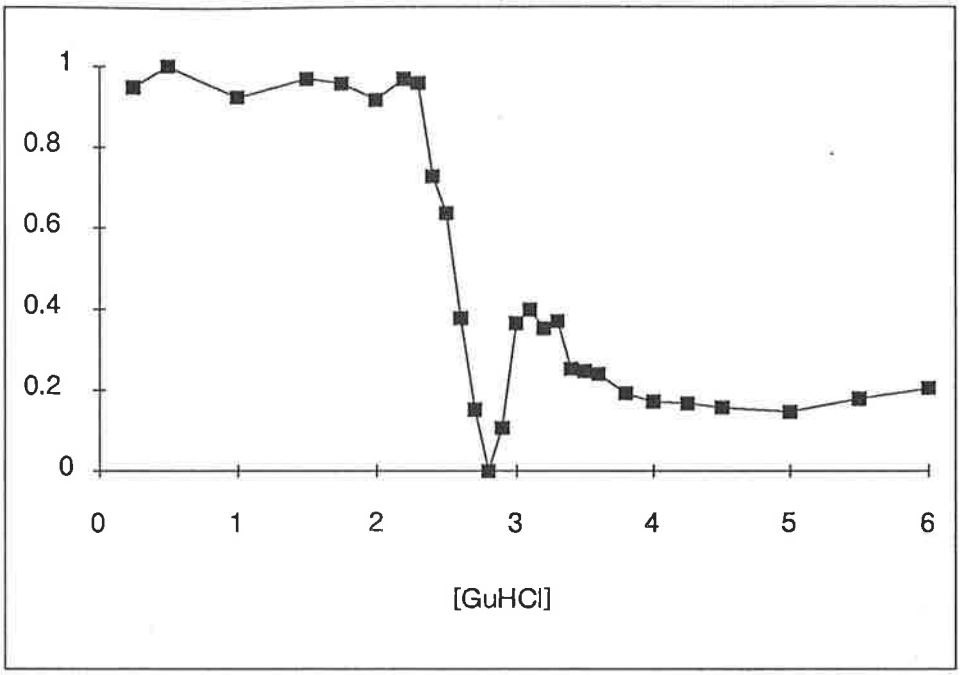

Figure 8.8 *THE 283.3nm BAND TRANSITION exhibits two sharp transitions between 2.4 and 3.0M GuHCl resulting in a 'transition state' centred at 2.8M GuHCl.*

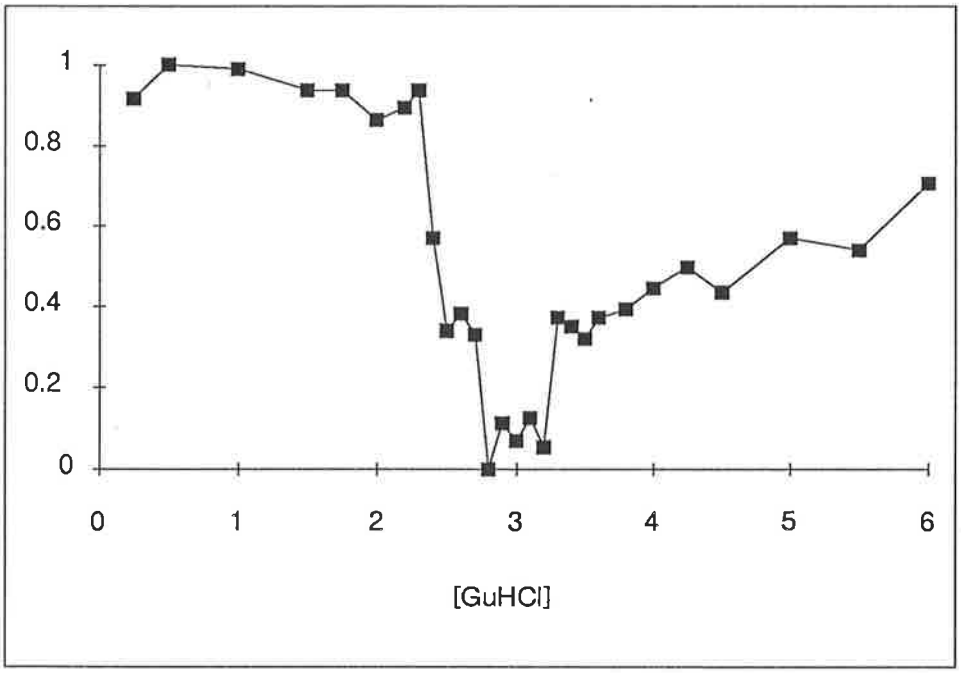

Figure 8.9 *THE 293.7nm BAND TRANSITION exhibits a broad transition state centred at 3.0M GuHCl. The gentle transition from 3.3 to 6M GuHCl is a featured shared by many of the variable bands.*

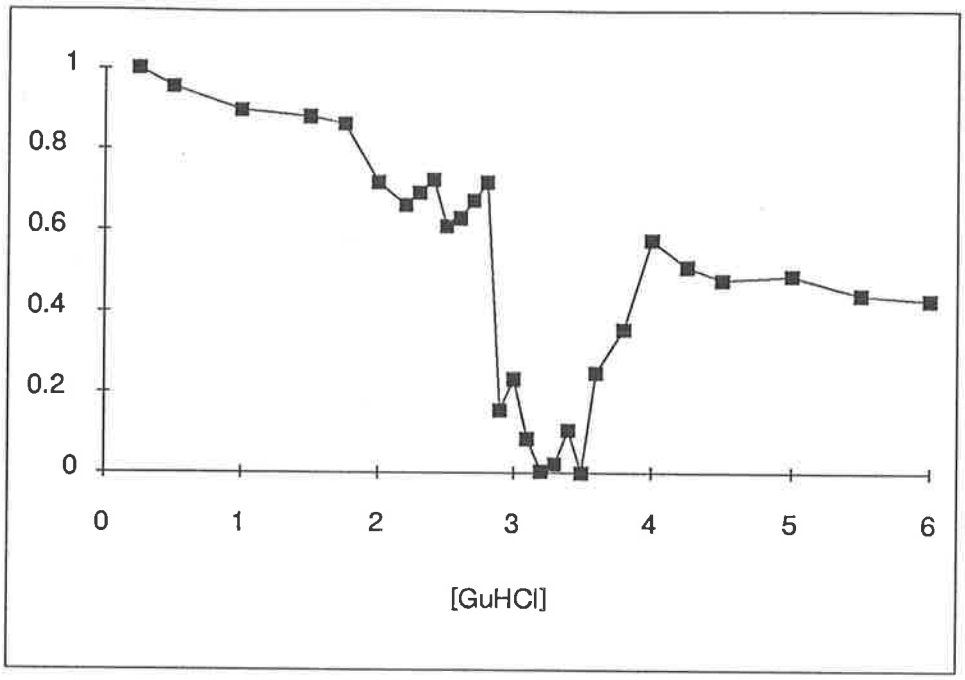

Figure 8.10 *THE 279.9nm BAND TRANSITION exhibits a very broad intermediate state between 2.9 to 3.5M GuHCl.*

While it is easy to determine the ΔG for the unfolding of PGH from its absorbance at 290nm vs [GuHCl] (figure 8.3), the validity of this must be questioned in view of all the different denaturation curves, only some of which are shown here. Which set of data and transitions should be used the determine the stability of the PGH? One can average all of the (normalised) denaturation curves and come up with a "global" denaturation curve which hopefully would be representative of the entire protein. However, there is no way of determining the correct weighting for the various denaturation curves and therefore the validity of any composite curve. The only valid approach I could suggest is (where possible) to determine the ΔG for each individual variable band; group the results relative to the major transitions (2.5M and 3.8M); and average these groups. This would give an average ΔG for each transition.

Presented with this wealth of detailed information it may be no longer valid to select a single wavelength (A290 nm) simply because it is easy to see the absorbance change as the protein is denatured. This is particularly so when considered in conjunction with the next section which shows that a number of complex changes are occurring to the bands centred at 290nm.

The 290nm Triplet of bands.

I have focused attention on the triplet of bands located at 290.2, 291, and 291.8 nm. This triplet of large bands exhibits a sharp blue shift of 0.5nm at 2.5M GuHCl and a red shift at 4.25M GuHCl. The blue shift is associated with a significant drop in intensity which is partially reversed when the bands shift back at 4M GuHCl. The 0.8 nm spacing between the three bands is maintained from 0 to 4.0 M GuHCl. At the 4.25 M transition the band spacing is altered. The 290.2 band is smaller than the others and suffers from a higher S/N as a consequence. Figure 8.11 shows the peak wavelengths of the three bands vs [GuHCl]. In character with all transitions observed between 2.3-2.9 M GuHCl, the first transition is extremely sharp, occurring over little more than 0.2 M GuHCl. The intensity of the bands clearly changes at the first transition. Unfortunately the S/N of the intensity is very poor above 2.5 M GuHCl. The intensity change vs [GuHCl] is shown in figure 8.12. The colour coding in the two figures (8.11, 8.12) is consistent to aid in comparison.

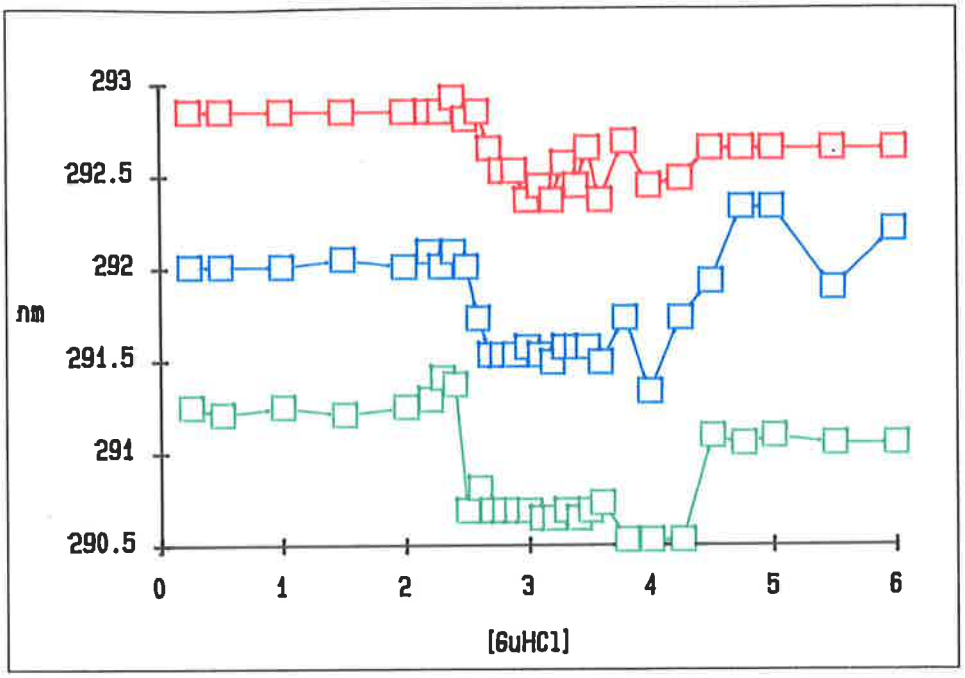

Figure 8.11 *A VERY SHARP RED SHIFT IS EXHIBITED by all three bands (292.8 red, 292 blue, 291.2 green) between 2.4 - 2.6 M GuHCl. The intermediate state responsible for the red shift is maintained up to 4.25 M GuHCl, where all three bands blue shift by different amounts. The 292.8nm band is smaller than the other two bands and has a lower S/N.*

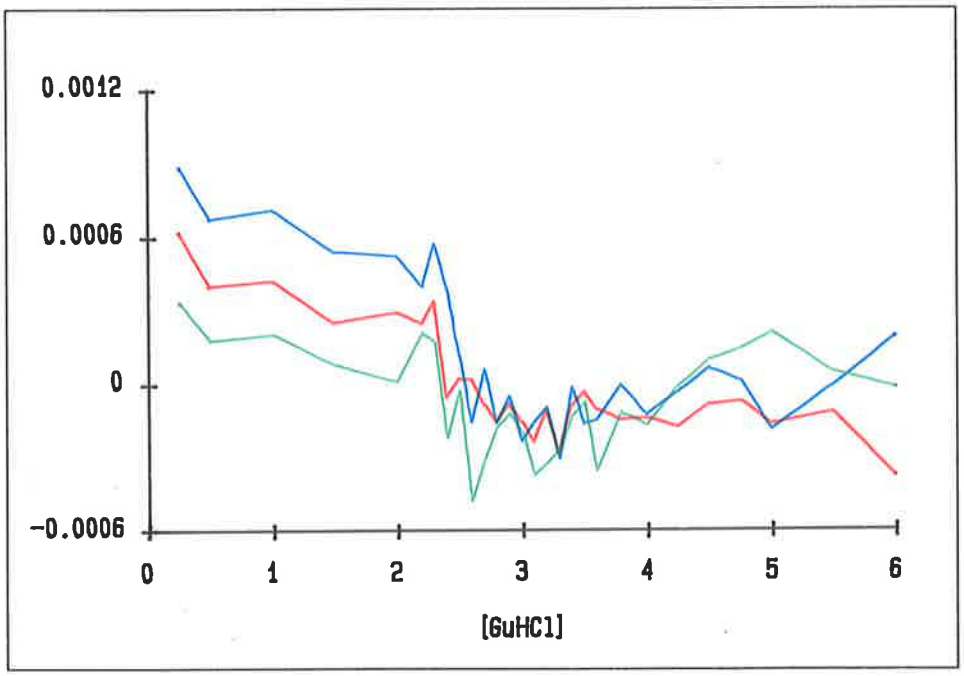

Figure 8.12 *A SHARP HYPOCHROMIC TRANSITION IS EXHIBITED by all three bands (292.8 red, 292 blue, 291.2 green) at 2.5 M GuHCl.*

Figure 8.13 shows sample spectra in the three regions at 0.25, 3.0 and 6 M GuHCl.

This is an excellent example of the power of the spectral enhancement methods developed here. The easily resolved bands in this triplet are only 0.8 nm apart and the shift is only 0.5 nm. In the first state (0.0-2.4 M GuHCl) the band locations vary by no more than 0.04 nm! Let us consider the various phenomena that this one example demonstrates.

First, hyper- and hypo-chromic effects.

a) Not accompanying shifts in the position (wavelength) of the bands.

In the 0 - 2.4 M state, all three bands exhibit an identical hypochromic effect. To a smaller degree (not shown well in figure 8.12, but quite evident in animations (this will be discussed later) of the spectra vs increasing [GuHCl]) the bands exhibit an overall hyperchromic effect above 4.5M GuHCl.

b) Accompanying shifts in the position (wavelength) of the bands.

This is to be expected when the energy levels (ground and/or excited) are altered. The first transition at 2.5M GuHCl is accompanied by a sharp hypochromic effect. The second transition at 4.25M GuHCl

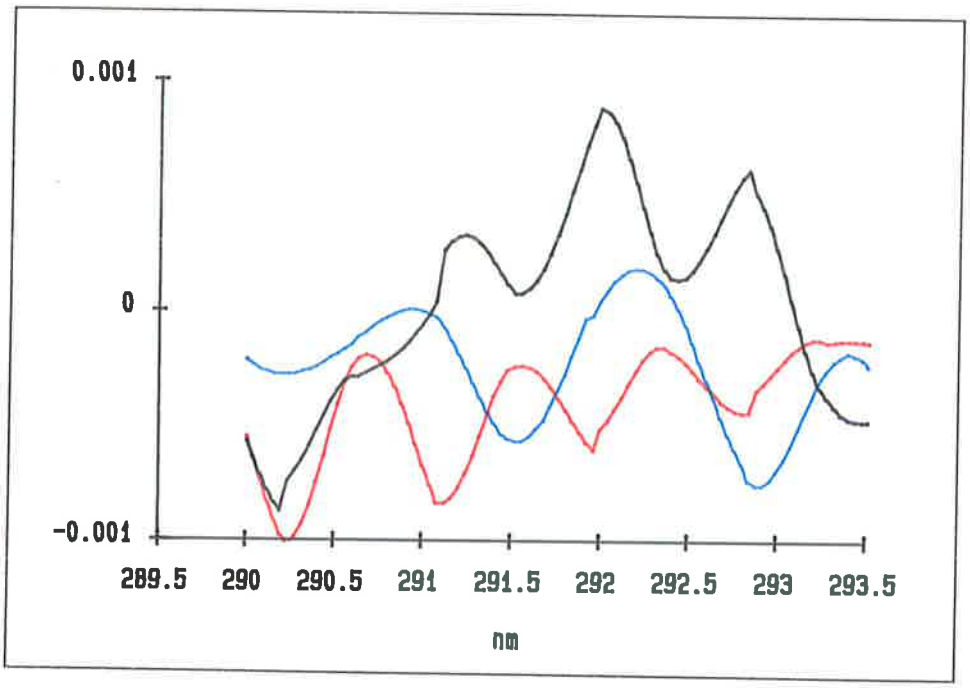

Figure 8.13 *SAMPLE SPECTRA AT 0.25M (black), 3M (red) and 5.5M (blue) GuHCl exhibit the wavelength shifts (red then blue) and hypo/hyper-chromic shifts.*

is accompanied by a smaller hyperchromic effect (again this is not shown well in figure 8.12, but is very evident in animations of the spectra vs increasing [GuHCl])

Second, shifts in band location as a consequence of alterations in ground and/or excited vibronic levels.

a) At 2.5 M GuHCl we see a shift to lower wavelength in all three bands. The shift is an identical 0.5 nm for all three bands.

b) At 4.5 M GuHCl the three bands shift to higher wavelengths, but not to the same degree.

These various effects are due to changes in the local microenviro-ment of the absorbing group. In the first stage (0 - 2.4 M GuHCl) the vibronic levels are not altered, but the probability of the vibronic transitions responsible for the observed bands are reduced resulting in the observed hypochromic effect. At the first transition the local microenviroment changes suddenly, resulting in a shift in either the ground or excited vibronic states corresponding to the three bands. In view of the fact that all three of the bands shift by an identical amount, the change is probably affecting either a single ground or excited vibronic state.

If it is a single excited vibronic state then the three bands result from transitions from three equally spaced ground states to the one excited state. At the first transition an increase in the energy of the one excited state would result in the observed identical blue shift of the three bands.

Alternatively, the three bands may arise from transitions from a single ground state to three equally spaced excited states. A decrease in the one ground state would also result in the observed identical blue shift of the three bands.

At 4.25 M GuHCl the bands red shift, but not in a co-ordinated manner as for the 2.5 M GuHCl transition, which implies a more complex transition pattern in this region.

Discussion of Variable Bands.

The aim of the work reported here was to demonstrate the quantity and quality of data provided when applying the enhancement techniques developed in the previous chapters. Specifically, the aim was to support the second hypothesis and strive to identify bands from individual amino acid residues.

In the 270-290 nm region examined, PGH has 7 tyrosine residues and one tryptophan residue contributing to the overall spectrum. In this region the existence of 23 variable bands has been reported. Of the 17 variable bands whose intensities were examined closely (listed in the second table), 8 distinctly different transition types were observed (A-H in the second table). Of the 17 variable bands, 7 clearly exhibited 2 transitions. Considering the eight transition types observed and combinations of these, all 17 of the reported variable bands undergo a unique denaturation pathway. How can this be when there are only 8 amino acids contributing to the spectrum in this region? The answer is simply that of all the multiple bands arising from a single residue, not all will undergo the same changes (or change at all) in response to the same change in the residue's microenviroment. I cannot claim to have uncovered sufficient information to uniquely identify all of the 8 amino acids involved, or even to link one of the amino acids to specific bands. However I do feel that the quantity and quality of the data revealed is of the right order so that with further clarifying analysis most (if not all) of the residues will be assigned to specific bands and transition combinations at some stage of the denaturation.

Towards this end I have designed (and Patented[3]) 20 analogues of PGH. The analogues were designed to fulfil several purposes: reduce aggregation during manufacture; increase binding (and hopefully activity) to the GH receptor; and purely as analytical tools. A significant number of these analogues have been produced and some proven to fulfil their intended roles. However I have chosen to strictly adhere to reporting the rigorous development and application of the techniques of spectral enhancement and not to report on the ever diverging work I have performed on PGH refolding through to successful field trials. Others are currently working on the unfolding/refolding of PGH utilising the spectral enhancement techniques and PGH analogues I have developed.

---

3 Provisional Patent covering all of these analogues and their applications limits any detailed discussion here

Protein Quantitation

Turning now to the validation of the third hypothesis, I will consider the spectral region of 250-270nm which is predominated by contributions from phenylalanine residues.

Figure 8.14 confirms the fact that the intensities of enhanced bands are linearly related to the intensities of the source bands. This may appear trivial but it is vital to confirm experimentally. The band chosen for the quantitations is located at 265nm and, as will be shown, is not affected by the various conditions examined (pH, [GuHCl], DNA & oxidised DTT contamination).

Having demonstrated a linear relationship between the peak intensity of the chosen enhanced band to PGH concentration, the following tests were performed: While holding the PGH concentration constant the following were varied

DNA contamination (salmon sperm) : 0-2.5% relative to PGH;

DTT (oxidised) contamination : 0 and 10mm;

[GuHCl] : 0 - 6 M; and

pH : 9 - 13.

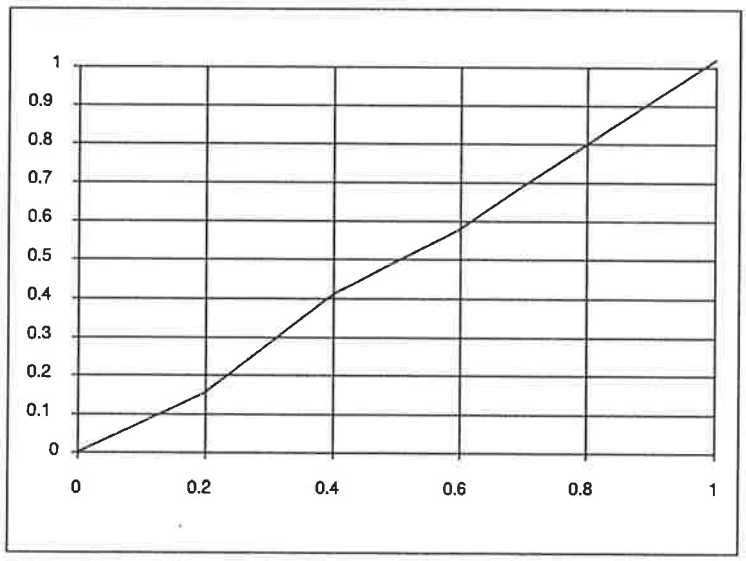

Figure 8.14 *THE ENHANCED SPECTRA IS QUANTITATIVE and can be used for quantitating the [PGH]. Using the 265nm band a standard curve of peak height vs [PGH] is generated. The scale factor is derived from the slope of this line. Having first established the quantitative nature of the enhanced 265nm band, subsequent experiments held the [PGH] constant and varied the environment.*

The intensity of the 265 nm enhanced band was measured from the peak at 265 nm down to the valley at 267 nm.

The individual spectrum in the following figures are colour coded for clarity, with the colour code legend arrearing on the figure. However, it is the overall variation due to the various conditions that is important, and the specific trends due to any of the conditions is immaterial for the purpose of finding a constant element for analysis.

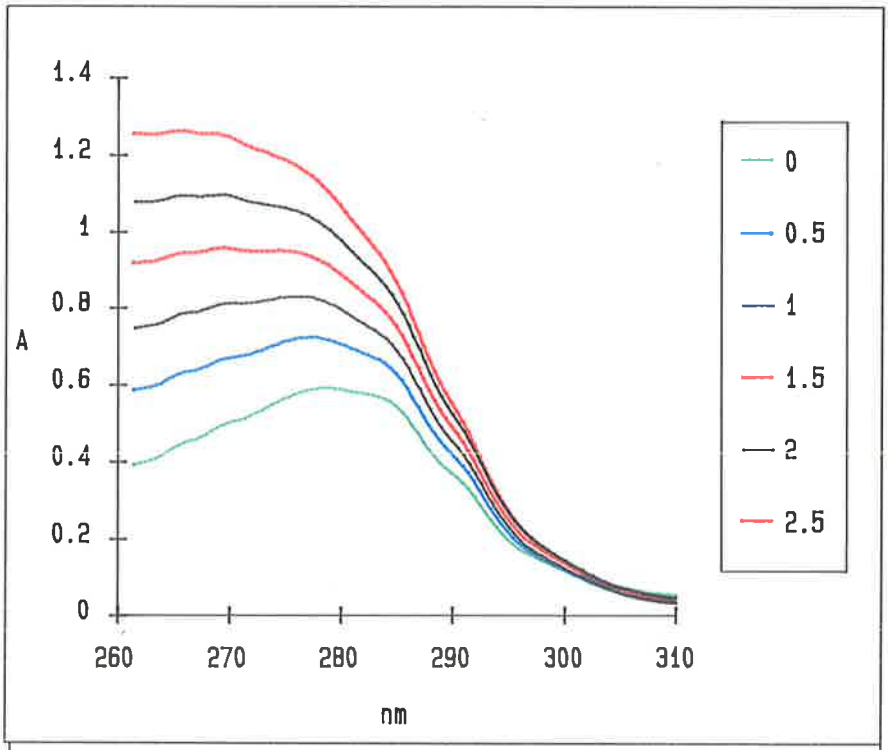

Figure 8.16 CONTAMINATION WITH SMALL AMOUNTS OF DNA *severely distorts protein spectra making normal spectroscopic quantitation impossible.*

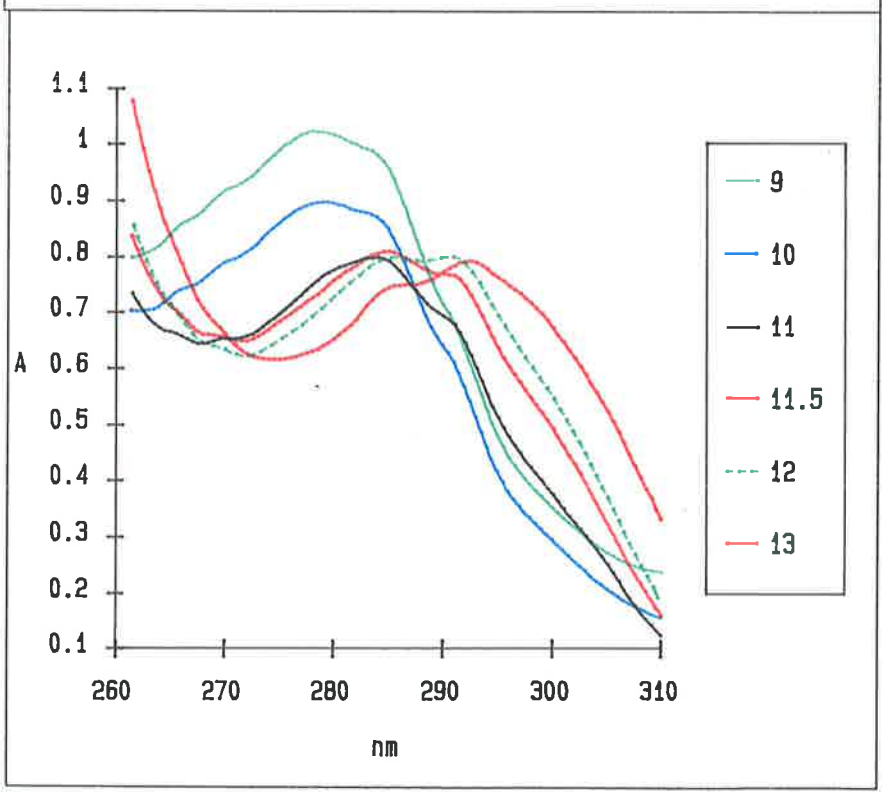

Figure 8.15 INCREASING pH IONISES TYROSINE *residues and shifts the peak absorbance from 280 to 295nm. PGH quantitation based on A280 can vary by over 40% with varying pH.*

The spectra for varying pH, DNA, DTT and [GuHCl] are shown in figures 8.15, 8.16, 8.17, and 8.18. Looking at these sets of spectra it is easy to appreciate the very considerable problems facing protein chemists in quantitating a known protein under such varying (and often unknown) conditions.

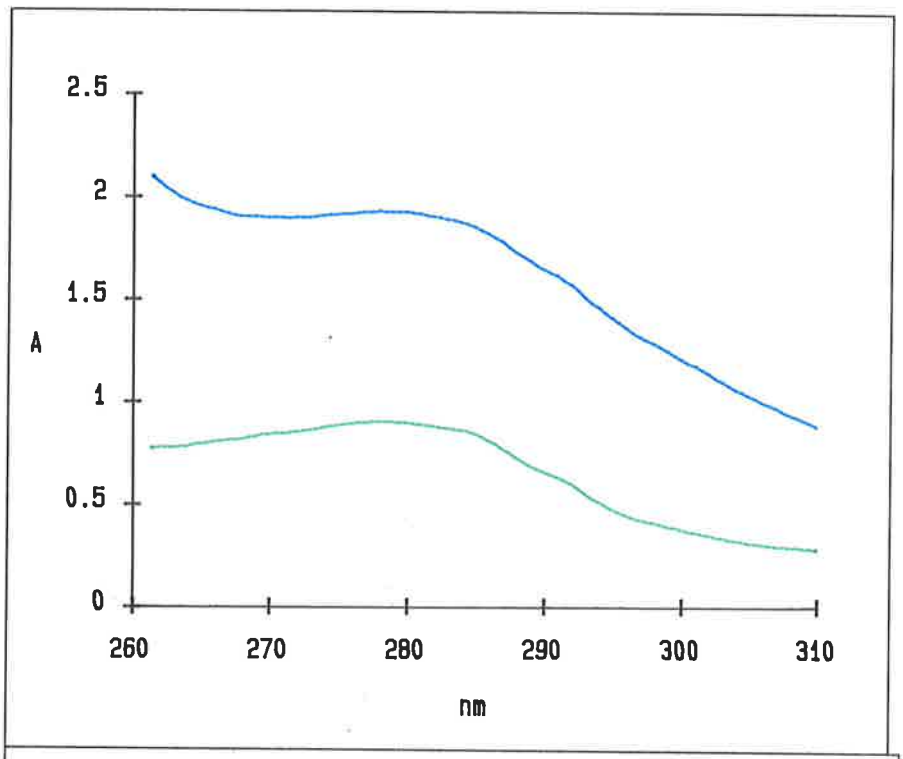

Figure 8.17 OXIDISED *DTT (upper spectrum) absorbs significantly over a wide range (as do most oxidised SH groups) making protein quantitation impossible.*

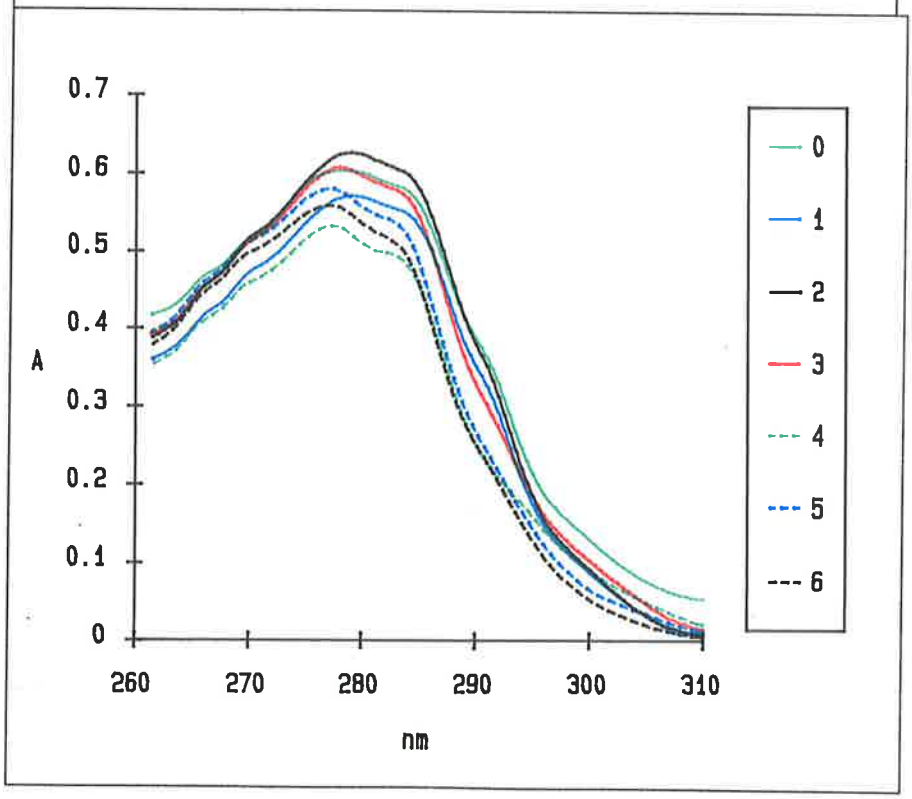

Figure 8.18 DENATURATION VARIES THE SPECTRUM *of PGH by 10-20% at most of the wavelengths shown, making accurate quantitation difficult for unknown conformational states of PGH.*

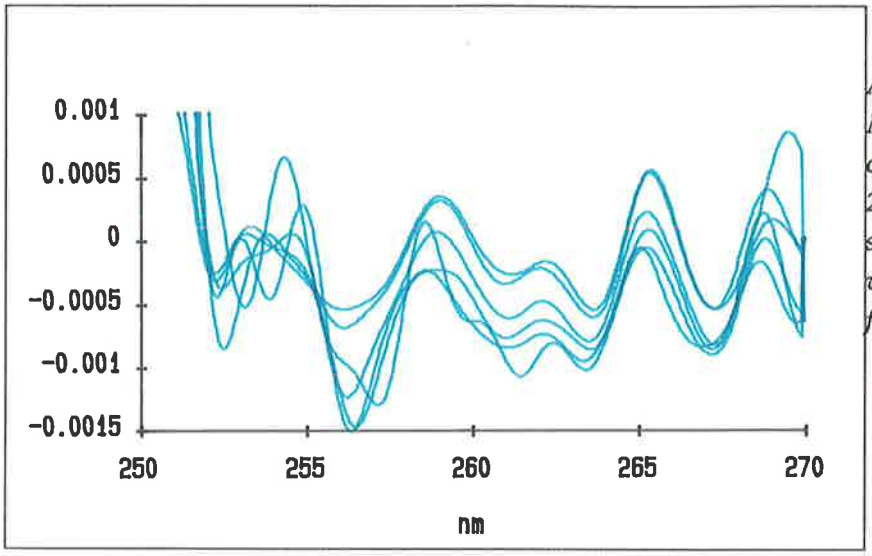

Figure 8.20 *HIGH pH HAS A SIGNIFICANT EFFECT ON MANY BANDS in this region of the spectrum. Fortunately the 265nm band intensity (measured as 265nm peak to 267nm valley) is not significantly affected.*

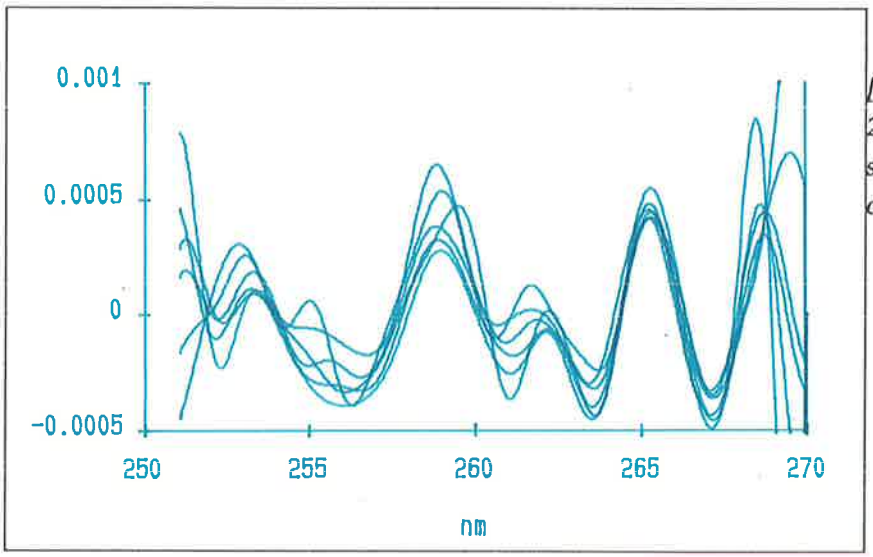

Figure 8.19 *VARYING [DNA] have no effect on the 265nm band of PGH, although significant spectral changes occur at lower wavelengths.*

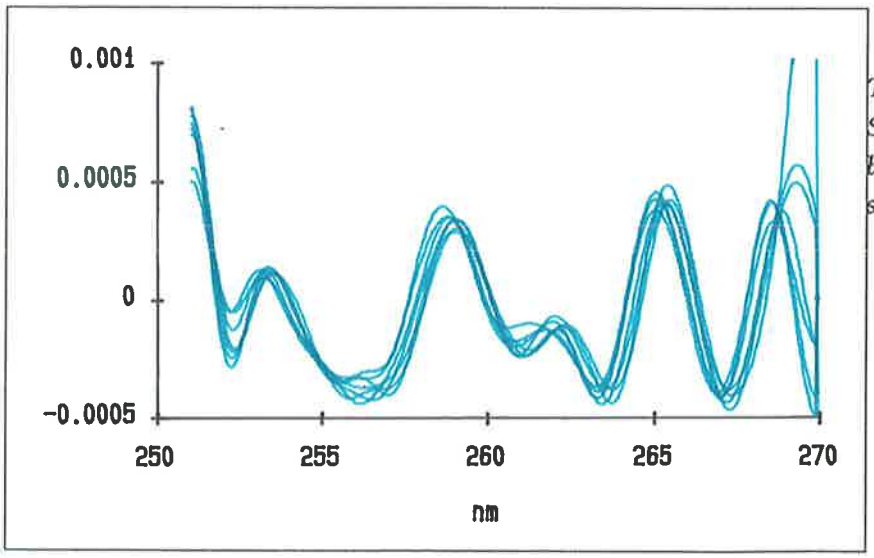

Figure 8.21 *GuHCl DENATURATION HAS NO SIGNIFICANT EFFECT on the bands in this region of the spectrum of PGH.*

The enhanced spectra from 250-270 nm for varying DNA, pH, and [GuHCl] are shown in figures 8.19, 8.20, and 8.21. It is immediately evident that the intensity of the 265 nm peak - 272 nm valley remains remarkably constant under all of the varying conditions.

I have tabulated the standard deviation around the mean for the protein concentrations determined from the enhanced 265 nm band (shown in figures 8.19, 8.20, and 8.21). This is compared to the % variation from the maximum to minimum absorbance (of the raw spectra) at 280 and 265 nm. In conjunction with the figures just presented, the following table demonstrates the stability of the intensity of the enhanced 265 nm band - 272 nm valley in the presence of these widely varying conditions.

	DNA (0-2.5%)	pH (9-13)	[GuHCl] (0-6M)	[DTT] (0-10mM)
280Nm	180%	71%	20%	110%
260Nm	290%	27%	14%	178%
Enhanced 265nm band	7%	5%	4%	2%

Table 8.3 *THE PERCENTAGE CHANGE in quantitative measures vs. the listed environmental changes are tabulated. The table summarises the data presented in figures 8.16-8.21.*

Discussion

I will discuss both electrophoretic and spectral enhancement advances here and put both into the context in which they were developed. From that starting point I will go on to consider some practical implications of the two inventions and finally future developments and advances.

Recombinant Protein Manufacture

This brief section describes the circumstances which required the development (and link) the two different processes reported on in this thesis.

In 1982 I was given the opportunity and freedom to develop commercial processes for the manufacture of PGH produced intracellularly as inclusion bodies in E.Coli. In reviewing the problems I was likely to encounter in the large scale purification of PGH (and any protein) it became apparent that all the current techniques had inherent limitations. Utilising combinations of chromatography and electrophoresis I set about to design a scaleable high resolution process that would be easy to implement. Initially designed as a thought experiment just to see how much detail I could work out without setting pen to paper, I devised the CEF process and initial device in their entirety. I predicted that the process would be controlled by three variables: pH, fluid velocity, and voltage gradient in the thick membrane. I also predicted that the limitation to the process would be wasted energy, the consequent heat production due to increasing conduction in the focused protein in the thick membrane. Some time later I was given the go-ahead to develop the process and, with the assistance of Nicholas Abbot (a recently graduated Chemical Engineer from the Chemical Engineering Dept. at Adelaide University), rapidly proceeded through 7 prototype apparati to prove the process in all but one aspect. It was extremely fortunate that the one limiting factor I had postulated did not arise. The focused protein did not increase the conductance (and therefore energy dissipation for the same voltage drop across the focused protein band) within the thick membrane, instead the conductance in this band rose sharply and the apparatus' efficiency rose dramatically. Unfortunately after proving the

technique and developing the apparatus and specialised power supplies, support for the project was discontinued due to a lack of funds.

Subsequently, as more work was put into the refolding of PGH, I turned to the use of second derivatives as an analytical tool. The early development of an interactive spectral analysis package on Sun work-stations provided the insights needed to inspire the development of improved techniques. In particular the ability to view a number of derivative spectra, and alter the digital filter parameters in real time revealed order where it was not expected. I noted that, as the filter widths were reduced, much of what appeared as noise when viewed as an isolated spectrum was in fact repeatable and significant bands when viewed as a group of related spectra. The major problem was one of S/N. From that point on the detailed second derivative spectrum has become the key tool in identifying and following the refolding of PGH. While techniques such as X -ray crystallography and 2D NMR yield similar (and greater) detail, I have not encountered any technique which provides such detailed information as spectral enhancement does in one simple and quick manner and under such a wide range of solution conditions.

During the time of the development of these two techniques, I personally developed a manufacturing process for recombinant PGH which remains essentially unchanged to date. This work has taken me to Biotechnology centres in Stockholm (Alfa Laval) and MIT (Chemical Engineering Department) in Boston to perform pilot production runs on two occasions each. The production of PGH as (dry weight content of PGH in) purified inclusion bodies went from 1.2Kg to 5Kg over the course of the four 1000L pilot runs at these sites. Over 100g of research grade PGH has been purified to date and utilised for research and development, and for a number of successful field trials here and overseas. It was my original intent to report on much of this work in this thesis. However much of the work was of an essentially technical nature. I felt that it was much more appropriate that I report on the two significant new processes I developed along the way.

CEF. Problems and solutions.

The serendipitous finding that the focused band in the thick membrane decreases the conductance of the band and increases the efficiency of the process may also yield one of the most serious problems of the technique. In a number of the experiments performed the [Hb] in the thick membrane rose to very high levels and aggregation occurred, fouling the membrane. Although this may have been a particular problem with Hb, it may also be representative of a more general problem.

The processes occurring in the apparatus are evidently considerably more complex than is initially apparent. Some exploratory experiments using pH indicator dyes showed a complex pattern of high and low pH bands/fronts that move through the thick membrane, first in one direction and then back again as the apparatus approached equilibrium. In addition, even though the gel material used for the thick membrane had no known interaction with the buffer ions, the operating apparatus demonstrated a very significant ion pumping action after reaching equilibrium. Also as noted, the thick membrane experiences considerable physical forces as equilibrium is reached and a stable focused band is formed. In all cases the force acts to push the membrane back against the liquid flow and is therefore an electrophoretically mediated force. In some of the early prototypes this resulted in the gel breaking out of its confines and heading for the electrodes.

I believe many of these problems would be overcome if the apparatus were developed to its conclusion as defined by these criteria: to reduce the distance between the electrodes and the thick membrane to a minimum; to reduce the depth of the thick membrane as much as possible; to reduce the voltage to a level where gas is not evolved; to maximise the surface area of the thick membrane within a minimum apparatus volume; to maximise turbulence in the volumes enclosing the thick membrane; and finally to design a cheap and easily manufactured apparatus.

All of these criteria could be met if the apparatus were constructed as a spiral wound cartridge in a similar manner to currently available spiral wound filtration cartridges. This would minimise all of the distances to the degree where the applied voltage would be low enough to avoid evolution of gas; and it would provide for turbulent flow (as is achieved in spiral wound cartridges) around the thick membrane. With such a cheap and easy to handle embodiment of the technique, low resolutions could be selected to avoid membrane fouling and serial units applied if greater resolution was required.

Spectral enhancement. Problems and solutions.

The first very real problem in spectral enhancement is the decision of just how much enhancement to apply before the S/N becomes unacceptable. Much of the problem is that the noise which is most serious is of the same frequencies as the signal. It is not the high frequency noise that is the real problem. It is a simple matter to suppress both low and high frequency noise without disastrously distorting the enhanced bands. As the higher frequency components of the bands being enhanced are increasingly amplified in a selective fashion, it is the noise at these very frequencies which is the problem. Clearly as the bands are further enhanced and the band pass nature of the frequency filters is narrowed, the noise and signal components converge in frequency envelope. The net result is an enhanced spectrum that looks good but in which repeat spectra reveal movement of the (good, noise-free-looking) bands in both position and intensity. This is the hall-mark of noise of the same frequency as the signal. An obvious solution is to collect a number of spectra of the sample and concurrently enhance all of them until the enhanced spectra begin to diverge. This is very time consuming considering the length of time needed to collect one good quality spectrum. In cases such as the denaturation study reported in the previous chapter, the experimental design provides a large number of closely related spectra and this method is applicable (and was applied).

The procedure I am about to describe also solves another related problem, which is that the response axis of the enhanced spectrum is almost meaningless. Although the intensity of the enhanced bands are linearly related to the intensity of their respective source bands, the scale factor will vary with every set of filter parameters used. Compounding this problem is the currently insoluble problem of deriving the normalising factors from the various filter parameters. A solution is: To represent the response axis in terms of S/N. This immediately yields a scale that has meaning for any spectrum whether enhanced or not. The procedure would be as follows:

First: Collect the spectrum and a blank spectrum at the same time. The RMS amplitude of the blank spectrum is calculated and the response axis of the actual spectrum represented as S/N ratios. @ONE_LINER = Second: Whenever an enhancement procedure is applied to the spectrum, the same procedure is applied to the blank spectrum and a new RMS noise amplitude calculated.

The enhancement of the spectrum can proceed until the S/N drops to some predetermined level (say 5). The validity of any enhanced spectrum is immediately apparent from the response scale, irrespective

of the enhancement technique and parameters used. When the final enhancement parameters have been set, a second scale of 'equivalent absorbance' could be added. The scale can be determined by applying the enhancement procedure selected to a computer generated noise-free band and measuring the ratio of source/enhanced intensities.

These procedures will be implemented in the next version of the software now being written.

A very real problem encountered in the analysis of the spectra used for the denaturation studies was 'information overload'. The enhancement worked well and presented me with 30 spectra each with 30+ bands. Although some enhanced bands were relatively noise free and unchanging, many smaller bands were noisy and many bands varied (as intended) in response to denaturation of the PGH. Concurrent viewing of the spectra presents the viewer with an ordered 'mess' containing nearly 1000 bands in 30 multi-coloured spectra. In addition to this problem, the spreadsheet containing the spectra was over 0.5Mb in size, which is well beyond the size which can be reasonably handled, even on the computer utilised (20MHz 386 + 387 PC compatible with 8Mb RAM using Excel 2.1c under Windows 3.0 with an additional 12Mb virtual RAM available). Fortunately processing time was not a problem and each spectrum (2000 points) required less than 5 seconds to process.

The only way it was possible to identify the variable bands was to fall back on the eye's remarkable ability to identify ordered motion against complex backgrounds. Small segments of the spectra containing 3 - 6 bands were isolated for examination. The spectra were ordered by increasing GuHCl concentration in the spreadsheet and when viewed were drawn in series. This resulted in approximately a two second animation as the 30 spectra were displayed. After viewing the 'animations' a number of times significant variations were easily identified. This technique was the only way to identify all of the variations occurring. Often very significant band variations and transitions viewed as animations appear very poor (noisy) when analysed as intensity variations at one wavelength or shifts of peak locations.

Resolution of dilemmas such as this is central to scientific analysis. So often 'scientific analysis' reduces down to the statistical analysis of visually obvious trends in data:

New data is manipulated to extract, enhance or highlight some relationship between the input and output variables to the extent that visual inspection of results will reveal a trend or relationship.

The data may then be further manipulated and processed in some defined and reversible way to enhance the visual trends and relationships.

The data may then be further manipulated and processed in some defined and reversible way to enhance the visual trends and relationships.

Finally mathematical (statistical) models are fitted to the data to validate and quantify what was visually obvious.

Thus the final results are endowed with scientific and quantifiable credibility and relationships between variables are validated.

In previous research (un-published software; company confidential to Applied Innovation P/L) I have had considerable success in developing highly automated chromatographic analysis software by considering the visual processes by which the eye identifies a 'peak' from 'baseline drift' and 'artifact' (noisy spikes). I hope that in a similar fashion I can determine the significant features and processes by which band variation is easily identifiable in the animations of serial spectra. Once programmed this will result in a repeatable and quantifiable method, resulting in improved S/N for the band transition graphs. The reasoning being that: the animations of whole spectra appear less noisy than the static plots of individual band intensities and position at a purely visual level. Automation of the visual processes should yield similar results in a quantifiable form. I hope that this will also lead to better ways for the analysis of band parameters of single or pairs of spectra. Such visual properties as band centre of mass, quality of shape, and useful part (ie. the 'top area' significantly unaffected by the baseline or neighbouring bands) should all be cast algorithmically and quantified.